MOLECULAR MODELLING OF TRANSITION METAL COMPLEXES WITH QM/MM METHODS

STRUCTURE AND REACTIVITY

A dissertation submitted by

Gregori Ujaque Pérez

in partial fulfillment of the requirements
for the degree of Doctor of Philosophy

Els sotasignants, **Agustí Lledós i Falcó** i **Feliu Maseras i Cuní**, Professors Catedràtic i Titular d'Universitat respectivament, del Departament de Química de la Universitat Autònoma de Barcelona

CERTIFIQUEM:

Que en Gregori Ujaque i Pérez, llicenciat en Ciències Químiques per la Universitat Autònoma de Barcelona, ha realitzat sota la nostra direcció, al Departament de Química de la Universitat Autònoma de Barcelona el treball que porta per títol:

"Molecular Modelling of Transition Metal Complexes with QM/MM Methods - Structure and Reactivity"

que es presenta en aquesta memòria per a optar al grau de Doctor en Ciències Químiques.

I per tal que consti a efectes legals, firmem aquest certificat.

Agustí Lledós i Falcó

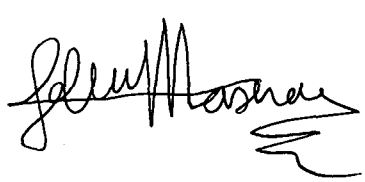

Feliu Maseras i Cuní

Bellatera, 9 de Febrer de 1998

Aquesta part de la tesi és possiblement la més curta de totes, i segurament la més consultada. Tot i així, és sens dubte la més important a nivell personal, ja que em dóna l'oportunitat de poder agrair a totes les persones que han col·laborat d'una forma o altra en l'elaboració d'aquest treball, o inclús diria més, que m'han ajudat en la meva formació tant personal com científica.

En primer lugar a mi familia, ya que ellos han sido la pieza clave para que yo pueda estar ahora escribiendo esta tesis. Desde que me vine a Barcelona, sus muestras de apoyo y confianza han sido constantes e inquebrantables, haciendo posible que todo lo difícil como por arte de magia se convirtiese en fácil. Así, el mérito de todo lo que estoy consiguiendo se debe principalmente a ellos, ya que es su empuje y su entusiasmo lo que me motiva para hacer todo lo que hago.

A la Sonia son también innumerables las cosas que tengo que agradecerle después del tiempo pasado juntos, y seguramente necesitaría un libro mayor que este para poder ponerlas todas.

Als "jefes" principalment una cosa, que és que no exerceixin com a tal, i m'explico: amb el tracte que donen han aconseguit un clima de "bon rotllo" dins el grup que fa que la ciència a vegades ens la prenguem com un oci. Així que més que jefes es pot dir que són uns autèntics "mestres".

A l'Agustí, el fet de què em donés l'oportunitat d'incorporar-me en el seu grup de treball sense posar cap inconvenient, ja que així he tingut l'ocasió de formar-me tant científicament com humanament. També m'agradaria agrair-li el seu enèrgic recolzament sobretot en alguns moments bastant delicats.

Al Feliu, (que com més temps passa més me n'adono que soc un simple mortal al seu costat), les seves múltiples i incansables assistències tant aquí com arreu del món a on he anat, ja que sense la seva ajuda tot hagués estat bastant més difícil. I a més sempre de bon tarannà. No sé si en tot això ha influït el fet de què soc el seu fill científic primogènit, però a mi es una cosa que m'enorgulleix profundament.

Je souhaiterais également remercier madame Odile Eisenstein pour m'avoir agreablement accueilli quelque temps au seir de son groupe de Montpellier.

Ara és el moment dels amics. Al Javi, Jose, Pau, ..., Esther, Javi, Xino, Toni, ..., Ignacio, Eugeni, ..., els hi estic molt agraït, ja que ha estat amb ells amb els que he passat molts dels millors moments que recordo ... les festes, les borratxeres, les escapades de cap de setmana, les maratons de "botifarra", etc. Tots ells han estat peces fonamentals que m'han ajudat en els moments que els he necessitat. També la penya d'inorgànics amb la que anem a dinar cada dia, i fotem les macro-partides de super-2.

A tota la gent de química física (als presents i als absents), el bon clima que generen (tant de treball com de festa) que fa que la vida en aquesta planta sigui molt més agradable. Moltes són les coses que compartim (a part de les cues a les màquines), com les partides de botifarra (que fèiem), o les de mus (que ara s'està posant de moda). A l'Óscar en concret totes les assistències de WordPerfect que m'ha donat durant l'escriptura d'aquesta tesi.

A tots els amics del poble, amb els que hem passat moments molt bons, i que sempre m'han donat un cop de ma quan m'ha fet falta. I molt especialment a l'Eloi, amb el ja que la seva amistat no te preu.

També m'agradaria fer una menció especial a la gent amb la que he compartit el pis durant tots aquests anys, i en particular a els "guiris": el "Doji" (Daíthí) i la "Gro" (Grainne); i a l'Enric, ja que ha estat amb ell amb el que hem arreglat i desarreglat el món infinites vegades, per arribar a concloure que no som res.

Al Carlos, por haber confiado en mi sobre todo en los momentos iniciales de mi carrera, ya que es entonces cuando uno necesita el más firme apoyo.

A tots ells GRÀCIES !

Gregori dixit. Bellaterra, Febrer de 1999.

A mis padres,

y a la memoria de mi abuela.

Contents

List of abbreviations

AM1	Austin Model 1
CI	Configuration Interactions
CFT	Crystal Field Theory
DF	Dirac-Fock
DFT	Density Functional Theory
ECP	Effective Core Potential
EHMO	Extended Hückel Molecular Orbital
IMOMM	Integrated Molecular Orbital Molecular Mechanics
LFT	Ligand Field Theory
MCSCF	Multi Configurational Self Consistent Field
MM	Molecular Mechanics
MP	Moller-Plesset
NDO	Neglect Differential Overlap
PPP	Pariser-Parr-Pople
QM/MM	Quantum Mechanics / Molecular Mechanics
SCF	Self Consistent Field
VB	Valence bond
VBT	Valence Bond Theory

Chapter 1

Introduction

Transition metal complexes play a very important role in chemistry, chemical industry, and in life itself. There are a lot of examples to prove this statement. For instance, one of the most important catalytic reactions in commercial use, the Monsanto process, uses a homogenous rhodium catalyst for producing acetic acid from methanol via carbonylation, allowing the production of more than 1.5 million tons annually. It is also known the importance of the hemoglobin for oxygen transport to animal cells, being involved in this case an iron complex. These examples give an idea of the importance of transition metal complexes.

At the beginning, the study of this kind of compounds emerged as a part of inorganic chemistry, and nowadays a number of transition metal complexes are also commonly used in organic chemistry. More recently, strong links with biochemistry and medicine are also being found. Consequently, theoreticians have also been interested in understanding the characteristics and behavior of this kind of compounds, and great efforts are being invested in the development of theoretical tools specially suited for the study of transition metal systems.

Early theoretical studies on transition metal complexes were mostly qualitative, and their explanations were generally successful. Nowadays, theoretical calculations are able to give quantitative results, providing a very powerful tool for the study and understanding of chemical problems. This change is principally due to the extraordinary increase of computational power and the development of new calculation algorithms. Quantum mechanical calculations (DFT or traditional ab initio methods) provide the most accurate results. However, the computational effort involved rises sharply with the size of the chemical system. Usually, calculations have to be carried out on model systems, because real systems are too large. Although this approach works very well in a large number of cases, the modeling of bulky ligands, specially when interactions between them are important, can drive to wrong conclusions. On the other hand, molecular mechanics methods are much simpler than quantum mechanics methods, giving less accurate results, but allowing the study of larger chemical systems. The main problem in the application of molecular mechanics methods to transition metal chemistry is that these methods are usually parameterized for the study of organic systems, and have to be used very carefully.

In order to solve the problems commented above, new methodologies are emerging which combine quantum mechanics (QM) and molecular mechanics (MM) methods. They are normally labeled as QM/MM methods. In these methods, the chemical system is divided in two parts. One part is treated by quantum mechanics methods, and the other part is treated by molecular

mechanics methods. The more significant part of the system, where the chemical bonds are breaking and forming, and where the metal atom is located, is treated at quantum mechanics level, while the rest of the system is treated at molecular mechanics level. Thus, this methodology is specially appropriate for the study of transition metal complexes. In a usual partition, the metal atom and the atoms belonging to the first coordination sphere are treated at quantum mechanics level, and the rest of the atoms are treated at molecular mechanics level.

Several QM/MM methods have been described in the literature, but most of them are designed to describe solvation effects in biochemical environments containing exclusively main group elements. The IMOMM (Integrated Molecular Orbital Molecular Mechanics) method, developed by Maseras and Morokuma, is specially designed to work with transition metal complexes. The work presented in this thesis is the application of the IMOMM method to different chemical problems related with transition metal complexes. On one hand, there are studies related to the understanding of structural features, such as agostic interactions or symmetry breaking distortions. On the other hand, there is an application of the IMOMM method to the discernment of a reaction mechanism, that of the asymmetric dihydroxilation of alkenes catalyzed by osmium tetraoxide.

This first chapter is divided in different sections and subsections. In the first section, there is a plain introduction to transition metal complexes from an experimental point of view, giving a general presentation of the chemical problems dealt in this work. In the second section there is a general overview on the theoretical methods applied to transition metal complexes, with special attention to the QM/MM methods. In the second chapter there is an explanation on the particular topics of this thesis and the obtained results. Afterwards, in the third chapter the main conclusions are enumerated. Finally, the last chapter are collects all the papers achieved with this work.

1.1 Transition Metal Complexes

Coordination compounds have always been a challenge to chemical knowledge. In the early days of chemistry they seemed unusual (hence the name "complex" ions) and seemed to defy the usual rules of valence. Although the usual bonding theories can be extended to accommodate these compounds, transition metal complexes still provide stimulating problems to be resolved.[1,2] In synthetic work they continue to provide unexpected reactions in the laboratory. The rapidly developing field of bioinorganic chemistry is centered on the presence of coordination compounds in living systems.[3]

Along the history of the chemistry, a lot of books, reviews, research papers, etc. have been written about transition metal compounds. Today these species still comprise a large body of current chemistry research. A survey in chemistry journals shows how active is this research field. For instance, ca. 70% of articles in recent issues of the journal *Inorganic Chemistry* can be considered to deal with coordination compounds. Therefore, it is quite difficult to make a brief and general overview of this important field of chemistry.

In spite of that, this part of the introduction will modestly try to fulfill this goal. In the first subsection there is a historical overview about transition metal complexes, where the main aspects are briefly commented. Afterwards, a general description about their structure is done, taking special emphasis on the particular topics dealt in this work. Finally, the last section deals with the reactivity of transition metal compounds, and their special ability to act as catalysts. One particular enantioselective catalytic reaction, the asymmetric dihydroxilation of olefins by osmium tretroxide is described in more detail.

1.1.1 Historical Background

It is not clear which was the first metallic complex discovered. It may have been the Prussian blue, discovered by Diesbach, a pigments' manufacturer at the beginning of the eighteen century.[4] However, hexamincobalt(III) chloride, brought to light by Tassaert in 1798, is normally cited as the first transition metal complex.[4,5] Since that moment, a lot of new complexes were discovered and studied, although more than one hundred years had to pass before a good model for the explanation of these compounds was presented. The first theory, labeled chain theory (due

to its similarity with the theories of valence common in those days), was proposed in 1869 by Blomstrand, and energetically defended later by Jorgensen. The chain theory was not able to explain all the experimental facts, and chemical researchers dedicated great efforts to the search of a better scheme. It was in 1893 when Alfred Werner (at the time only 26 years old!) proposed the coordination theory,[6] providing a new concept of chemical bond. His contribution to chemistry was so important that he was awarded the Nobel price in 1913, becoming thereby the first inorganic chemist to receive it.

The theory of Werner put the first principles for a general explanation of the behavior of transition metal complexes. Afterwards, more theories have been developed, although the most important were done in the 1930's. In spite of this, they have been applied during different periods along this century. The first one, the Valence Bond theory (VBT) developed by Linus Pauling,[7] was mainly used from the 1930's, becoming less important in the 1960's. The second one, the Crystal Field Theory (CFT), was developed by Bethe[8] and Van Vleck[9] although not largely applied until the 1960's. The third one, the Molecular Orbital Theory (MO), was initially developed by D. R. Hartree[10] and V. Fock,[11] and later popularized by Roald Hoffmann[12] in the 1970's, being now the most extensively used. In fact, most of the ab initio procedures nowadays utilized, are based on this MO theory.

These theories have been allowed a better understanding of the structure and reaction mechanisms where transition metal complexes are involved. As far as structure is concerned, transition metal complexes present a large structural diversity. They have several coordination numbers and different geometries associated with each coordination number. Moreover, there are various types of bonds among the metal center and the ligands, depending on their nature.

As far as reactivity is concerned, there are two leading types of reactions. They are the ligand substitution and the reduction-oxidation. In spite of this, not all processes can be labeled with only one reaction type, and there are examples where the two types are involved. A chiefly characteristic of transition metal complexes reactivity, is the power of these compounds to act as catalysts in a very wide variety of chemical reactions. The impact of catalysis on a number of chemical processes, and on industrial technology, has grown substantially in the past thirty five years. This is the main reason why nowadays they are very important in chemistry.

Another important utility of transition metal complexes arises from their use in biochemical reactions. In biological systems catalysts are called enzymes. More than half of all

enzymes have metal ions in their structure; these are called metalloenzymes. In many cases, the metals are essential to the action of the enzyme, and are often at the active site where the substrate is bound.

In summary, as has been commented above, transition metal complexes are very important compounds in chemistry, and in life itself. Their importance arises mostly from their ability to make a diverse number of chemical bonds. Main-group elements are able to form from one to four chemical bonds around one atom center, while transition metal atoms are able to form from one to nine chemical bonds. This special ability of transition metal atoms to make so many bonds is due to the participation of the *d* orbitals in the valence shell. In the case of the main-group elements, the valence shell orbitals are formed by the *ns* and *np* orbitals. For transition elements, apart from the *ns* and *np* orbitals, the *(n-1)d* orbitals take also part in the valence shell. So, it is easy to guess that they will be able to lead up to a great number of different molecules.

1.1.2 Structure

The structure assignment of transition metal complexes has always been a difficult problem for inorganic chemists. Nowadays there are several physical methods to resolve the structure of a complex, although the better and most commonly used is the X-ray diffraction. On the other hand, theoretical methods are also becoming a powerful tool to solve the structure of this kind of compounds.

The structure of transition metal complexes is determined by the nature of the metal center, and the nature of their ligands. Thus, there are complexes with the same ligands in their coordination sphere but different metal center leading to a change in their geometric structure. For instance, the $[Co(Cl)_4]^{2-}$ and $[Pd(Cl)_4]^{2-}$ complexes have four chloride ligands, but in the first case the geometry is tetrahedral, while in the second one is square planar. There are also complexes with the same metal center and the same number of ligands, the geometry dependign of the nature of the ligands. This is the case of the $Ni(CO)_4$ and $[Ni(CN)_4]^{2-}$ complexes. The first one is tetrahedral, and the second one is square planar. Therefore, it is easy to guess how complicated can become the prediction of the geometry of a given transition metal complex.

The different factors which depend the structure of transition metal complexes, can be summarized as:

- nature of the metal atom

- metal-ligand interactions
- ligand-ligand interactions

There are no rules to exactly predict the structure of a complex. In spite of this, the analysis of the different factors on which the structure depends, can be very fruitful in order to try to predict a geometric structure.

Next three subsections are focused in the description of each of these factors. Last subsection is dedicated to describe more extensively the agostic interactions. This is a particular case where all these factors can be analyzed.

1.1.2.1 The Nature of the Metal Atom

The geometry of a transition metal complex is intimately related with the electronic configuration of the metal atom. Thus, the arrangement of the ligands around the metal center is affected by the number of valence electrons on the metal. In turns, the electronic configuration is intimately related with the oxidation state of the metal atom. The concept of oxidation state is arbitrary and the assignment of appropriate oxidation states is often a mere matter of convenience. Nevertheless, oxidation states are useful, and as such, are commonly used by chemists working on transition metal chemistry. The assignment of an oxidation state implies the assignment of the number of electrons that the metal atom has in its d shell. The metal atom can lose its valence electrons, becoming its electronic configuration d^0, as in OsO_4 or $[TiF_6]^{2-}$ complexes, or they can have a full d shell, being thus d^{10} as in $[Ag(NH_3)_2]^+$ or $[Au(CN)_2]^-$ complexes.

The most obvious structural characteristic of a complex is probably its coordination number. The coordination number is the number of coordination sites occupied by the ligands. In general, the coordination numbers of metal ions range from 1, as in Na^+ Cl^- ion pairs in gas phase, to 12 as in the solid crystal lattice of perovskite. Nevertheless, the lowest and highest coordination numbers found in transition metal compounds are 2 and 9, respectively, with the intermediate number 6 being the most important, followed by number 4. The fact that the maximum coordination number is 9 can be readily explained because the metal ion has 9 valence orbitals. In most cases the coordination number is less than 9, because some of the metal 9 orbitals are either lone pairs or engaged in back bonding. This fact is also the origin of the well known 18 electrons rule. This rule says that the metal atom can not have more than 18 valence electrons.

This is just due to the metal atom only has 9 valence orbitals.

Few complex ions are known with coordination number 2. They are generally limited to the +1 ions of the Group 11 metals and the closely related Hg(II) species. The geometry of this coordination number is generally linear. Coordination number 3 is a rare one. Many compounds which might appear to be 3-coordinate as judged from their stoichiometry are found upon examination to have a higher coordination number. The usual geometry is an equilateral triangle with the metal atom at the center. Coordination number 4 occupies an important place in coordination chemistry. The structures formed can be conveniently divided into tetrahedral and square planar forms, although intermediate and distorted structures are known. In the past a coordination number 5 was considered almost as rare as coordination number 3, but the number of known compounds has increased rapidly in recent years. Their structures range from perfect trigonal bipyramids to perfect square pyramids with various degrees of intermediacy. Coordination number 6 is by far the most common. The most common structure for this coordination number is the octahedron. Two forms of distortion of octahedral complexes are of some importance. The first is the tetragonal distortion, either elongation or compression along one of the fourfold rotational axes of the octahedron. The second major distortion, the trigonal distortion, consists in either elongation or compression along one of the four threefold rotational axes of the octahedron. This second type of distortion, taken to the limit would lead to a trigonal antiprism. The bicapped tetrahedron is also found in 6 coordination number. Coordination numbers above 6 are uncommon. For coordination 7 there are three distinct geometries known: pentagonal bipyramid, capped octahedron, and a capped trigonal prism. There are several coordination polyhedra available for 8-coordination. The most regular, the cube, is not found in discrete complexes but occurs only in lattices. The two usual structures are the square antiprism and the dodecahedron. Other geometries as bicapped octahedron are also known. Discrete 9-coordinate structures are known for several complexes. The most common structure is obtained by adding a ligand to each of the rectangular faces of a trigonal prism.

Transition metal complexes also present isomerism. There are compounds with the same chemical formula, but with very different structure (structural isomerism). This is the case of the $[Co(NH_3)_4Cl_2]NO_2$ and $[Co(NH_3)_4(Cl)(NO_2)]Cl$ complexes. Besides the structural isomers, there are other cases where the difference is only in the spatial arrangement. These are still called often geometrical isomerism, but the more modern designation should be stereoisomerism. The most

typical example are the cis and trans isomers of the square planar geometries. There is also optical isomerism in some species.

1.1.2.2 Metal-Ligand Interaction

Metal-ligand interactions have a crucial weight in the structure of transition metal complexes. Thus, the nature of the ligand has a decisive influence on the degree of splitting of the metal orbitals, and therefore on its ability to form low or high spin species. Different ligands cause different degrees of splitting. In general it is possible to list ligands in order of increasing field strength in a spectrochemical series.[13] Although it is not possible to form a complete spectrochemical series of all ligands with one metal ion, it is possible to construct one from overlapping sequences. The result is that the presence of empty π orbitals in the ligand able to receive back-bonding from the metal produces an increase of the splitting, while ligands with the presence of occupied π orbitals produce a decrease of the splitting on the d orbitals.

Bonding interactions between metals and ligands have been a controversial matter since transition metal complexes were discovered. The bond with the metal center is done by a lot of different kind of ligands, leading thus to very different types of bonds. Thus, it is convenient to do a general classification of the ligand-metal bonds, attending to their main characteristics.

The main type of interaction between a ligand and a metal is usually electron donation from the ligand to the metal. Although the back-donation interaction is also important, it comes usually accompanying the main donation interaction. Ligands can be classified according to the origin of the electrons they donate in three different classes.[14] The first one is formed by ligands that use one lone pair of electrons to bind to the metal center. Typical examples would be ammonia or phosphine. This is the most typical kind of ligands, and were the first to be discovered. The second class is constituted by ligands that donate electrons from one of its π-bonds. The archetype of this kind of ligands would be ethylene. The third class of ligands are those that coordinate to the metal by donation of electrons from one of its σ bonds. This third kind of ligands is the most recently discovered and will be briefly discussed in the next paragraph.

The first transition metal complex where a ligand uses σ-electron density to bind with the metal center was the Kubas complex.[15] In 1984 the neutron diffraction technique allowed to solve the structure of the $W(CO)_3(P\text{-}i\text{-}Pr_3)_2H_2$ complex. In this complex a hydrogen molecule binds to the metal without breaking of the H-H bond. It was the beginning of a new type of compounds

with a different bonding kind between a metal and a ligand.[16] In a similar way, in agostic interactions there is a covalent interaction between a metal center and electron density from a σ C-H bond. Agostic interactions will be discussed in detail later in this same section.

1.1.2.3 Ligand-Ligand Interactions

Usually, interactions among ligands in transition metal complexes are considered less important compared with metal-ligand interactions to decide their structures. In spite of this, sometimes these interactions become the most important ones to decide the arrangement of the ligands around the metal center. Normally, the most important ligand-ligand interactions considered are the steric hindrance, and the chelate effect.

As far as the chelating ligands is concerned, they classified in several types. A ligand capable of occupying only one position in the inner coordination sphere and forming one bond to the central atom is called a monodentate ligand. When a ligand is capable of bonding to the central atom in two places, it is said to be bidentate. When a ligand is bound to the metal center by three places is called tridentate, by four places tetradentate, and so on. Ligands that have up to six coordinating groups are known. Because the two bonds from a bidentate ligand appear to enclose the metal atom in a pincerlike structure, the resulting compound is known as a chelate (Greek, "chele" for "claw").

The most important property of the polidentate ligands comes from their higher stability than the monodentate ones. This extra stability is termed the "chelate effect". The chief factor of this stability arises from the entropy factor when monodentate ligands are substituted by polidentate ones. A simple manner to illustrate this effect is by means of an example. For instance, the difference in dissociation energy between ethylenediamine complexes and ammonia complexes, where the electronic effects of ethylenediamine and ammonia are practically identical. If a molecule of ammonia dissociates from the complex, it is quickly swept off into the solution and the probability of its returning to its former site is remote. On the other hand, if one of the amino groups of ethylenediamine dissociates from a complex it is retained by the other end still attached to the metal. Thus, the complex has a smaller probability of dissociating and is therefore experimentally found to be more stable toward dissociation.

Taking the chelate effect out, ligand-ligand interactions in transition metal complexes are usually lumped together in the so-called steric effects. The term "steric effects" is one of the most

used terms among the chemical community. However, the concept is not defined very precisely, and in fact is defined in different ways by different authors.[17] In any case, the general idea is that steric effects are the interactions (repulsive and/or attractive) between bulky groups that are not far away each other in the space.

Perhaps, the best way to understand the nature of steric effects is by means of some examples. One example could be the cis-trans equilibrium in planar platinum(II) complexes such as those presented in scheme 1.1:[18]

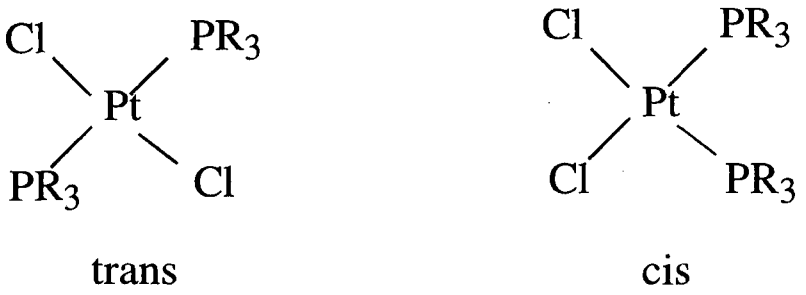

Scheme 1.1

Results from the study of this system show that in equilibrium the concentration of the trans isomer is larger than that of the cis isomer. Bond energies however, favors the cis isomer, as might be expected from simple π-bonding arguments. Increasing of steric hindrance from either increasing the size of the alkyl groups (R) on the phosphines or replacing the chloride ligand by iodide favors the trans isomer. This is thus a case where the relative stability between two isomers is affected by the steric hindrance.

Another example can be found in some edge-sharing binuclear square planar complexes of d^8 transition metal atom.[19] These compounds are formed by two square planar units, which share two of their ligands (see scheme 1.2). Thus, they are able to adopt different conformations depending on the angle between the planes. In this way, this movement can be compared with the wings of a butterfly. In the particular case of the $[Pt_2(dppy)_4(\mu\text{-}S)_2]$ complex (dppy = 2-diphenylphosphanopyridine) experiment shows that the angle between the two square planar units is 180 degrees, being therefore strictly planar.[20] On other hand, theoretical ab initio studies on the $[Pt_2(PH_3)_4(\mu\text{-}S)_2]$ (cite 4 chem-com) complex,[21] show that the angle between the two square planar units is approximately 120 degrees. The main difference between these two complex is the

size of their ligands. The first one has much bulkier ligands than the second one. Thus, the reason for the change of the angle between the square planar units is attributed to the steric hindrance between the ligands.

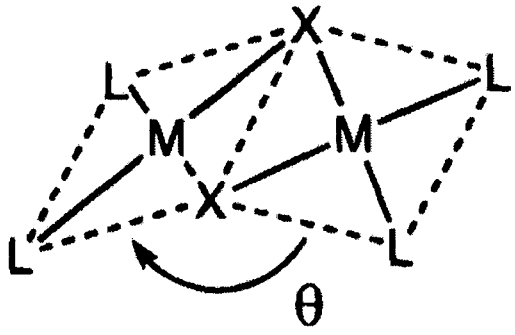

Scheme 1.2

As has been showed above, steric effects can decide the preference between two isomers (first example), or they can lead to a geometric distortion (second example). As a result, a transition metal complex can present a geometric structure with small ligands, and another one with bulkier ligands.

In fact, general trends in transition metal complexes show that coordination numbers lower than 4 use to be found with bulky ligands, where a larger coordination number would lead to prohibitive steric interference between the ligands. For example, the complex $Pt(PCy_3)_2$ can be isolated as such.

Sometimes it is difficult to say if a distortion is provoked by steric or electronic effects. In the particular complexes studied in this thesis some geometrical distortions were analyzed. Distortions that had originally been attributed to electronic effects, are proved here to be caused by steric hindrances. In particular, the complexes studied are $Os(H)_2(Cl)_2(P\text{-}i\text{-}Pr_3)_2$, $Ir(H)_2(Cl)(P\text{-}i\text{-}Bu_2Ph)_2$, and $[Ir(biph)(X)(QR_3)_2]$ (biph=biphenyl-2,2'-diyl, Q=P, As, and X= Cl, I). This will be discussed in detail in the next chapter.

1.1.2.4 An Interesting Case: Agostic Interactions

The study of agostic interactions is a very interesting topic due to their importance in inorganic chemistry, and more concretely in organometallic chemistry. Moreover, there are several different effects taking place together in complexes with this kind of interactions. On one

hand, the chelat effect, giving thus an extra stability. On other hand, the nature of the metal center and its oxidation state are also important, since an empty orbital from the metal center is needed for this interaction. Moreover, steric effects can play a very important role, as will be proved in one of the complexes studied in this work. In that way, this kind of interactions provide a challenge for theoretical study.

The bond between the metal center and the ligand in the agostic interactions belongs to the third bonding type commented above. In this interaction, a X-Y σ-bonding electron pair acts as a 2-electron donor to give an (X-Y)-M type complex. The most typical cases of agostic interactions are those where the X-Y group is a C-H group. These kind of interaction are becoming very usual in transition metal complexes, and they have not only been found in the ground state but also in the transition states of many important organometallic transformations such as Ziegler-Natta catalysis[22] and sigma bond metathesis.[23]

1.1.2.4.1 The Nature of the Agostic Bonding

Carbon-hydrogen bonds, especially those of saturate carbon (sp^3) centers, normally are considered chemically inert. Nevertheless, experimental evidences have been found to show an interaction between metal centers and the C-H bond.[24] This kind of interaction are commonly considered as three center two electrons (3c-2e) bond. Thus, important effects to the structure and reactivity are found in complexes which present this interaction.

The "agostic" term* was initially used for intramolecular covalent interactions between the metal center and the C-H group. Nowadays, this term is used to design any interaction between a σ bond which belongs to a ligand already bonded to the metal center and the metal center.[25] Nevertheless, this terminology is not clear in the literature, and it is very often confused. In fact, agostic interaction and agostic distortion have not the same meaning. Agostic interactions occur when there is a covalent interaction between the metal center and a σ bond. In contrast, agostic distortion is a more general expression. It describes the fact that a σ bond is brought to the metal center, but a covalent interaction between this σ bond and the metal center is not necessary. A graphic explanation is showed in figure 1.1.

---

* The agostic term is derived from the Greek word *αγοστοσ* . which may be translated as to clasp, to draw towards, to hold to oneself. [Homer, "*The Iliad*", 11.425 etc., D. B. Monro and T.W. Allen, Eds., Oxford, 3rd Ed. (1920), often reprinted.]

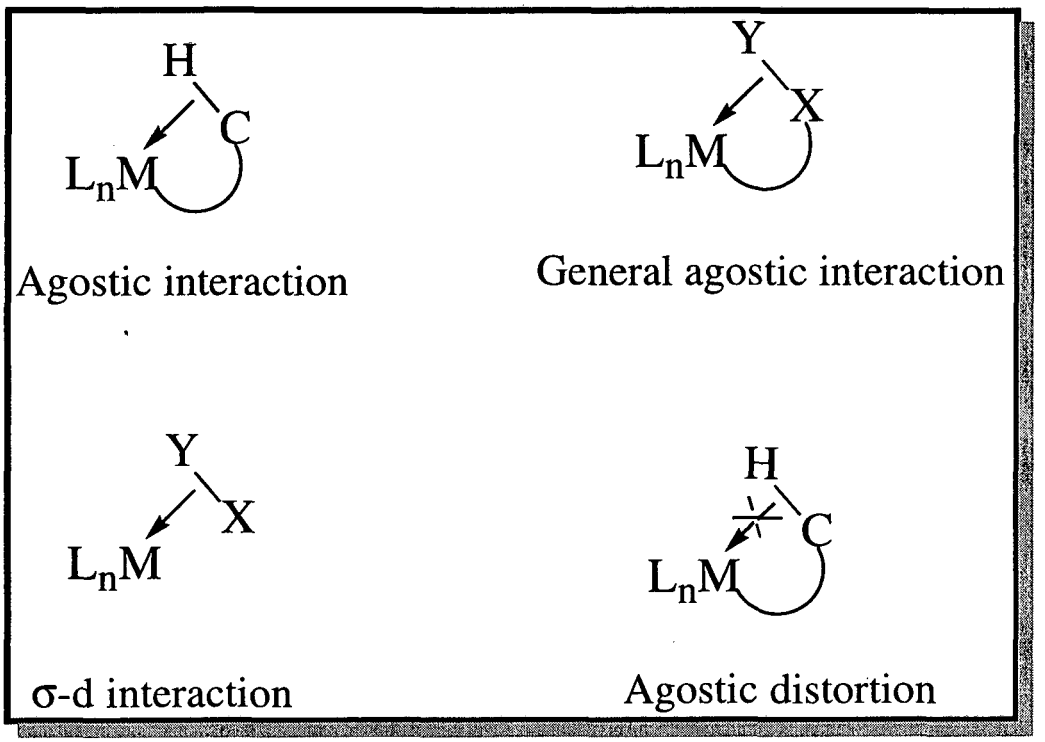

Figure 1.1 Difference between agostic interaction and agostic distortion.

The discovery of compounds with short distances between the metal center and C-H bonds made suspect that there were some interaction among these centers. In 1965 Mason et al.[26] synthesized the $PdI_2(PMe_2Ph)_2$ and $RuCl_2(PPh_3)_3$ compounds, and they found that the orto hydrogen of the aryl-phosphine was very close to the metal center. The characterization in 1978 of the $[Fe(n - C_8H_{13})\{P(OMe)_3\}_3]^+$ complex by neutron diffraction was the first experimental evidence of an agostic interaction.[27,28] The ab initio study in 1984 of the $TiEtCl_3(dmpe)$ complex was the first theoretical evidence of an agostic interaction.[29]

The metal center has to have an empty d orbital to receipt electron density from the C-H bond. This orbital has to be a good acceptor, and its energy and spatial orientation have to be appropriate to interact as much as possible with C-H. Therefore, it is necessary an electron deficiency in the metal center to lead up an agostic interaction.

When the 18 electrons rule is applied, it can be observed that agostic interactions are found in complexes with less than 18 electrons. However, early EH (Extended Hückel) studies showed that electron deficiency in the metal center is not sufficient by itself to give rise to interaction.[30,31] It has been also noticed that agostic interactions with β or γ electrons are

relatively easy when they are not very hindered by steric effects.

From an orbitalary point of view, an agostic interaction is considered as a sum of two effects. The first and more important is the donation from the σ C-H bond to an empty d orbital of the metal. The second interaction, although less important, is the back-donation from a full d orbital from the metal (with π symmetry respect to the bond) to the antibonding σ* C-H orbital. These two interactions are depicted in figure 1.2.

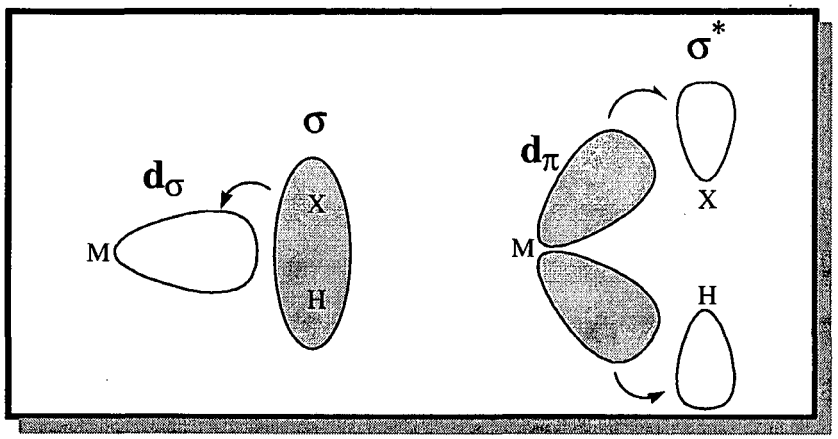

Figure 1.2 Orbitals involved in the agostic interaction. (Occupied orbitals dark, empty orbitals blank).

1.1.2.4.2 Characterization and Classification

The leading structural characteristic of the agostic interactions are the C-H and M-H distances. These distances are very difficult to obtain, since the neutron diffraction technique has to be utilized to locate the hydrogen atom. Results obtained by X-ray diffraction to the position of the hydrogen atoms are only indicative. At this point, theoretical calculation can be very useful, since it is able to locate the hydrogen atom, besides the usual theoretical analysis. Apart from these techniques where the location of the hydrogen atom is direct, there are some other indirect techniques to point out this kind of interaction. They are mostly the spectroscopic techniques.

The most useful spectroscopic technique for detecting the presence of M-H-C systems in compounds is Nuclear Magnetic Resonance (NMR). Where spectra of static agostic systems can be obtained, the ^{1}H and ^{13}C chemical shifts, and in particular J(C-H) values can be used with confidence to assign agostic structures. The most characteristic feature of a M-H-C agostic interaction is the low value of J(C-H) due to the reduced C-H bond order in the three centers two electrons (3c-2e) system and the resulting elongated C-H bond. Typical values for J(C-H) are in

the range of 60-90 Hz. These values are significantly lower than those expected for normal $C(sp^3)$-H bonds (120-130 Hz) in a saturated structure. Conversely, they are much higher than expected for a classical C-M-H alkyl hydride system, where the J(C-H) value is normally less than 10 Hz.

The chemical shift of agostic hydrogens in C-H-M systems for d^n, $n > 0$, metal centers normally occur at high fields [$\delta(h) < 0$ ppm and up to – 16 ppm] and occur in the range typical for normal terminal metal hydride. For this reason, care must be exercised in interpreting these values; there are several examples in the early literature where such high-field shifts led to incorrect assignments of agostic structure as classical (normally olefin-hydride) structures. For d^0 systems, resonances due to the agostic hydrogens normally do not occur at higher fields than 0 ppm.

As far as reactivity is concerned, the most usual characteristics are: (a) the C-H group, as a weak ligand, can be substituted by better donor ligands; (b) in the system M-C-H, the metal center is "electrophylic" leading to a more acid character of the hydrogen in the C-H group.

The number of compounds where an agostic interaction has been proposed has largely increased in recent years. Thus, it is important to have a classification of the compounds that present an agostic interaction, in order to understand and to rationalize their behavior. One of the different classifications found in the Literature, and maybe the most appropriate, is that done by Brookhart, Green and Wong.[24]

In this classification, agostic interactions are divided in four large groups, depending on the nature of the ligand where the interaction is found:

A. Agostic compounds of alkyl ligands.

The ligand is an alkyl group, and the interaction can be done by any C-H bond of the ligand. In that way, this group can be subdivided in α-agostic, β-agostic, etc.

B. Agostic compound of alkylidenes.

Now, the ligand is an alkylidene ($M=CH_\alpha R$) and the interaction is found with the H_α. A set of these kind of compounds has been synthesized by Schrock et al.[32]

C. Agostic compounds of unsaturated hydrocarbon ligand.

In this kind of compounds, the π system of the ligand is used to form the bond with the metal. Moreover, the agostic interaction is done by a C-H group which is close to the π system.

D. Remote M-H-C Bond.

In this kind of compounds, the agostic interaction is done by a C-H group which is located very far away in the ligand chain from the part of the ligand that is directly bonded to the metal.

Agostic interactions have been more extensively explained here because some particular transition metal complexes with this kind of interactions have been studied in this thesis. This compounds are $[Ir(H)_2(PPh_2{}^tBu)_2]^+$, where the agostic interactions are very related with steric effects, and the complexes $Mo(COR)(S_2X)(PPh_3)_2$ (R=CH_3, H, CH_2SiH_3 and X=CNH_2, $C(OH)(PH_3)$), where the agostic interactions are the main reason of the geometry distortion in these compounds. This will be discussed in detail in the next chapter.

1.1.3 Reactivity

Reactivity of transition metal complexes is a very important, and at the same time, very difficult field in inorganic chemistry. Its importance emerges from its application to several topics in chemistry, biochemistry, geochemistry, ..., in science in general. Great efforts have been invested in its understanding. In this concern, the joint use of experimental work and theoretical developments has been very useful. Nevertheless, the full understanding of the reaction mechanism of a process involving a transition metal complex requires still a large volume of work. This work presents our small contribution to the advance in the understanding of some particular processes.

The application of transition metal complexes in catalysis, and more specifically in asymmetric catalysis, is one of the most active research topics in chemistry. The importance and practical use of asymmetric synthesis as a tool to obtain enantiomerically pure or enriched compounds has been fully acknowledged by chemists in synthetic organic chemistry, medicinal chemistry, agricultural chemistry, natural products chemistry, the pharmaceutical industries, and the agricultural industries.[33] This prominence is due to the explosive development of newer and more efficient methods during the last decade. In that sense, asymmetric dihydroxylation of olefins

is one of the most vigorously catalytic asymmetric reactions studied at this moment.[34]

1.1.3.1 Reaction Mechanisms

The reactivity of transition metal complexes is normally separated in two leading types,[35] although sometimes they are very related. The first one is the ligand substitution reaction. In this kind of reactions, metal oxidation state is kept constant while the metal center coordination is changed through the process. The second one is the reduction-oxidation reaction. In this kind of reactions electrons are transferred between the metal and the ligands or between two metals, while the metal coordination is not modified. Nevertheless, as usual when classifications are done in chemistry, there is not a clear limit between them, and in a large number of cases these two processes take place together.

As far as substitution reactions are concerned, there are three different established mechanisms: dissociative, associative and interchange. In the first one, the mechanism goes through an intermediate where the coordination number of the metal center is less than the coordination number in the reactant. In the second one, the intermediate has a larger number of coordination than the reactant. In the third class, there is no intermediate, and the entry of a new ligand is simultaneous with the departure of an old one.

A term related with the substitution reaction is lability. Lability is the capacity of a complex ion to undergo a substitution reaction of one or more of its ligands. Those complexes where the substitution reactions are fast are called labile, while those complexes where the process is slow, or does not occur, are labeled inert. It is important to underline that the term is mostly kinetic, referred to the reaction rate, and must not be confused with the concept of stability, which relates to the thermodynamic state of equilibrium. In other words, there is no direct relationship between the thermodynamic stability of a complex and its lability.

As far as the reduction-oxidation reactions of transition metal complexes are concerned, there are two types. In the first type, called the outer sphere mechanism, the coordination of the metal center is not altered. In general, the rate of the redox reaction is faster than that of the exchange of the ligands, so one may consider the reaction to be a simple electron transfer from one stable complex to another. In the second mechanism, called the inner sphere mechanism, a ligand is intimately involved in the transfer of the electron from one metal to another. Normally it consists in a transfer of the ligand from one complex to another, which decrease the oxidation

state of the former and increase that of the latter.

Apart from these two types of reactions, there are several reactions where these two processes (substitution and redox reaction) take place together. These reactions are commonly labeled as oxidative addition and reductive elimination.

Despite extensive study, inorganic chemistry has yet to achieve the understanding of reaction mechanisms enjoyed by organic chemistry. Substitution reactions usually too fast, or too slow, to be studied by conventional physical methods. Moreover, substitution at a coordinate metal center (with coordination number eventually as large as 8) has many more stereochemical possibilities than the substitution at a tetrahedral carbon atom. Specific problems exist also with electron transfer reactions.

The lack of understanding of mechanisms carries over into synthesis. Occasionally, synthetic "tricks" are discovered that allow the synthesis of a desired compound or isomer without interference from an undesired one. Only in rare cases predictions can be made about a wide variety of complexes involving different ligands. In that sense, theoretical methods can provide a powerful tool to help to understand transition metal complexes reaction mechanisms.

Until here, general reactivity of transition metal complexes has been briefly described. However, one of the main reasons of its importance comes from their power to catalyze a very wide variety of chemical reactions. Lability and redox properties make them privileged systems to act as catalysts. Because of that, the impact of transition metal complexes as catalysts on a great number of chemical reactions, including some of industrial relevance, has grown largely in the past thirty-five years. New knowledge regarding structure and reactivity of this kind of compounds has created new catalytic processes or has improved the efficiency of old ones. Thus, next subsection is dedicated to this special topic.

1.1.3.2 Catalysis

The power of transition metal complexes to act as catalysts, has been shown in a large number of valuable chemical reactions. For instance, the ethylene polymerization by the Ziegler-Natta catalyst[22] (an aluminum-titanium complex in its first generation), or the alkene hydrogenation by the Wilkinson catalysts[36] (a rhodium complex).

The effect of a catalyst is to change the rate of conversion of a substrate into products in some reaction. So, they act increasing the reaction rate, or reducing the reaction rate. In the first

case they are labeled *catalysts*,* and in the second case they are labeled *inhibitors*. Normally, the reactant (called substrate) for the reaction binds to the metal complex which serves as catalyst. The metal then brings about the rearrangement and the product dissociates, leaving the metal fragment free to bind a new molecule of substrate and go around the catalytic cycle again and again. It is this feature of a catalyst that distinguishes it from a simple reagent: a mole of catalyst converts many moles of substrate into products.

Depending on the nature of the catalyst, there are different kinds of catalysis. Homogeneous catalysis takes place when the catalyst and substrates for the reaction are in the same phase. In heterogeneous catalysis, the catalysis takes place in a phase boundary or at the surface of a solid. Finally, one must mention catalysis in biological systems, in which case the catalysts are called enzymes. All these different kind of catalysis are very important and interesting.

Transition metal complexes act usually as catalysts in the same phase that the substrate. It is usually in dissolution, although it can also be in catalytic enzyme site. A general classification of the mode how transition metal complexes begin the catalytic cycle, is the following:

- Coordination of the reaction partners to a transition metal brings them into close proximity (Ex. cyclooligomerization of alkynes).

- Through coordination to a transition metal, a reaction partner becomes activated for subsequent reactions. (Ex. hydrogenation of alkenes).

- Coordination of an organic substrate to a transition metal facilitates nucleophilic attack. (Ex. $PdCl_2$-catalyzed oxidation of ethylene to acetaldehyde).

- Through interaction with other ligand(s), a reaction partner becomes activated for subsequent reactions. (Ex. dihydroxylation of alkenes)

It is not very easy to guess which of these different reaction mechanisms is taking place. Because of that, a lot of experiments and theoretical work are being carried out to determine reaction mechanisms.

1.1.3.3 A Particular Case: Osmium Catalyzed Dihydroxylation of Olefins

* The word catalyst was suggested by Berzelius in 1835 to note substances which accelerate the reaction rate. The root of the term comes from two Greek words; "kata", which means down, complete, and "lysis", which means rupture.

Among enantioselective reactions, the oxidation of olefins with osmium tetraoxide is probably both the most general and most selective organic reaction known to date: osmium tetraoxide reacts with almost all olefins, it is an extremely mild oxidizing agent, and it tolerates almost every other organic functional groups.

In 1936 Rudolf Criegee, in his pioneering work on the stoichometric reaction of OsO_4 with olefins, showed that pyridine accelerates the reaction considerably.[37] However, cost considerations make the stoichiometric osmylation uneconomical. Not surprisingly, catalytic variants of the reaction, which employ relatively inexpensive reagents for the reoxidation of the osmium(VI) glycolate products, greatly enhance its synthetic utility.[38,39] Inorganic cooxidants, such as sodium or potassium chlorate or hydrogen peroxide,[40] were the first to be introduced, but in some cases these reagents lead to diminished yields due to over-oxidation. Better results are obtained with others cooxidants.[41,42,43]

Once OsO_4 was shown as a good catalyst for dihydroxylation, there were several attempts to introduce asymmetry in the reaction. Initial efforts to induce enantioselectivity in the osmylation with chiral pyridine derivatives failed due to the low affinity of these ligands for OsO_4. It was found that the binding constant of a ligand is extremely sensitive to the steric hindrance near the reacting center. Consequently, quinuclidine derivatives were used instead of pyridines for further investigations due to their intrinsically higher affinity for OsO_4.[44] (cite 17revS) This logic proved correct, and in 1980 it allowed Sharpless et al.[45] succeeded in isolating diols with moderate to good enantiomeric excesses using acetate esters of cinchona alkaloids as chiral ligands. From their studies, they found that the better alkaloid was a bis-cinchona ligand, more concretely the $(DHQD)_2PHAL$ ligand.[46] Later on, Corey and coworkers[47] found practically the same yields with $(DHQD)_2PYDZ$ ligand (another bis-cinchona). In fact, these two systems are very similar as can be seen in figure 1.3.

Cinchona alkaloids are the best ligands found to date to induce enantioselectivity in the osmium dihydroxylation of olefins. Besides, there are also a few other catalytic systems leading to good yields. The most important are probably a monodentate 1,4-diazabicyclo[2.2.2]octane, or some chiral isoazolidines.[48] More recent methods employ chiral diamine ligands for the asymmetric osmylation of olefins.[49] Despite the good to excellent enantioselectivities that can be obtained with them, a serious drawback results from their bidentate nature. They form very stable chelate complexes with the osmium(VI) glycolate products and this leads to inhibition of

hydrolysis. As a consequence, in situ recycling of the osmium and the ligand cannot be achieved. Thus, all the reactions involving bidentate ligands are stoichiometric in both OsO_4 and the chiral ligand.

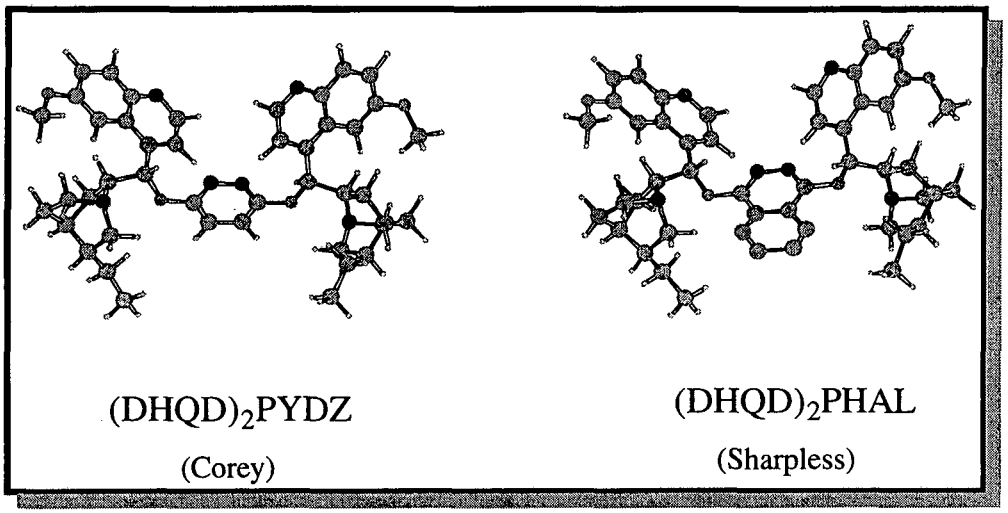

Figure 1.3 Alkaloids ligands (bis-cinchona) used by Corey and Sharpless in the asymmetric dihydroxylation of olefins.

The osmium-catalyzed dihydroxylation reaction has been the center of extensive mechanistic investigation, and two different mechanisms have been suggested: Böseken[50] and Criegee[37] originally proposed a concerted [3+2] pathway, while Sharpless et al. suggested a stepwise reaction which is initiated by a [2+2]-like addition of the olefin across an Os=O bond, followed by rearrangement of the resulting osmaoxetane intermediate to the glycolate product.[51,34] In the case that bis-cinchona alkaloids are used as osmium ligands to induce an asymmetric dihydroxylation, a modified version of the [3+2] mechanism is proposed by Corey and Noe, called as CCN (for Criegee-Corey-Noe) model.[52,53] It supposes the existence of an olefin-OsO_4·(bis-cinchona) complex before the concerted [3+2] pathway.

Initially, the accepted "textbook mechanism" was the concerted [3+2] mechanism proposed by Criegee, where a direct interaction between the two carbons of the double bond and two oxygens from the oxide is present from the initial step. Later on, after an extensive study on different oxo metal compounds as OsO_4, MnO_4^- or CrO_2X_2, Sharpless and coworkers suggested a stepwise [2+2] process in 1977.[23] This mechanism proposes an olefin addition to the M=O bond. Thus, it introduces the existence of an organometallic "intermediate" where one of the carbons is bonded to the metal, and the other is bonded to the oxygen. Most mechanistic investigations

have been carried out using OsO_4 with bis-cinchona alkaloids as ligands, since it is the best catalyst for the enantioselective reaction. In the case of the OsO4•(bis-cinchona) catalyst and styrene, the intermediate proposed by Sharpless and coworkers is depicted in figure 1.4.

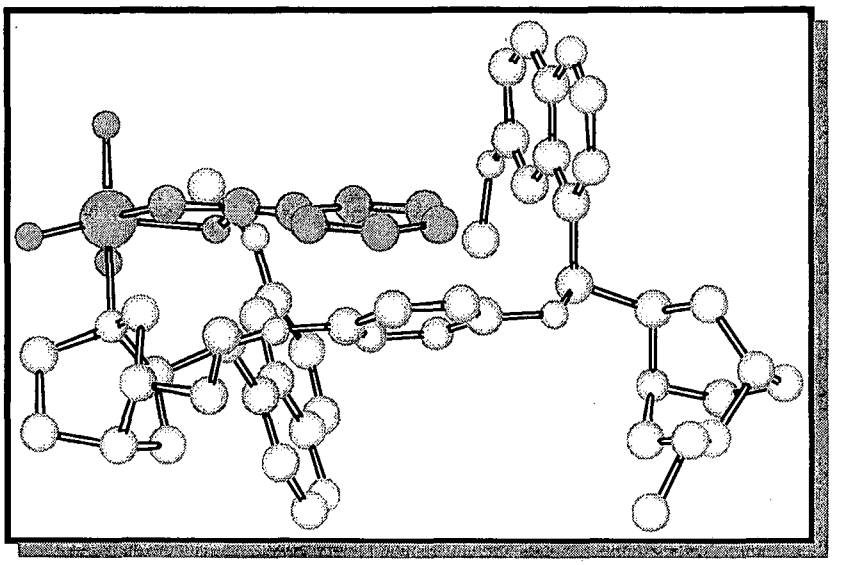

Figure 1.4 Intermediate for the asymmetric dihydroxylation of olefins proposed by Sharpless and coworkers. Styrene and OsO_4 subunit are depicted darker.

The proposal of an intermediate by Sharpless and coworkers is based on the temperature dependence of the enantioselectivity, shown by its Eyring plot.[54] The reaction proceeds via at least two different pairs of diastereomeric transition states. This results are not consistent with a concerted mechanism, and lead them to propose the [2+2] stepwise mechanism.

In contrast, kinetic investigations carried out by Corey and coworkers, led to them to argue in favor of the [3+2].[55,56] The major problem of this proposed mechanism arises from its incapacity to explain the non linearity in the Eyring-type diagrams. Corey et al. also propose the existence of an intermediate (in what becomes the CCN model),[23,23] but it is not the osmaoxetane proposed by Sharpless. The intermediate proposed by Corey is a complex with a donor-acceptor interaction between the π orbital of the olefin and a d orbital from the osmium, stabilized by attractive van der Waals interactions between the rest of the olefin and the U-shaped binding pocket formed by the alkaloid. A minimum motion from this intermediate leads to the [3+2] cycloaddition. This intermediate is depicted in figure 1.5.

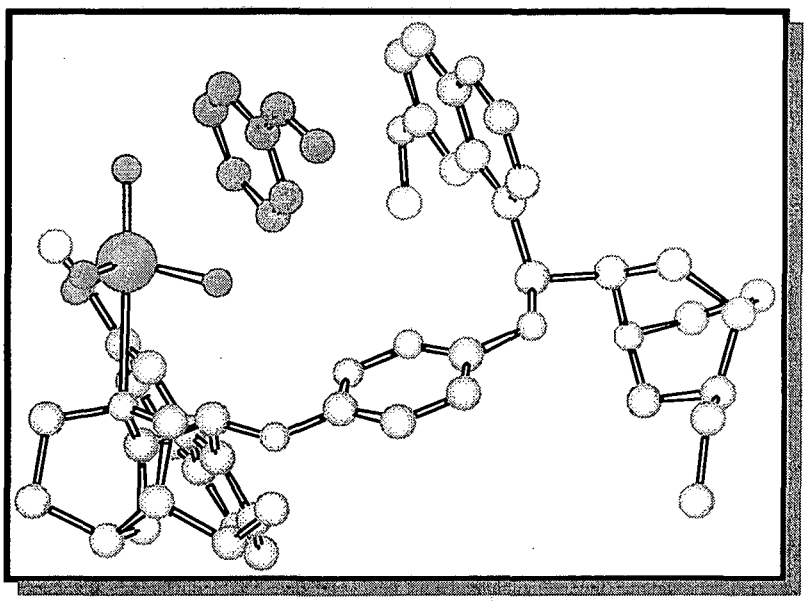

Figure 1.5 Intermediate for the asymmetric dihydroxylation of olefins proposed by Corey and Noe. Styrene and OsO_4 subunit are depicted darker.

The existence of intermediates is also supported by additional kinetic investigations.[56] The observation of Michaelis-Menten behavior on this reaction, which implies the intermediacy of a reversibly and rapidly formed olefin-catalyst complex, is presented as fully consistent with the [3+2] mechanism by Corey and coworkers.[56,53]

In summary, a lot of experimental works have been carried out in order to discern which is the real mechanism. In spite of that, experimental data does not allow to decide between them. All the kinetic observations could be explained by the two main proposals, being thus impossible to discard one of them. Early, theoretical studies with EH[57] or RHF[58] methods were also inconclusive. In this work we present our own quantum mechanic calculations on a model system, which was published simultaneously with other works and gives strong support to the [3+2] mechanism.[59],[60] We will also present a wider study on the real system (OsO4·(bis-cinchona) complex) using the IMOMM methodology.[61]

1.2 Theoretical Methods for the Study of Transition Metal Complexes

There is nowadays a wide and expanding variety of methods in computational chemistry, ranging from the very approximate to the very precise. Computer power has been growing steadily through the years, and it seems that it will not stop increasing in the foreseeable future. As a result an external observer could get the impression that performance of computations on any system at the highest computational level will be possible in a short time, and that one should not worry any more about the design of approximate methods. This situation is however far from reality.

The goal of the application of theoretical methods to chemical problems is obtention of information on molecular structure, stabilities, reactivities, electronic properties, etc. There are many theoretical models currently available to chemists. They range from the very simple to the very sophisticated. Available methods include molecular mechanics, extended Hückel, Austin Model (AM1), density functional, and large-scale computer intensive ab initio electronic structure procedures using extended basis sets and highly correlated electronic wave functions. Each of these methods has been successfully applied to chemical problems and each has its practical limitations. For example, ab initio electronic structure procedures can be applied to any combination of atoms because the model is not directly parameterized on experimental data, and hence does not require experimental input. But use of ab initio electronic structure procedures requires usually a lot of computer time, a great deal of disk space, and a significant amount of memory. This means that use of the model is restricted to systems with a few to several atoms. Molecular mechanics represents the other extreme of mathematic complexity. It requires several orders of magnitude less computational effort, so it can be used on large systems. The range of application of molecular mechanics methods is nevertheless more limited because of its close relationship to the validity of experimental data on which it is parameterized.

As an alternative to solve the chief problems of these methods, new methodologies are emerging which combine quantum mechanics with molecular mechanics. The idea of these new

methods, is to obtain results with a quality of pure quantum mechanics methods, and at the same time being able to study systems of a size that could be only achieved with pure molecular mechanics methods. Therefore, in an ideal case, these methodologies would take all the advantages from both quantum mechanics and molecular mechanics methods. The downside is of course that a careless use could bring together the disadvantages of both methods.

This section is divided in four subsections. First, a general introduction to the theory and theoretical aspects on transition metal compounds is given. Afterwards, the next two subsections deal with the two leading theoretical methods used on transition metal chemistry, ab initio and molecular mechanics. In the last subsection a more detailed explanation of the QM / MM methods is given, and more concretely of the IMOMM method, which has been especially designed to work with transition metal compounds, and that has been applied in most of the calculations of this doctoral thesis.

1.2.1 Historical Background

The modern study of coordination compounds begins main with two men, Alfred Werner and Sophus Mads Jorgensen. Both men were astute chemists, not only in the laboratory synthetic aspects but also in the area of interpretation and theory. As it turned out, they differed fundamentally in their interpretation of the phenomena they observed and thus acted as antagonists, each prompting the other to perform further experiments to augment the evidence for his point of view. From our viewpoint, a century later, we can conclude that Werner was "right" and Jorgensen was "wrong" in the interpretation of the experimental evidence they had, but a lot of work and theory development had to be done to achieve this conclusion.

Initially, two different theories were proposed to explain the "complex" behavior of these new compounds. The first one, was proposed in 1869 by Blomstrand, and defended later by Jorgensen. It was labeled the chain theory due to its similarity with the valence theories current in those days. Nevertheless, this theory was unable to accommodate all experimental data. Thus, in 1893 Alfred Werner proposed the coordination theory, providing a new concept on the chemical bond. This theory put the first principles for a general explanation of the behavior of transition metal complexes. Afterwards, newer and better theories have been developed to make possible a better explanation of these complexes, but Werner's theory played a very important role in this evolution.

The first successful application of bonding theory to coordination compounds was made by professor Linus Pauling.[7] It is usually referred as the Valence Bond Theory (VBT) of coordination compounds. His contribution to chemistry was so important, that he was awarded with the Nobel price in 1954. From the valence bond point of view, the formation of a complex is a reaction between a Lewis base (ligand) and a Lewis acid (metal or metal ion) with the formation of a coordinate covalent (or dative) bond between the ligand and the metal. Until about 40 years ago, the VBT was almost the only one applied to coordination compounds by chemists. Nowadays, few inorganic chemists use simple valence bond theory in discussions of transition metal complexes.

The crystal field theory (CFT) was developed by Bethe[8] and Van Vleck.[9] Its development was contemporary with that of Pauling's valence bond approach. Although used to some extent by physicists, it remained largely unknown to chemists until the 1950s. This theory is completely different from the VBT, because it rejects the covalent bond and supposes that the interaction among metal center and ligands is purely electrostatic. The CFT theory is not able to appropriate describe the bonds in the transition metal complexes. Hence, a modified version of this theory was developed trying to solve this problems. This theory has been called as ligand field theory (LFT). Thus, while in the CFT the electrons are forced to stay on the central transition metal ion, the LFT carries the CFT one step further: it generates molecular orbitals and allows the electrons on the transition metal ion to share these orbitals with a pair of electrons from each ligand.

Just as crystal field theory (and its modified version ligand field theory) largely replaced valence bond theory in treating coordination compounds, the latest is in turn being replaced by molecular orbital theory. This theory was also developed in the 1930's,[10,11] the major contribution being done by two brilliant theoreticians as D. R. Hartree and V. Fok. In spite of that, it was not commonly used in transition metal chemistry until the 1970's. The Molecular Orbital Theory is based on the extension to a molecule framework of the concepts obtained in solving the Schrödinger equation through the Hartree-Fok methods, which leads to atomic orbitals. Molecular orbitals are obtained by quantum mechanics, and this theory will be discussed in detail in the next subsection.

Apart from these theories which are principally concerned on the nature of bonding, another type of methodologies began to be developed in the 1940s. These are called molecular mechanics methods. Their principles are completely different from any of the others presented

above. They represent a molecule as a set of "balls" and "springs", neglecting thereby the effects associated to the behavior of electrons and nuclei as subatomic particles. Initially, these methods were designed to study organic systems, although since early they are also being applied to transition metal complexes. A more detailed explanation on these methods is the object of one of the following subsections.

Finally, methods which combine quantum mechanics and molecular mechanics are making a powerful entry in the field of computational transition metal compounds. These methods began to be developed at the end of the 1970's for application in others fields of chemistry, and their utilization in transition metal complexes has not started until this decade. The basic approach is the use of different methods to describe different parts of the same molecule. In the most common partition, the transition metal atom and its first coordination sphere are dealt at the quantum mechanics level, while the rest of each ligand is dealt at the molecular mechanics level.

1.2.2 Quantum Mechanics Methods

A large portion of the computational methods, and certainly the most accurate, rely on quantum mechanics (QM). Quantum chemistry has been very successful as a predictive tool in the study of small or medium size organic molecules, allowing the study of properties such as the ground state molecular geometries, conformational preferences, transition state geometries and energies, Born-Oppenheimer potential energy surfaces, reaction pathways and the rates of organic reaction.[62,63] At the same time, quantum chemistry has also been applied in the field of transition metal compounds and organometallic.[64,65,66] However, despite the greatly improved computational facilities and the availability of sophisticated quantum chemical calculations, the quantum chemistry of molecular systems containing heavy atoms appears to be less advanced.[64,66] On one hand, this is due to methodological problems arising in the treatment of heavy atoms and molecules containing them, such as the quasi-degeneracy of their lowest electronic states, relativistic effects, etc. On the other hand, there are also problems arising from the large size of the chemical systems, which make its study usually very demanding in terms of computational effort.

Electron correlation is necessary to obtain high accuracy in systems containing light atoms, but qualitatively accurate descriptions can already be obtained without electron correlation. In transition metal compounds, the correlation effects need to be considered even for a qualitative

description of the electronic structure. This is because the energy associated with electron correlation, although being a small fraction of the total energy, is comparable in magnitude with the energy cost of processes of chemical significance such as bond dissociation, activation, barriers of rotation, etc. Therefore, nowadays, it is generally accepted that the minimal approaches required in order to get reliable results require the introduction of dynamic correlation.[67,68]

Thus, when ab initio methods are used to study transition metal compounds, one has to go beyond the Hartree-Fock (HF)[10,11] approximation by using more sophisticate methods, such as post-Hartree-Fock methods [perturbational approach based on Moller-Plesset partition (MP),[69] multiconfigurational self-consistent (MCSCF) techniques,[70] configuration-interactions (CI)[71], or methods based on the Density Functional Theory (DFT) especially with gradient corrected [non-local functionals].[68,65,72]

To reduce computational effort in transition metal complexes calculations, one of the most common approximations is the use of the effective core potentials (ECP).[73,74,75,76] In this approximation, the core electrons are replaced by an effective one-electron potential. The ECP includes the Coulombic exchange and orthogonality interactions between the valence electrons and the core. They may be derived from atomic HF or Dirac-Fok (DF) wavefunctions by any of several methods, including direct inversion of a HF equation,[77] or direct optimization of parameters.[78]

As an alternative to ab initio methods to reduce computational effort, one can also mention semiempirical SCF MO procedures. Although electronic correlation is not introduced by these methods, they sometimes provide successful results. Many of the semiempirical SCF MO methods are modifications of the Pariser-Parr-Pople (PPP) scheme and contain various degrees of neglect of differential overlap (NDO). Along this line, attempts have been made to extend their applicability by including transition metal parameterization and introducing modern algorithms.[79,80,81] At this point it is worthy to note the extended Hückel molecular orbital (EHMO) approximation, popularized by Roald Hoffmann and his coworkers,[12,82] since it has been extensively used during the last 20 years. The EHMO theory, together with orbital interaction rules, frontier orbital theory and symmetry consideration, provided the experimentalists in coordination and organometallic chemistry with a very popular tool for the study of structure, dynamics and reactivity problems concerning chemically interesting molecular systems. Its popularity is mainly due to its low computational cost, and to the fact that its results are very easy

to interpret, presenting the clearest picture of how the electronic structure of small and large molecules varies with respect to the structure of the molecule.

Another important quantum chemical method of high quality, also applied in the field of transition metal compounds and organometallics, is the generalized valence bond (GVB) method proposed by Goddard.[83] GVB is a method based on the ideas of the old valence bond (VB) method which, uses the mathematical approach of MO methods.

In general, the evolution of "black-box" quantum chemical programs, coupled with the increasing performance of computer hardware, has resulted in a tremendously expanding role for ab initio techniques in different applications. However, in the investigations of large molecules, as common transition metal compounds, the ab inito methods are still computationally too expensive.[84] The costs grow sharply as the size of the system increases.

An approach that has been extensively applied to circumvent this problem is the use of model systems.[64,65,66] The calculation is not carried out on the real system but on a model system that has hopefully the same behavior. These model systems are obtained through simplification of the ligands of the system, usually in the regions further away from the metal center. For instance, the researcher interested in the $Pt(P(t\text{-}Bu)_3)_2$ system would compute instead the $Pt(PH_3)_2$ system, where the *tert*-butyl groups attached to phosphorus are replaced by hydrogen atoms. This strong approach is nevertheless very efficient in a number of cases. The reason for this efficiency is that the metal-ligand interaction remains well reproduced. In the example mentioned above, the $Pt\text{-}P(t\text{-}Bu)_3$ bond is not very different from the $Pt\text{-}PH_3$ bond, and because of that the electronic properties of the metal atom remain mostly unchanged. This approach is obviously not so good as far as the ligand-ligand interaction are concerned. Therefore, the challenge of studying problems where ligand-ligand interactions, essentially of steric nature, play an important role cannot be met by calculations on model systems.

The introduction of this ligand-ligand interaction, even at a less accurate level, would improve the description of the chemical system. This is precisely one of the main ideas of the hybrid quantum mechanics / molecular mechanics methods.

1.2.3 Molecular Mechanics Methods

Molecular mechanics can be considered also to arise from the Born-Oppenheimer approximation, which assumes that the motions of the nuclei of a molecule are independent of

the motion of the electrons. The approach of molecular mechanics is much more radical, assuming a simple empirical "ball-and-spring" model of molecular structure. Atoms (balls) are connected by springs (bonds) that can be stretched or compressed by intra- or intermolecular forces.[85] Hence, the basis of molecular mechanics is that a good estimate of the geometry of a molecule can be obtained by taking into account all the forces between the atoms, calculated using a mechanical approach. For example, bonded atoms are treated as if they are held together by forces that behave as mechanical springs, and non-bonded interactions are taken to be made up of attractive and repulsive forces that together produce the typical van der Waals curve. The parameters that define the strength of the springs or the steepness of the van der Waals curves are derived, in the first instance, from experimental observables such as infrared vibrational frequencies and gas compressibility data. However, the parameters are normally modified empirically to enhance the reproduction of experimentally determined values as geometries or thermodynamic stabilities. To optimize the geometry of a molecule, the total energy that arises from these forces or stresses, is minimized by computational methods. The minimized total energy is taken to be an indication of the strain present in the molecule. It is related to the molecule's potential energy and stability.

Some of the potential energy functions used to calculate the total strain energy of a molecule are similar to the functions used in the analysis of vibrational spectra. Because the parameters used to derive the strain energies from these functions are fitted quantities, which are based on experimental data (for example X-ray structures), molecular mechanics may be referred to as "empirical force field calculations" (more often the simplification "force field calculations" is used).[86] The quality of such calculations is strongly dependent on the reliability of potential energy functions and the corresponding parameters (the force field). Thus, the selection of experimental data to fit the force field is one of the most important steps in a molecular mechanics study. An empirical force field calculation is in essence a method where the structure and the strain energy of an unknown molecule are interpolated from a series of similar molecules with known structures and properties.

Over the past 50 years molecular mechanics has grown into a technique used extensively by chemists to quantify the role that steric strain plays in determining molecular structure, conformational structure, the energy differences between conformations of a molecule, and the binding interactions between molecules.[86]

Molecular mechanics treatment of transition metal compounds is complicated, by the partially filled d-orbitals of the metal ions that are responsible for the multifarious structures of coordination compounds with a large variety of possible coordination numbers and geometries.[87,88] There is a much larger variety of elements and binding modes than in organic chemistry, and much less examples of each class of compounds. The coordination geometry of a metal complex is always a compromise between the size and electronic structure of the metal center, and the type, size and geometry of the coordinated ligands. The fact that the ligand-metal-ligand angles vary over a much larger range than the corresponding parameters of organic molecules, as shown, for example, by the lower values of force constants determined from vibrational spectra, indicates that the competition between the ligand and the metal center in terms of coordination geometry is generally dictated by the ligand.[87] Moreover, the assumption that the nature of the bonding does not change with the structure may not be valid when there is π-bonding between the metal and the ligand or when there is an equilibrium between two spin-states with similar energies. In any case, the structure of a coordination compound, and therefore its thermodynamics, reactivity, and electronics, is strongly influenced by the ligand structure. One possible solution is the use of QM calculations on model systems to adjust the MM parameters involving the transition metal atom.[89,90] This approach can yield precise MM parameters, which can be used subsequently for extremely fast calculations. The downside is the that the parameterization process is very computer demanding, much more than that of a normal calculation on the model system, and that these parameters are valid for a very limited range of system. Coupling of the molecular mechanics method with quantum mechanical can provide a very powerful theoretical tool to study of chemical problems, and particularly to study transition metal complexes.

1.2.4 Quantum Mechanics / Molecular Mechanics (QM / MM) Methods

A logical answer to all the problems exposed above for the calculation of transition metal systems is the use of QM methods for the part of the molecule involving the metal, and of MM methods for the part removed from the metal. This is precisely the general idea of hybrid QM/MM methods.

Hybrid QM/MM methods have already a certain history of their own in computational chemistry.[91,92,93,94,95] Most work on this field has been on the introduction of solvation effects, with special focus on biochemical systems. A usual partition is to have the solvate computed at the QM level and the solvent molecules introduced at the MM level. If the solvate is composed exclusively of a few organic molecules, the QM part of the calculation can indeed be carried out very efficiently through the use semiempirical methods. As a result, hybrid QM/MM calculations have been used extensively in the performance of molecular dynamics calculations of solvation effects, and there are indeed a variety of different methods to carry out this type of calculation.

The application of the QM/MM algorithms in the description of solvation to transition metal chemistry has not been so far very productive. There is a main difference concerning the nature of the interaction between the QM and MM parts of the systems. While in a solvate/solvent system there are no bonds between the two parts, in a typical transition metal complex there are chemical bonds crossing the interface between the QM and MM regions of the molecule. The design and application of QM/MM methods in systems where there are chemical bonds between the two different regions of the molecule is more recent. Two major lines of applications seem to be developing, one concerning zeolite solid systems[96,97,98] and another concerning transition metal complexes.[25,99,100]

Hence, as far as transition metal complexes are concerned, following the same example mentioned above in the quantum mechanics subsection, the hybrid QM/MM calculation on the $Pt(t\text{-}Bu_3)_2$ system would use a QM level to describe the interaction between platinum and the phosphines, and an MM level to describe the steric interaction between the bulky *t*-Bu substituents of the phosphine ligands, having thus chemical bonds between the two different regions of the molecule.

This section will try to review the current state of these methods. After this introduction, in the next subsection there is a general overview, followed by a second subsection dealing with one-step QM/MM methods, and a final subsection dealing with multistep QM/MM methods, and particularly the IMOMM method.

1.2.4.1 General Overview

The simple idea of partitioning a chemical system in QM and MM regions gives rise to a number of different methodologies depending on the particular way the calculation is performed.

It is not the goal of this subsection to enter in depth in the technical details, which can be found elsewhere, but a minimum description is necessary to evaluate the quality of the different calculations.

The common feature of all hybrid QM/MM methods is the partition of the system in at least two regions: one where the quantum mechanic description is applied (to be referred as QM region), and another one where the MM description is applied (to be referred as MM region). The calculation of the hybrid QM/MM energy of the whole system can be in all generality expressed as:

$$E_{tot}(QM,MM)= E_{QM}(QM) + E_{MM}(MM) + E_{interaction}(QM/MM) \qquad \text{(Eq. 1)}$$

where the labels in subscript refer to the type of calculation and the labels in parenthesis correspond to the region under study. The interaction energy between the QM and MM regions has to be in principle computed by both the QM and MM methods, and the previous expression becomes:

$$E_{tot}(QM,MM)= E_{QM}(QM) + E_{MM}(MM) + E_{QM}(QM/MM) + E_{MM}(QM/MM) \qquad \text{(Eq. 2)}$$

The energy expression in a general hybrid QM/MM method has thus four components. Two of them are simply the pure QM and MM calculations of the corresponding regions, and their computation is straightforward. The other two correspond to the evaluation of the interaction between both regions, in principle at both computational levels. Different computational schemes are defined by the choice of the method to compute the $E_{QM}(QM/MM)$ and $E_{MM}(QM/MM)$ terms.

The $E_{QM}(QM/MM)$ term accounts for the direct effect of the atoms in the MM region on the QM energy of the system. This term is usually critical on solvation problems, because one of the points of interest is precisely how the wavefunction of the solute is affected by the presence of the solvent. In the case of a transition metal complex, this term accounts mainly for the electronic effects of the ligand substituents on the metal center.

A simple way to introduce the $E_{QM}(QM/MM)$ term is to put electrostatic charges in the positions occupied by the MM atoms.[101] One first problem with this kind of approach is the choice

of the electrostatic charges, which is by no means trivial. A more serious problem appears when there are chemical bonds between the QM and MM regions, where this approach breaks down in the proximity of the interface and needs to be reformulated. A more elaborate scheme that overcomes this limitation has been proposed through the introduction of localized orbitals,[102,103,104] although it has been applied so far mostly on organic systems. The Integrated Molecular Orbitals Molecular Mechanics (IMOMM) scheme,[61] that will be discussed below in detail, simply neglects this E_{QM}(QM/MM) term.

The E_{MM}(QM/MM) term accounts for the direct effect of the atoms in the QM region on the MM energy of the system. This term is usually important in transition metal complexes, because it accounts for the steric constraints introduced by the presence of a metal center on the geometry of the ligands. In other words, it is mostly related to the steric effects of the ligand substituents. The E_{MM}(QM/MM) term is usually introduced through the parameterization of the QM atoms with the same force field used in the MM region. When there are no bonds between the QM and MM regions, it corresponds simply to non-bonded interactions between the QM and MM regions, with things being slightly more complicated when the two regions are connected through chemical bonds.

It has been repeatedly mentioned in the previous paragraphs that the presence of chemical bonds between the QM and MM regions poses a problem to the use of hybrid QM/MM methods. One of the reasons is that most approaches require the introduction of additional atoms (usually hydrogen) in the QM calculation because of the impossibility to have dangling bonds. The way to deal with these additional atoms introduces another wide range of methodological details that will not be discussed here.

1.2.4.2 One-Step QM/MM Methods: Combined MO + MM Method

The simplest approach to the use of hybrid QM/MM methods is the performance of two independent calculations. First, the geometry of the atoms in the QM region is optimized in a pure QM calculation. Afterwards, the real ligands are added in an MM calculation where the structure of the atoms in the model system is kept frozen. This approach has its big advantage in the simplicity: the researcher needs only access to two independent standard programs able to carry out the QM and the MM calculations. No special computer code is required, and the addition of the results of both calculations can be done by hand.

In the terms exposed in the previous subsection, this approach has a series of implications. The first of them is the neglect of the E_{QM}(QM/MM) term. This is usually reasonable in transition metal complexes, where the MM regions has mostly a steric effect. A more serious limitation of this approach is the lack of relaxation of atoms in the QM region. They stay frozen at the geometry of the model system, regardless of any steric strain that might exist on them. These methods are labeled here as one-step methods to distinguish them from multistep methods, where the geometry of the QM part is relaxed through an iterative procedure. The have also been labeled elsewhere as combined MO + MM methods[105,106,107] and MO-then-MM methods.[97]

Houk and coworkers had already applied in the 80's one-step hybrid QM/MM methods to the study of organic systems .[108,109] Later on, they have been applied to transition metal systems in a number of cases. In particular, one-step QM/MM methods have been used extensively by Morokuma and coworkers to the study of a number of problems, like olefin polymerization ,[106,110,111] and fluxionality of hydride complexes of iron.[105] Other studies with this type of methods were carried out by Eisenstein and coworkers on the structure of $OsCl_2H_2(P(i\text{-}Pr)_3)_2$ systems[112] and by Maseras and Lledós on the fluxionality of $[Me_2Si(NSiMe_3)_2]_2InLi$ species.[113]

The particular features of one-step methods can be probably better understood with an example taken from a study by Matsubara et al. on the $Pt(PR_3)_2 + H_2$ system (Scheme 1.3) [26]. In this study, which is in fact a calibration of the multistep IMOMM procedure, the authors compare the results obtained with different hybrid approaches with those of a much more expensive pure MO study of the complete system. In particular, they consider four different structures: the reactants, the *trans* product, the *cis* product, and the transition state connecting the reactants to the *cis* product. In the case of R= *t*-Bu, the relative energies at the HF level of each of these four stationary points are 0.0, -10.1, 18.5 and 33.6 kcal•mol^{-1}, respectively. The one-step hybrid QM/MM calculation carried out with a $Pt(PH_3) + H_2$ model for the QM part at the same computational level and the MM3 force field for the MM part yields values of 0.0, -13.9, 87.3 and 39.7 kcal•mol^{-1}. Relative energies computed with the hybrid method are thus quite close to those of the pure MO calculation (within 7 kcal•mol^{-1}) except for the case of the *cis* isomer, where the deviation is as large as 68.8 kcal•mol^{-1}. The reason for this huge difference can be easily traced back to the geometry distortion. The value computed at the pure MO level for the P-Pt-P angle is 104.7° in *cis*-$Pt(PH_3)_2H_2$, and 129.2° in *cis*-$Pt(P(t\text{-}Bu)_3)_2H_2$ system. The one-step hybrid QM/MM calculation uses the value of the model system (104.7°) for the real system, resulting

in a large steric repulsion that leads to the corresponding increase in the relative energy. Things are not so bad for the other stationary points, where the steric repulsion is smaller, and the P-Pt-P bond angles are more similar.

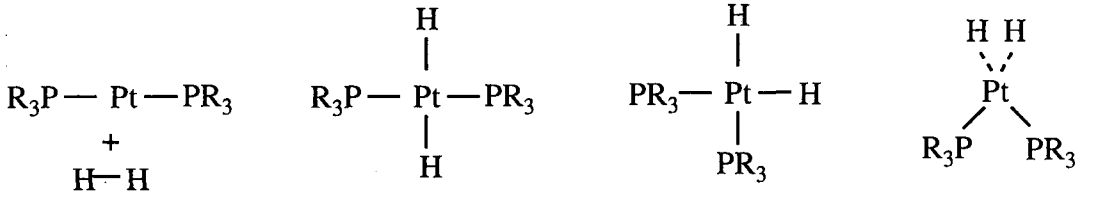

Reactants Trans Products Cis Products Transition State

Scheme 1.3

This example illustrates the advantages and limitations of one-step hybrid QM/MM methods. They are able to produce results in reasonable agreement with those of more elaborate methods, and as such, they cannot be neglected as a valuable tool. On the negative side, they can fail dramatically if there is an important distortion of the geometry of atoms in the QM region. An additional inconvenient of these methods is that no analysis can be carried out on the geometries of the QM atoms, simply because they are not optimized. A more troublesome problem is that the validity of the method cannot be assessed in absence of external data, either coming from experiment of from more elaborated calculations. All these limitations are overcome by multistep QM/MM methods.

1.2.4.3 Multi-Step QM/MM Methods: the IMOMM Method

The natural extension to single-step methods is the use of multistep methods, where the geometry of the model system is corrected to account for the effect of atoms in the MM part. The basic equation of the energy in multistep methods is not very different from that of single-step methods, and it can be indeed the same if one neglects the E_{QM}(QM/MM) term, as is done in a number of schemes. However, there is a substantial difference in the choice of the geometries. In single-step methods the geometry of each region is optimized independently, in particular with the QM method for the QM region. As a result, in general, the final geometry is not the best possible from the QM/MM point of view. In multistep methods the geometry optimization is complete within the QM/MM formalism, and as a result the best possible geometry is obtained

and used for the computation of the energy. In other words, the fully optimized QM/MM geometry is neither the optimal QM nor to the optimal MM arrangement of the atoms, but the arrangement that reaches the best compromise between the two of them.

The performance of a full geometry optimization has important implications both from a technical point of view and from the point of view of applications. From a technical point of view it requires the use of QM/MM gradients, the consistent computation of the which from the pure QM and MM gradients has a number of pitfalls which will not be discussed in detail here. In any case, authors use different approaches to solve this problem, giving rise again to different methods.

The difference in the applications is illustrated again by the study of Matsubara et al. discussed above.[99] Let us recall that a one-step method yielded for the *cis*-$Pt(P(t\text{-}Bu)_3)_2H_2$ complex an energy 87.3 kcal•mol^{-1} above that of $Pt(P(t\text{-}Bu)_3)_2 + H_2$, a result which was in sharp disagreement with the pure MO difference of 18.5 kcal·mol^{-1}. The use of a multistep hybrid QM/MM method is in very good agreement with the pure MO result, with the energy difference between both species falling down to 17.2 kcal·mol^{-1}. This success is closely related to the improvement on the P-Pt-P angle by the multistep method, with a value of 124.9° (to be compared with 129.2° in the full MO calculation, and with the 104.7° used in the one-step calculation).Therefore, in this case, the geometry optimization feature of the multistep method is able to overcome the limitations of the one-step approach and give a correct result.

Within the variety of available multistep hybrid QM/MM methods,[92,93,114,115] the one that has been applied more often to transition metal complexes is the Integrated Molecular Orbitals Molecular Mechanics (IMOMM) method.[61] The most remarkable of its characteristics are the following:

- It is a full multistep method. The final geometry is optimized within the hybrid QM/MM formalism.
- It is not associated to any particular QM method or force field. It can be used with any combination of them.
- It neglects the E_{QM}(QM/MM) term. Therefore, it does not introduce electronic effects of ligands. The effect of the ligands is nevertheless introduced indirectly in the QM energy through the geometry distortions they induce.
- In its original formulation it freezes the lengths of the chemical bonds between the QM and

MM regions of the molecule.

- It includes an algorithm to perform a geometry optimization of the MM region (microiteration) in each step of the geometry optimization of the QM region (macroiteration). Although this technical feature improves highly the computer efficiency, it does not alter the final outcome of the calculation.

The general philosophy of the IMOMM method is therefore to provide a simple and robust algorithm for the application of hybrid QM/MM methods to transition metal systems. This is achieved to the price of losing a part of precision, especially in what concerns the neglect of electronic effects and freezing of bonds between the QM and MM regions. A number of applications of the IMOMM method to transition metal chemistry constitute the bulk of this thesis. The QM and MM computational levels are usually expressed in a compact way in the form IMOMM(QM-level:MM-level).

Chapter 2

Results

This chapter presents a summary of the work carried out during this doctoral thesis, a work that is presented in full detail in the articles collected in the third chapter. Our main goal has been the application of theoretical tools to the understanding of the behavior of transition metal compounds. Because of that, theoretical calculations have been performed with ab initio (HF or DFT - based) methodologies, and a special focus has been set on the IMOMM method, combining quantum mechanics with molecular mechanics, that is emerging as a new powerful tool for transition metal compounds. This work also serves as a test on the quality of this methodology.

The chapter is divided, somewhat arbitrarily, between studies concerning structures and studies concerning reactivity. The first section is dedicated to structural problems: the origin of agostic interactions and other geometrical distortions in some transition metal compounds. The second section is dedicated to reactivity problems, focused in particular on the reaction of dihydroxylation of olefins catalyzed by osmium tetraoxide.

2.1 Structural Analysis

This section is concerned about structural problems. A first subsection analyses the origin of the agostic distortions in the $Ir(H)_2(P^tBu_2Ph)_2^+$ complex, and in the $Mo(C(O)CH_2R)(S_2CNH_2)(CO)(PH_3)_2$ (R = H, SiH_3) compounds. A second subsection discusses the origin of geometrical distortions in the $Os(H)_2Cl_2(P^iPr_3)_2$ and $Ir(H)_2Cl(P^tBu_2Ph)_2$ complexes and in the [Ir(biph)(X)(QR_3)$_2$] (biph = biphenyl-2,2'-diyl; X = Cl and Q = P, X = Cl and Q = As, X = I and Q = P) family of compounds.

2.1.1 Agostic Interactions

Results presented here are a summary of the first and second articles collected in the last chapter. These are concerned with agostic interactions. General aspects on agostic interactions have been discussed in chapter 1.

2.1.1.1 Agostic Interactions in the $Ir(H)_2(P^tBu_2Ph)_2^+$ Complex

The first study on a complex with agostic interactions presented in this thesis (article I) was carried out during an stage in the laboratory of Prof. Odile Eisenstein (Montpellier). It was done

in collaboration with the group leaded by Prof. Kenneth G. Caulton (Indiana). In fact, the experimental part of the work was carried out by Prof. Caulton's group, and the theoretical study is our own contribution.

The compound studied is $Ir(H)_2(P^tBu_2Ph)_2^+$ (see figure 2.1). This is a complex with a formal count of 14 valence electrons, having thus two empty valence orbitals in the metal. Moreover, the ligands are occupying four coordination sites in a saw-horse shape, and the molecule can be viewed as the result of abstracting two ligands from an octahedron. Hence, it is an excellent candidate for the formation of agostic bonds, and in fact, the crystal structure of the complex reveals two agostic bonds.

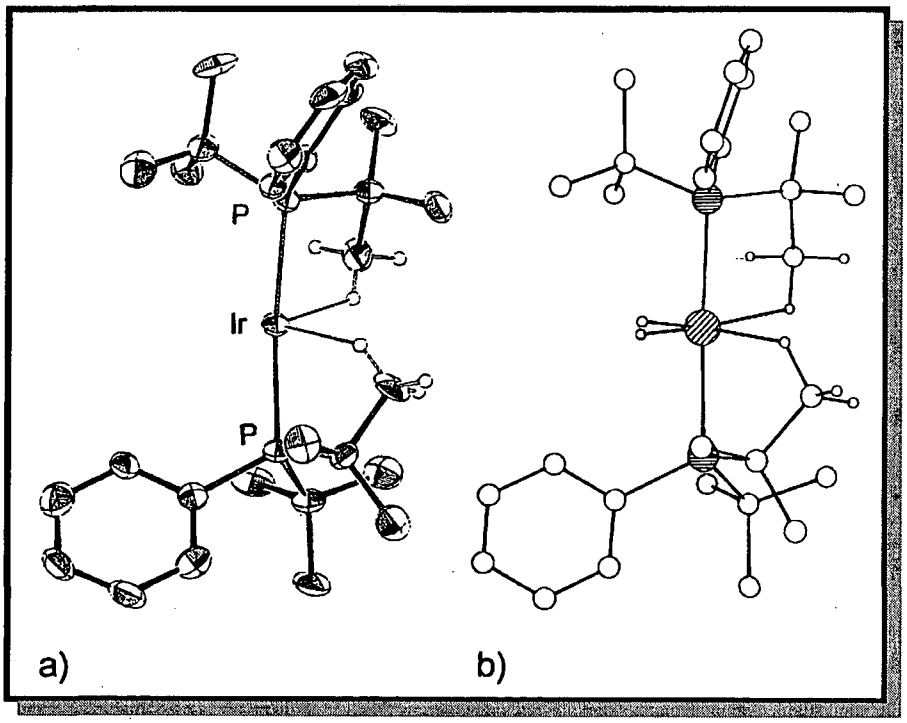

Figure 2.1 (a) Observed structure of $Ir(H)_2(PH_2Et)_2^+$; hydrogens were not located by X-ray diffraction, and the agostic hydrongens shown were placed in idealized positions, assuming staggered conformations. (b) Optimized geometry of the same cation from the IMOMM(Becke3LYP:MM3) method.

To theoretically characterize the agostic interaction, we initially calculated a highly simplified system in which we kept only those atoms involved in the agostic interaction and the groups around the metal which are necessary to properly describe the ligand field. The calculations were thus carried out on the $Ir(H)_2(PH_2Et)_2^+$ model system. This calculation was done at DFT

Becke3LYP level. Results obtained show that the geometry of the atoms directly bonded to the metal center is practically identical with that of an even simpler model, $Ir(H)_2(PH_3)_2^+$ and very similar with the geometry of crystal structure. This confirms that the saw-horse shape of this complex is determined by the coordination of two hydrides and two phosphines to the d^6 metal, and not by the presence of agostic interactions. However, this calculation does not show any evidence of agostic interaction. The shortest Ir ··· C (being the last carbon of the ethyl chain) distance is 4.0 Å (compared to 2.811 Å in the X-ray structure) leading to a Ir ··· H distance of 3.511 Å which is too long for establishing any significant interaction. This is also evident from the essentially equal distance for all CH bonds of CH_3 (1.096-1.097 Å).

Improvements to the model were done in several ways. On one hand, one H of each PH_2Et model ligand was replaced by a vinyl group, as a model of the phenyl group; on the other hand, polarization functions to C and H involved in the agostic interactions were added. No significant changes in the final structure were brought about by any of these two improvements.

The steric bulk of the ligand was introduced in the calculations by means of the IMOMM method. The difference with the calculation on the model system discussed above is striking. The IMOMM calculation shows a clear agostic interaction. Now, the Ir ··· C nonbonding distance is 3.138 Å, which is still a bit longer than the experimental value of 2.811 Å, but is significantly shorter than the 4.0 Å distance calculated in the model system. The corresponding Ir ··· H distance is also relatively short, 2.446 Å.

The steric bulk of the phosphine plays a central role in constraining the agostic C-H bond in proximity to the iridium. Inclusion of the complete ligand forces one methyl group of each phosphine ligand to get closer to the metal atom. In spite of this, there is a real bonding interaction of the CH_3 group with the metal center. The final prove of the existence of the agostic interaction arises from the C-H distances founded. They are stretched to 1.109 Å and are significantly longer than the other C-H bonds of the CH_3 group, 1.094 Å (average value). Hence, these results show that the bulk of substituents is essential for the formation of an agostic interaction in the $Ir(H)_2(P^tBu_2Ph)_2^+$ complex.

2.1.1.2 Agostic Interactions in Acyl Complexes of Molybdenum

Continuing with the study of agostic interactions, a family of molybdenum complexes containing unusual agostic interactions involving the acyl group were analyzed (article II). This

work was also carried out in collaboration with an experimental group. In this case, it was the group leaded by Prof. Ernesto Carmona (Sevilla). This group synthesized several acyl complexes of molybdenum containing several S-donor ligands. The experimental compounds have the general formula $Mo(COCH_2SiMe_2R)(S_2CX)(CO)(PMe_3)_2$ (R = Me, Ph; X = NMe_2 , N-i-Pr_2, NC_4H_4, O-i-Pr, O-t-Bu). These are 6-coordinate compounds with a distorted bicapped tetrahedron structure. The two sulphur atoms and the acyl and carbonyl ligands occupy the tetrahedral sites, with the phosphines in the capping positions. NMR data on all these compounds are consistent with an agostic distortion of the acyl ligand; a distortion that is confirmed by X-ray data when available.

Theoretical calculations on models of several of the experimental complexes were carried out, the results being collected in article II. In this summary, however, only MP2 results on the $Mo(COCH_3)(S_2CNH_2)(CO)(PH_3)_2$ (**8**) and $Mo(CH_2CH_3)(S_2CNH_2)(CO)(PH_3)_2$ (**12**) are discussed. The optimized structures of both are presented in figure 2.2

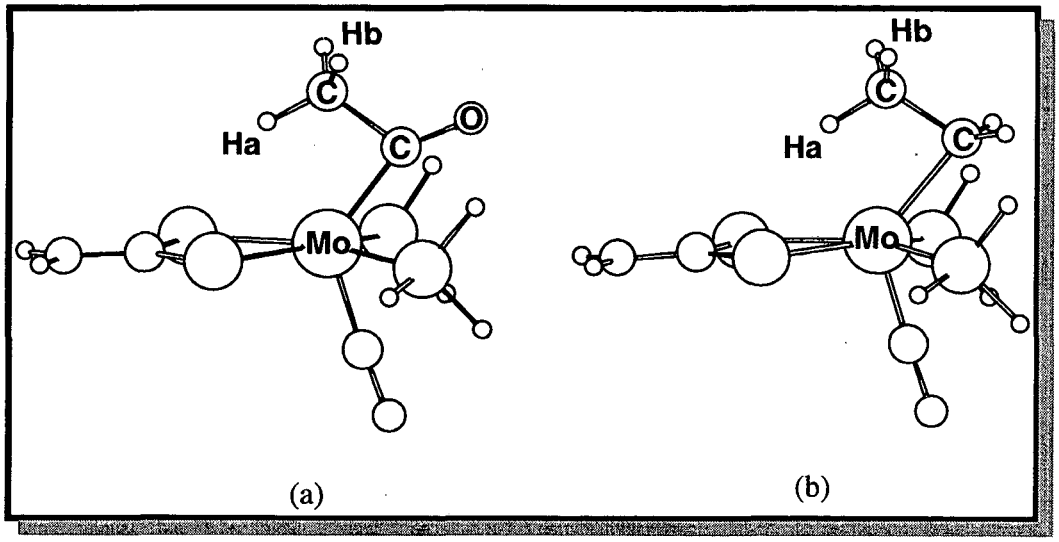

Figure 2.2. (a) Optimized geometry of the $Mo(COCH_3)(S_2CNH_2)(CO)(PH_3)_2$ complex. (b) Optimized geometry of the $Mo(CH_2CH_3)(S_2CNH_2)(CO)(PH_3)_2$ complex.

Complex **8** is a model for the experimental species $Mo(COCH_3)(S_2CNMe_2)(CO)(PMe_3)_2$, and optimized parameters are in good agreement with the X-ray structure. In order to quantify the agostic interaction, a series of additional calculations were performed (Scheme 2.1). The starting point was the fully optimized structure **8e** , where the C_β-H bond is in an eclipsed conformation with respect to the Mo-C_α bond. A second structure **8s,** was obtained by forcing the methyl to a

staggered conformation around the C_α-C_β bond. Finally, two more structures (**8ef** and **8sf**) were obtained by adding a restriction tot the Mo-C_α-C_β, forcing it to a non agostic value of 120°.

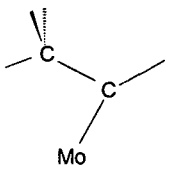

8e

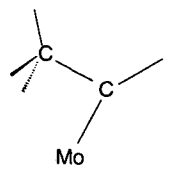

8s

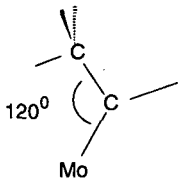

8ef

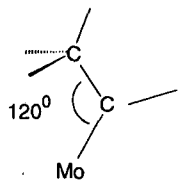

8sf

Scheme 2.1

8s happens to be 2.9 kcal/mol above **8e**, and we attribute this difference to the lack of Mo-H interaction in the **8s** complex. Therefore 2.9 kcal/mol is the energy associated to the Mo-H interactions. Quite unexpectedly, the agostic distortion is still present in **8s**, with a Mo-C_α-C_β bond angle of 92.3°. This agostic distortion must therefore be associated to a Mo-C_β interaction. We estimate its value through the energy difference between **8s** and **8sf**, which is 9.8 kcal/mol. Thus, the agostic distortion yields an energy gain of 11.7 kcal/mol; divided in 2.9 kcal/mol associated to the Mo-H interaction and 9.8 kcal/mol associated to the Mo-C_β interaction.

A similar analysis was carried out on the ethyl complex $Mo(CH_2CH_3)(S_2CNH_2)$ $(CO)(PH_3)_2$ (**12**) to check for the possible specificity of the acyl ligand. In the case of the ethyl complex, the agostic distortion has an associated energy of 11.3 kcal/mol, very close to that of the acyl complex. However, the partition between the two terms is different. In the case of the ethyl complex, 4.4 kcal/mol correspond to the Mo-H interaction, and 6.9 kcal/mol to the Mo-C_β interaction.

Therefore, our theoretical study confirms the existence of agostic distortions in these species, but points out the main contribution is not the Mo-H interaction, but the Mo-C_β interaction. A further extension of this interaction would lead to breaking of the C_α-C_β bond and insertion of Mo

in this bond. The viability of this process agrees in fact with experimental reports and was confirmed through a set of additional theoretical calculations also presented in article II.

2.1.2 Other Geometrical Distortions

The two last articles dealing with structural problems, are concerned with other geometrical distortions presented by several transition metal complexes. They correspond to papers III and IV.

2.1.2.1 Different van der Waals radii for the same halogen atom

In paper III, geometrical distortions on the $Os(H)_2Cl_2(P^iPr_3)_2$ and $Ir(H)_2Cl(P^tBu_2Ph)_2$ complexes are studied. This work was carried out in collaboration with the group of Prof. Odile Eisenstein (Montpellier). In these two particular complexes, the original implementation of the IMOMM method failed to reproduce the X-ray geometry. The problems were analyzed from a

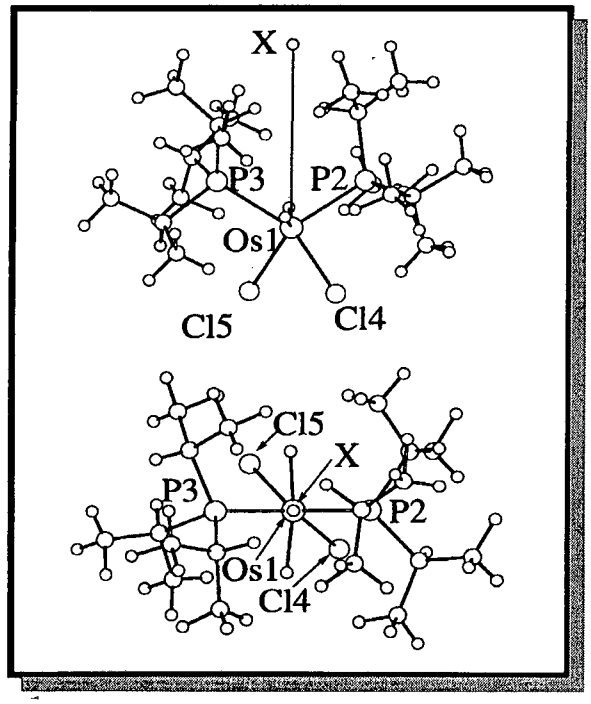

Figure 2.3 X-ray structure of $Os(H)_2Cl_2(P^iPr_3)_2$. X is a dummy atom on the bisector of the P2-Os1-P3 angle. Two different views are shown for clarity.

methodological point of view, and a simple and satisfactory solution was found.

The critical parameter ruling the distortion in the $Os(H)_2Cl_2(P^iPr_3)_2$ complex is the dihedral

angle between the plane defined by the P-Os-P atoms and that defined by the Cl-Os-Cl atoms. This dihedral angle can be precisely defined as X-Os-Cl-P (where X is on the bisector of the P-Os-P angle, see figure 2.3). The X-ray structure shows a value of 41.9° for this dihedral angle. However, the geometry optimization of the $Os(H)_2Cl_2(PH_3)_2$ model complex at RHF level, gave a value of 0.0°. The same result of 0.0° was obtained when a more sophisticated calculation (DFT Becke3LYP level) was carried out. A geometry optimization of the complete system at the IMOMM (Becke3LYP:MM3) computational level using the aforementioned model system for the quantum mechanics part and the default MM3(92) parameters yielded a dihedral angle of 27.2°. This is a remarkable improvement from the 0.0° obtained on the model system, but still far from the experimental value of 41.9°.

A second system presenting a similar problem is $Ir(H)_2Cl(P^tBu_2Ph)_2$. The geometry of this pentacoordined complex is better seen as derived from a trigonal bipyramid with the phosphine ligands in the axial positions (figure 2.4). The metal center and the other three ligands (Cl, H, H) lie essentially in a plane. The X-ray structure shows a remarkable asymmetry between the two Cl-Ir-H bond angles. Their values are 131.1° and 156.2°. The geometry optimization of the model system $Ir(H)_2Cl(PH_3)_2$ at the RHF level gives a C_{2v} structure with two identical Cl-Ir-H values. This unsatisfactory result could not be corrected when calculations on the same model system were carried out at Becke3LYP level. The resulting geometry was again C_{2v} with a Cl-Ir-H angle of 145.3°. A geometry optimization of the complete system using the same model system for the quantum mechanics part, and the default MM3(92) parameters did not produce any significant improvement.

The fact that the improvement was only partial for the first studied system, and non-existent for the second one, hints at the existence of a methodological problem in these particular systems. One peculiarity of both systems is that the steric repulsion is mostly caused by interactions between the anionic Cl^- and H^- ligands attached to the metal and the alkyl substituents of the phosphine ligands. Interactions of this type are essentially controlled by the van der Waals interaction between the atoms in the MM3 force field. It is hard to argue on the accuracy of MM3 parameters for alkyl substituents, since the force field is especially designed for this kind of atoms, however, the parameterization of the inorganic Cl^- and H^- ligands is much less reliable, since this force field considers them to be in an organic environment. Thus, the accuracy of this parameterization was analyzed in detail.

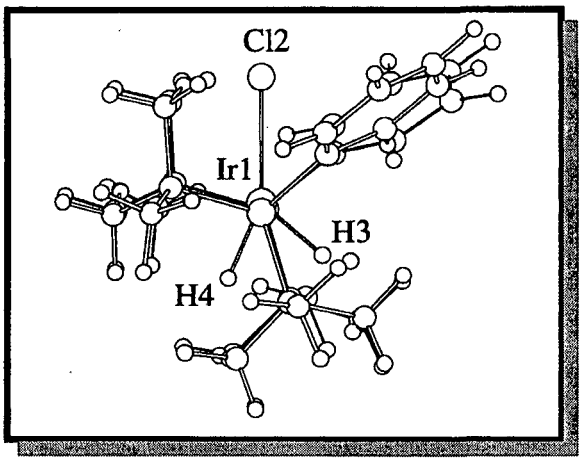

Figure 2.4 X-ray strucrure of $Ir(H)_2Cl(P^tBu_2Ph)_2$.

We calculated the van der Waals radii for the chlorine atom, in both an organic and an inorganic environment. The method to calculate the radius for chlorine atoms in both environments consisted of using the helium atom as a probe in geometry optimizations at the Moller-Pleset (MP3) level with 6-311++G(3d,3p) basis set. One simple model was chosen for each environment. The model organic system was H_3C-Cl ··· He, and the model inorganic system was Na-Cl ··· He. For further simplification, the helium atom was restricted to a head-on approach on the chlorine atom . The resulting van der Waals radius for chlorine were 1.73 Å and 2.13 Å, respectively.

The agreement of the value of 1.73 Å for the organic environment with the MM3 van der Waals radius for this element (2.07 Å, which has been surely fitted for an organic environment) is unexpectedly poor. A comparison between the experimentally accepted van der Waals radii [116] value (1.75 Å) and the MM3 value for a sp^3 carbon atom (2.04 Å) gives a difference of 0.34 Å. This is because what MM3 calls van der Waals radius is a parameter inserted in a mathematical expression, the value of which is adjusted to reproduce properly the overall experimental properties. Hence, it probably incorporates corrections to other errors in the force field, and as a result, it does not correspond exactly to the van der Waals radius, although it is directly related to it. Thus, our assumption is that this difference between the "correct" value and the MM3 value for van der Waals radii is constant for all the atom types. Hence, the van der Waals radii for the inorganic chlorine is 2.13 + 0.34 = 2.47 Å. The validity of this approximation was tested for the two transition metal complexes above presented.

The geometry optimization for the $Os(H)_2Cl_2(P^iPr_3)_2$ complex was repeated at the same

IMOMM(Becke3LYP:MM3) computational level, using as a van der Waals radii the new value of 2.47 Å. The resulting value for the dihedral angle between the P-Os-P and Cl-Os-Cl planes is 35.7°. This is substantially closer to the experimental value of 41.9° than the 27.2° obtained when the default radius for chlorine atom (2.07 Å) was used, and much better than the 0.0° obtained in the pure ab initio calculation on the model system. In the case of $Ir(H)_2Cl(P^tBu_2Ph)_2$, the experimental breaking of symmetry was also properly reproduced once the corrected radius was used. In particular, the resulting values for the two Ir-Cl-H angle bonds were 122.0° and 162.6° . Again, this is in much better agreement with experiment (131.1° and 156.2°) than the results obtained with the standard MM3 radius for chorine (147.1° and 146.0°).

2.1.2.2 Geometrical Distortions in the $[Ir(biph)(X)(QR_3)_2]$ Complexes

Article IV presents a study on $[Ir(biph)(X)(QR_3)_2]$ family of complexes carried out on collaboration with the theoretical group of Prof. Odile Eisenstein (Montpellier) and the experimental group of Prof. Robert H. Crabtree (Yale). The $[Ir(biph)(X)(QR_3)_2]$ family of complexes (biph = biphenyl-2,2'-diyl; X = Cl and Q = P, X = Cl and Q = As, X = I and Q = P) are related to the iridium complex presented before in subsection 2.1.2.1. All these complexes have five ligands in their coordination sphere, they are trigonal bipyramids, and they present a distortion in the trigonal plane.

In the family of complexes discussed here, we have quantified the difference by the angle ϕ, defined in figure 2.5. These complexes are especially interesting because experimental X-ray data show a gradual change of this angle, with values from 8.2° to 17.2°.

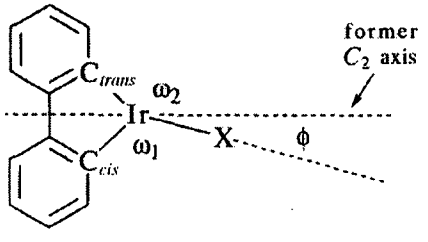

Figure 2.5 Ligands in the equatorial plane of $[Ir(biph)(X)(QR_3)_2]$ family of complexes , showing the deviation of the halide from the ideal C_2 axis (dotted) of pure Y structure. QR_3 ligands are located above and below the equatorial plane. Angle ϕ is the deviation of the X group from the C_2 axis, ω_1 is the C_{cis}-Ir-X angle and ω_2 is the C_{trans}-Ir-X angle. X always lies in the C_{cis}, C_{trans}, Ir plane.

The optimized structure on a model system, $Ir(C_4H_4)Cl(PH_3)_2$, computed at Becke3LYP level, is close to the experimental geometry with the exception of the presence of a C_2 symmetry (ϕ=0°)

which is present in the calculated structure and lacking in the experimental systems (ϕ=10.15°). Having established that $Ir(C_4H_4)Cl(PH_3)_2$ has an electronic preference for a symmetrical structure with $\phi = 0°$, the observed deviation in the presented complexes seemed likely to be a steric effect.

Examination of the experimental structures of these complexes showed that in each case the same ligand conformation is adopted. This conformation was therefore taken as the departure point for the IMOMM study so as to minimize the risk of falling into a series of local minima of no relevance to the experimental solid state conformation. IMOMM (Becke3LYP:MM3) calculations were carried out with van der Waals radii for the halides corrected with the method presented in the previous subsubsection. The IMOMM calculation on $[Ir(biph)(X)(QR_3)_2]$ always reproduce the experimental conformation, indicating that this is a local minimum for the isolated complex and that the crystal packing is not a determining factor. The calculation also shows a displacement of the halide from its electronically preferred position on the C_2 axis in a direction which allows the Ir-X bond to stay coplanar with the metalacycle. In complex $Ir(biph)Cl(PPh_3)_2$ the optimized structure comes remarkably close to the experimental one (calc. ϕ = 11.4° ; exp. ϕ = 10.15°). For all Q and X studied, the displacement, the ϕ angle obtained is close to the experimental value, see figure 2.6.

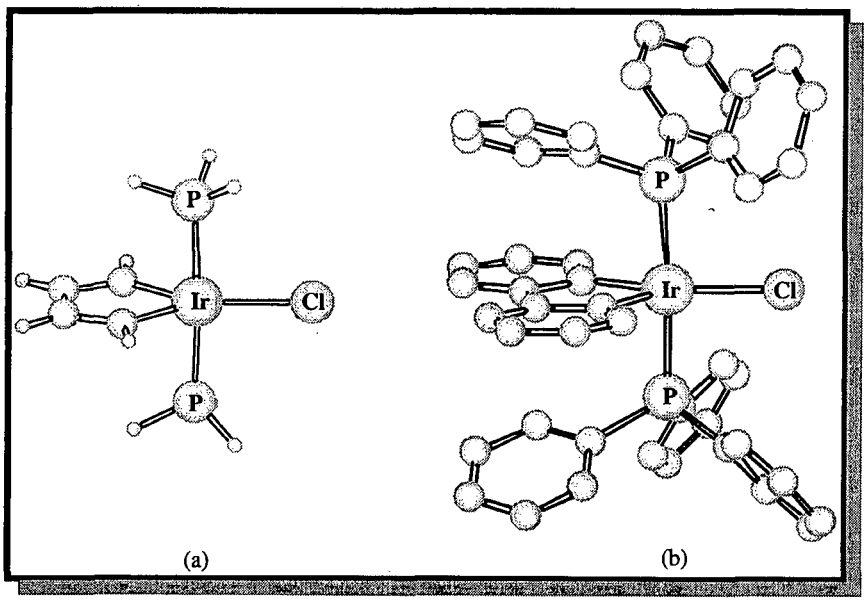

Figure 2.6 (a) Optimized structure of $Ir(C_4H_4)Cl(PH_3)_2$ model complex. (b) IMOMM(Becke3LYP:MM3) optimized geometry of $Ir(biph)Cl(PPh_3)_2$ complex. In this picture hydrogens are omitted for clarity.

On going from PH_3 to PPh_3 (X = Cl), all the calculated metal-ligand distances increase

slightly, probably as a consequence of the increased steric bulk around the metal. The C = C bond of the metalacylopentadiene is not changed on moving from the IrC_4H_4 to the Ir(biph) model since the adjacent phenyl rings of biph are represented only at the MM3 level and therefore delocalization of the electrons of the C = C bond is not possible.

The calculated value of ϕ increases on going from Cl to I (L = PPh_3) as is also the case for the experimental results (calc.: from 11.4° to 14.6° ; exp.: from 10.15° to 17.2°). The increased distortion is clearly associated with a bigger steric interaction with the larger halide. Changing Q from P to As (X = Cl) diminishes the experimental distortion by only one degree (ϕ = 9.15° (av.) for Q = As and ϕ = 10.15° for Q = P); the calculation show no change (ϕ = 11.3° for Q = As and ϕ = 11.4° for Q = P). The longer Ir-Q distance presumably causes the ligand cone angle to decrease.

The calculations thus closely mimic the experimental system, even though the substituents on QR_3 are represented in a purely MM (steric) manner; this suggests that the interactions between the substituents and the other ligands are essentially controlled by steric factors and not by electronic effects as it was thought in a previous study.[117] It is also very satisfying that the IMOMM hybrid method is able to reproduce subtle structural changes even on a potential energy surface known from ab initio calculations to be very flat.

2.2 Reactivity: Mechanistic Analysis of the Osmium catalyzed dihydroxylation of olefins

This section is concerned about reactivity problems, and more concretely about the dihydroxylation of olefins by means of osmium tretraoxide, and its enantioselective application. It has already been mentioned in the first chapter that the mechanism is very difficult to characterize from a experimental point of view, and that different models have been proposed.

The work presented in this section is the application of the theoretical tools to discern which is the best reaction mechanism. It is divided in two subsections. In the first subsection there is a

methodological study, where several quantum methods and basis sets as well as the IMOMM method are tested to prove their validity in the study of this system. In the second subsection there is the study of the reaction mechanism, where the different possible pathways are checked.

2.2.1 Methodological Study

This subsection, starts with a pure quantum mechanical study of the OsO_4 molecule to choose the most appropriate method and basis set for the calculation. Afterwards, an IMOMM study on different $OsO_4(NR_3)$ systems is carried out in order to establish the reliability of this methodology to study this kind of systems.

2.2.1.1 The Choice of the QM Method

First of all, a preliminary study was carried out on the OsO_4 molecule to find the most appropriate quantum mechanical method. Several basis set were tested, and the performance of conventional ab initio methodologies and density functional procedures were compared using the geometries and harmonic frequencies obtained. These results corresponds to paper V.

The most widely extended criterion for evaluating the quality of methods is comparison of optimized geometries. This molecule has the big advantage of being tetrahedral, and there is thus only one parameter to be considered, the Os-O distance.

First of all, different basis sets were tested, and afterwards, different methods were compared with the most appropriate basis set. The comparison of basis sets was carried out with the DFT Becke3LYP method. Up to 9 different basis sets were tested. The optimized values for the Os-O distance oscillate between 1.695 Å and 1.742 Å. In particular, it was found that the addition of polarization functions on both osmium and oxygen affects the outcome of the calculation, while the addition of diffuse functions or a shift to valence triple-ζ quality brought no improvement. Thus, a valence double-ζ basis set with polarization would be the optimal choice. Nevertheless, the lack of analytic gradients for f functions in the programs we were using made us choose LANL2DZ for Os and 6-31G* for O.

Once the basis set was chosen, it was used for the election of the computational method. The performance of different methodologies in the computation of optimal geometries and harmonic frequencies was checked. The comparison was made between methods based on HF and post-HF theory, and methods based on Density Functional Theory.

As far as Os-O bond distance is concerned, the value obtained by the best method used (CCSD(T)) is 1.736 Å. It must be noted that this value is quite different from experiment, 1.711 Å, but should be substantially improved by the addition of f functions at the CCSD(T) level (1.710 Å). Bond distances obtained by HF and post-HF methods, are systematically shorter than the CCSD(T) 1.736 Å value. They are 1.664 Å, 1.681 Å and 1.728 Å for the RHF, CISD and MP2 methods respectively. For DFT calculations the obtained values are 1.737 Å, 1.727 Å, 1.712 Å and 1.710 Å for the BLYP, BPW91, B3LYP and SVWN functionals respectively. Thus, it is shown that the bond distances obtained by DFT are closer to the value obtained at CCSD(T) level than the bond distances obtained by traditional ab initio methods.

As far as vibrational frequencies are concerned, the OsO_4 molecule has four normal modes of vibration, one A_1, one E and two T_2. The average error obtained with the CCSD(T) method, compared with the experimental values is 1.7 %. In the case of the HF and post-HF methods, the average error range between 9 % and 14 %, while for DFT methods the average error are in general smaller, being in the range of 2.4 - 3.6 %. Despite of this, the average error of the calculated frequencies are in general quite small, independently of the methodology used.

The seeming failure of HF based methods seems to be related to the presence of instability in the RHF wave function, indicative of an important presence of non dynamical correlation in this system. The DFT method corrects this error, and shows no instability. It is not clear how non dynamical correlation is included by DFT methods, but it certainly is, as has been also reported by other authors.[118] Since all the functionals tested give good results, the most commonly used Becke3LYP functional was chosen.

This test lead us to chose the LANL2DZ basis set for osmium and the 6-31G* basis set for oxygen; and the DFT Becke3LYP computational method. Thus, the quantum mechanics calculations presented will be using the mentioned method and basis set.

2.2.1.2 Validation of IMOMM for This System

Another methodological test was carried out to probe the reliability of the IMOMM method to deal with the active forms of the catalyst where a chiral amine ligand is added. In this way, several calculations were carried out on the $OsO_4(NR_3)$ system with different NR_3 ligands. This is the content of article VI.

The chosen systems for the IMOMM calculations were those where X-ray geometries are

available, together with the not synthesized $OsO_4(NH_3)$ model complex. In particular, the experimental systems are OsO_4(quinuclidine) and OsO_4\{(dimethyl-carbamoyl)dihydroquinidine\} (see figure 2.7). The test consists in proving the ability of this scheme to reproduce the X-ray structure, paying special attention to the Os-N distances, which are 2.37 Å and 2.49 Å for the experimental systems.

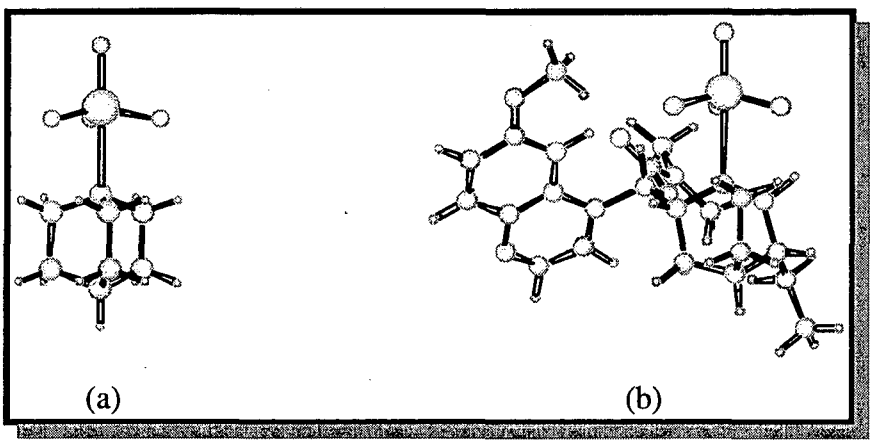

Figure 2.7 IMOMM(Becke3LYP:MM3) optimized structures of: (a) OsO_4(quinuclidine) and (b) OsO_4\{(dimethyl-carbamoyl)dihydroquinidine\}.

In the IMOMM calculations, the part described quantum mechanically (at Becke3LYP level) corresponds to the $OsO_4(NH_3)$ fragment, while the rest of the system is described at the molecular mechanics (MM3) level. For the quantum mechanics part, the basis set used is the mentioned above, LANL2DZ for osmium, 6-31G* for the oxygen, and 6-31G basis set for the nitrogen and hydrogen atoms.

IMOMM geometry optimizations show that the molecule adopts a trigonal bipyramidal structure around the metal center, with one oxygen and the NR_3 ligand in the axial positions. A staggered conformation around the Os-N bond, with O-Os-N-C dihedral angles near 60° , is found, in agreement with the X-ray structures. The most significant result, from a quantitative point of view, of the geometry optimization is the Os-N distance. Values obtained for this parameter are 2.466 Å, 2.546 Å and 2.619 Å for the $OsO_4(NH_3)$, OsO_4(quinuclidine) and OsO_4\{(dimethyl-carbamoyl)dihydroquinidine\} complexes respectively. The trend in the difference between the complexes is reproduced by the calculations. Comparing the two systems where X-ray structures are available, the third complex has a longer Os-N distance than the second one,

being this difference 0.07 Å. Thus, although the computed differences fall short of the experimental one (0.18 Å), we consider this qualitative agreement itself a remarkable achievement of the integrated method.

Besides allowing the study of much larger systems, the IMOMM scheme provides additional tools to analyze the results.[100] For instance, it is possible to quantify the relative weight of steric and electronic effects in the distortion of the system. In order to do this, some additional calculations were carried out. These were restricted geometry optimizations of the experimental systems, with the Os-N distance fixed to the optimized value for $OsO_4(NH_3)$. From direct comparison of these restricted optimizations with the full optimizations discussed above, the energy gain associated to the elongation of the Os-N distance in presence of the bulky ligand can be measured. It comes out to be quite small. For the OsO_4(quinuclidine) complex it is 0.24 kcal/mol, and for the OsO_4\{(dimethyl-carbamoyl)dihydroquinidine\} complex it is 0.69 kcal/mol. This total energy gain can be further decomposed in QM and MM contributions. For the first complex it is found that the gain of 0.24 kcal/mol comes from a 0.46 kcal/mol gain at the MM level and a 0.22 kcal/mol loss at the QM level. For the second complex, there is an MM stabilization of 1.34 kcal/mol and a QM destabilization of 0.65 kcal/mol. These numbers bear an important consequence for the nature of bonding in these complexes. Certainly, they indicate that the Os-N bond is elongated essentially because of its intrinsic weakness (low force constant), and not because of the existence of strong steric repulsions, which are absent.

After the test on the methodology for the quantum chemical calculations, and the test of the performance of the IMOMM method in reproducing the subtle differences between the different tested complexes, a study of several features of the reaction mechanism for the dihydroxylation of olefins by OsO_4 will be presented.

2.2.2 Mechanistic Study

Once the methodology has been tested and chosen, the problem of the reaction mechanism is attacked. First, a study on a model system, $OsO_4 \cdot NH_3$ as catalyst and C_2H_4 as olefin, at pure quantum mechanics level is carried out. Then, the reaction mechanism on the real system is studied by means of the IMOMM method. This means the full consideration of the bis-cinchona

$(DHQD)_2PYDZ$ as a ligand catalyst, and the styrene as a olefin.

2.2.2.1 [3+2] or [2+2] Mechanism?

It has already been mentioned in the first chapter that it has existed for some time a strong controversy between the experimental groups of Profs. Sharpless and Corey on the mechanism of the reaction of asymmetric dihydroxylation. The two proposes are the so-called [2+2] and

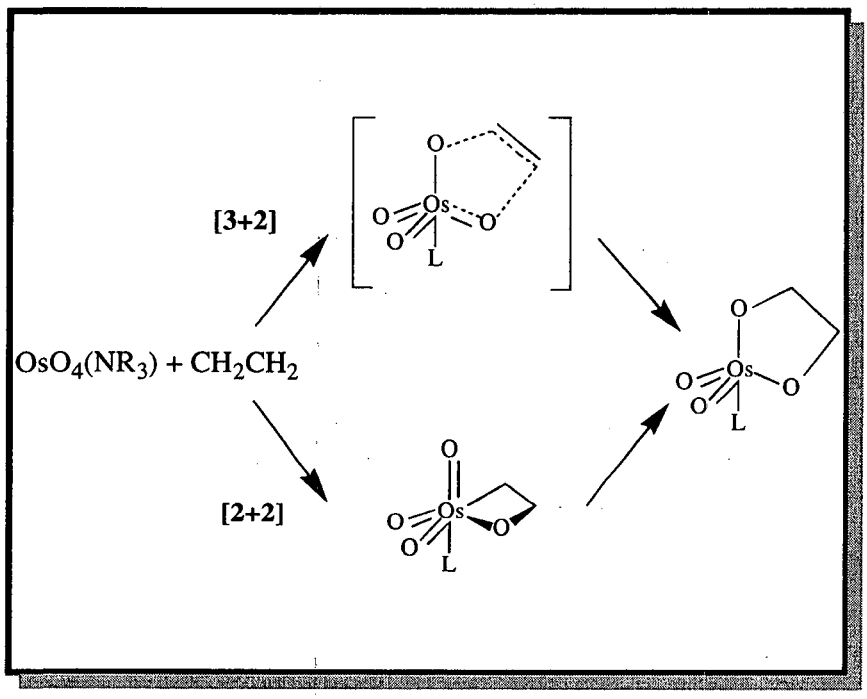

Figure 2.8 Schematic presentation of the concerted [3+2] mechanism and the stepwise osmaoxetane [2+2] mechanism.

[3+2] mechanisms (presented in figure 2.8), the key difference between them being the existence in the [2+2] mechanism of an osmate intermediate containing a direct Os-C bond. This controversy has been solved recently with the help of theoretical calculation, and our work (presented in article VII) carried out in collaboration with the group of Prof. Morokuma (Emory) has contributed to settle this point. Other theoretical works confirming the same results have also been published by other groups almost simultaneously.[60,59] Even Prof. Sharpless, who was the main proponent of the [2+2] mechanism has agreed on the validity of the [3+2] mechanism.[119]

Our study on the two mechanism is performed by means of pure quantum mechanics methodologies and on a model system. The cycloaddition steps with catalyst OsO_4, $OsO_4(NH_3)$,

$OsO_4(NH_3)_2$ are studied. The structure and relative energy for the reactants, the transition states and the products have been calculated, for both the [2+2] and [3+2] pathways.

As far as transition states are concerned, the activation barrier for the [2+2] pathway is 43.3 kcal/mol. In contrast, the activation barrier for the [3+2] addition is only 1.9 kcal/mol, which is even much lower than the energy of the intermediate associated to the [2+2] mechanism. This result makes a [2+2] cyclization as an initial step of the osmium-catalyzed dihydroxylation very unfavorable. The transition state is very reactant-like with a carbon-oxygen distance of 2.365 Å. The carbon-carbon bond (1.374 Å) is slightly elongated in comparison with free ethene (1.348 Å). Our calculations strongly suggest that the osmium-catalyzed dihydroxylation involving [2+2] cycloaddition step is practically impossible under base-free conditions.

When the model catalyst $OsO_4(NH_3)$ is considered, the energetical changes of the reaction profile are minor. Coordination of one NH_3 molecule stabilizes slightly the four-membered ring intermediate with respect to the reactant, the process being endothermic by 13.1 kcal/mol. The activation barrier of 50.4 kcal/mol is even higher than under base-free conditions. The formation of the osmium(VI) glycolate ester is more exothermic (-23 kcal/mol) with $OsO_4(NH_3)$ than with OsO_4 (-15.8 kcal/mol). There is a very low energy transition state for the [3+2] mechanism only 1.4 kcal/mol above the reactants. These facts are compatible with the observation that the reaction is accelerated in the presence of bases. Results are similar when the model catalyst is $OsO_4(NH_3)_2$.

These calculations have clearly shown that the reaction mechanism of the osmium-catalyzed dihydroxylation of olefins can not involve a [2+2] intermediate, whether it is base-free of base-assisted. Even when the Gibbs free energies are used, the conclusion is the same.

2.2.2.2 Location of the Intermediate

The results of the $OsO_4(NH_3)$ + C_2H_4 model mechanism are not able to give an explanation of the observed nonlinear Eyring relationship, or the Michaelis-Menten kinetics behavior, which are attributed to a stepwise process. In order to solve this problem, it seems necessary the introduction of the complete system to study the reaction mechanism, since it has been suggested that interactions between the olefin and large bases used in experiments have important influences. In fact, an olefin-Os(VIII) complex stabilized essentially by a π-d interaction between the olefin and the metal has been suggested in the CCN model.[53] At this point, the Integrated Molecular Orbital / Molecular Mechanics (IMOMM) method is an appropriate theoretical tool to the study

of this reaction mechanism, since its reliability with this kind of systems has been already proved in the previous test mentioned above.

For the IMOMM study, the selected catalyst is OsO_4·$(DHQD)_2PYDZ$ [$(DHQD)_2PYDZ$ = bis(dihydro-quinidine)-3,6-pyridazine] and the olefin is the $H_2C{=}CH(C_6H_5)$ (styrene). This system is chosen because, despite its relative simplicity, it provides a high experimental enantioselectivity for the R product and because there are a lot of experimental data available as a result of the extensive work carried out by the group of Prof. Corey.[52,56] These available data are used to choose the conformation of the reactant, as well as the disposition of the phenyl group substituent in the attacking styrene. At any rate, the orientation of the phenyl group is confirmed by our own later studies (see below).

The quantum mechanics part of the system is defined by $OsO_4(NH_3)$ for the catalyst, and C_2H_4 for the olefin. The rest of the system is treated at the molecular mechanics level with the MM3 force field. The basis set used is LANL2DZ for Os, 6-31G* for O and 6-31G for N, C and H atoms.

Full geometry optimizations succeeded in locating four different stationary points: the separated reactants, the intermediate, the transition state and the osmium(VI) glycolate product. The transition state has a negative eigenvalue of –0.070 a.u. in the approximate Hessian, with the corresponding eigenvector having large components in the O-C distances. The connection of reactant and product through the transition state is further proved by downhill geometry optimizations with small step size from the transition state.

The optimized geometries for the transition state and product are very close to those obtained by pure quantum mechanics optimizations. Bond distances in the 5-membered ring are practically the same in both calculations for the product, with the larger difference being 0.016 Å. For the transition state there are slightly larger differences, with one of the C-O distances being shorter by 0.078 Å (2.011 vs. 2.089 Å) in the IMOMM calculation than in the quantum mechanics calculation. Energies are also similar. The IMOMM energies for the intermediate, transition state and product with respect to the reactants are –9.7, -3.3 and –34.3 kcal/mol, respectively.

The geometry of the intermediate (figure 2.9) presents several interesting features. In first place, the cinchona ligand takes the U-shape conformation predicted by Corey and Noe (CCN model), an orientation that is conserved in the transition state and the product. The validity of the CCN model is thus confirmed. The nuance introduced by these calculations is that the importance

of the two sandwiching nearly parallel methoxyquinoline walls seems to be quite unbalanced. While there is an almost perfect overlap with the styrene substrate with one of the methoxyquinoline rings, the overlap with the other one is quite small, even if it increases as one goes toward the product.

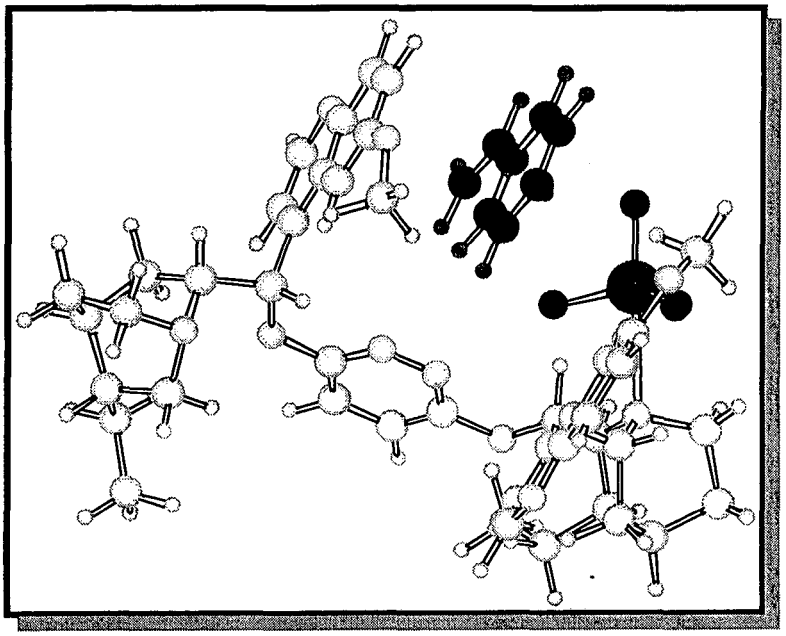

Figure 2.9 IMOMM(Becke3LYP:MM3) optimized structure of the intermediate. Atoms in the styrene and the OsO_4 subunit are depicted in black.

The second remarkable aspect of the geometry of the intermediate is the large distance between the osmium catalytic center and the styrene substrate. The C_{olefin}-O_{Os} distances are 3.136, 3.202 Å, to be compared with values of 2.011, 2.109 Å in the transition state and 1.462, 1.488 Å in the product. The distance of the olefin carbons to the osmium atom are even larger, 4.163, 4.114 Å. The methoxyquinoline ring located further away from the OsO_4 unit is not much closer to the substrate, with C(styrene)-C(quinoline) distances between 3.5 and 3.7 Å, but it is in the optimal orientation for a π-π attractive interaction. In order to identify the main contribution to the binding of the substrate in the intermediate, additional calculations were carried out on the isolated $(DHQD)_2PYDZ{\cdot}OsO_4$ and H_2C=CHPh fragments frozen at the geometry they have in the intermediate. These frozen fragments have an energy 2.7 kcal/mol above the optimized reactants and, therefore, 12.4 kcal/mol above the intermediate. The decomposition of this difference in QM and MM contributions is very clarifying. The QM component, representing the direct interaction

between the OsO_4 unit and the olefin, is only 0.8 kcal/mol, while the MM component, representing the interaction of the styrene substrate with the cinchona ligand, is 11.6 kcal/mol. Therefore, these results show that the stabilization of the intermediate comes essentially from the π-π interaction between one of the methoxyquinoline rings of the cinchona ligand and the phenyl substituent of the substrate.

This results provide the first theoretical characterization of an intermediate for the [3+2] cycloaddition of a substituted olefin to a $OsO_4(NR_3)$ catalyst. The formation of this intermediate seems to be associated to an attractive π-π interaction between the aromatic ring of the substrate and one of the methoxyquinoline rings of the ligand, rather than with π-d interaction of the olefin with the metal center, that have been proposed in the CCN model.

2.2.2.3 The Origin of the Enantioselectivity

Once the [3+2] reaction mechanism for the asymmetric dihydroxylation of olefins by osmium tetraoxide has been established and the intermediate has been characterized, the next logic step is to study the origin of the enantioselectivity for this reaction, since the determined reaction mechanism by itself does not provide any explanation for the origin of the enantioselectivity. This is the subject of article IX.

Calculations on the same experimental system [$(DHQD)_2PYDZ{\cdot}OsO_4$ +H_2C=CHPh] were carried out considering all possible reaction paths leading to R and S products. The experimental selectivity achieved by this catalyst on styrene is very high, being its enantiomeric excess of 96 for the R isomer.

In order to search the transition state associated to the formation of the osmate ester all the different ways in which the olefin can approach to the catalyst have been taken into account. These different paths are depicted in figure 2.10. Figure 2.10(a) shows the possible regions of approach of the olefin to the catalyst from a top view along the O-Os-N axis. The alkene forms bonds with the axial and with one of the three equatorial oxygen atoms. Since the three equatorial oxygen atoms are not equivalent, the approach to each of them defines therefore a distinct family of reaction paths, which have been labeled as "regions" **A**, **B** and **C**, following the same nomenclature proposed by Sharpless and coworkers in a previous study. A second question is the placement of the phenyl substituent of the styrene substrate, which is illustrated in figure 2.10(b). The phenyl can replace any of the four hydrogens of ethylene, giving rise to four different

"orientations" of the substrate, which have been labeled as **I**, **II**, **III** and **IV**. The joint consideration of the three regions of approach and the four possible positions of the phenyl ring per region yields a total of twelve different pathways.

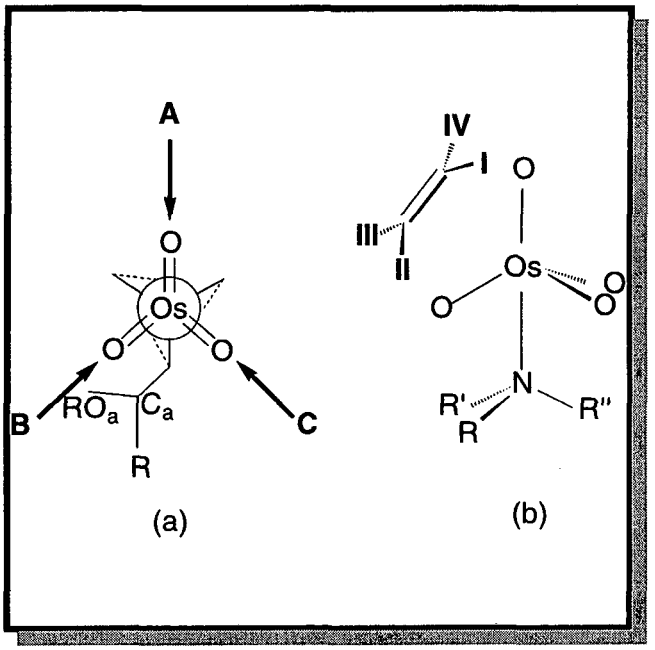

Figure 2.10 Definition of the possible reaction paths in the IMOMM calculations. (a) Top view along the O-Os-N axis showing the three different regions (**A**, **B**, **C**) of approach of olefin. (b) Side view perpendicular to the O-Os-N axis showing the four possible positions (**I**, **II**, **III**, **IV**) of the phenyl ring of styrene.

Each of these twelve possible paths have been theoretically characterized through the location of the corresponding transition state, their energies being collected in table 2.10. The energies are relative to that of the lowest transition state, **B-I**, to emphasize the comparison between different paths.

Looking at table 2.10, it can be seen that the three lower energy saddle points correspond to region **B**: **B-I**, **B-III** and **B-IV**, with relative energies of 0.00, 0.09 and 2.65 kcal/mol, respectively. This computed preference for region **B** is in full agreement with the suggestions emerging from kinetic observations by Sharpless and coworkers.[120] The fact that the region **B** is preferred over the region **A** has a direct consequence on the nature of the steric interactions between catalyst and substrate. It can only mean that the steric interactions are of an attractive nature, because region **A** is the least sterically hindered.

After showing that the reaction goes through region **B**, the analysis shifts to which is the preferred orientation of the substrate within this region. This is the point where selectivity is decided, since isomers **I** and **III** lead to the R product, and isomers **II** and **IV** lead to the S product. Theoretical results on this system show that the product is the R enantiomer, being therefore in good agreement with experiment. The agreement reaches even the value of the enantiomeric excess, since the value reported by the experiment is 96, and the calculated value is 99.4.

		A	B	C
I	QM	-0.72	0.00	-0.05
	MM	5.57	0.00	6.59
	Total	4.84	0.00	6.54
II	QM	-0.40	-0.09	0.29
	MM	6.87	5.49	4.67
	Total	6.47	5.40	4.96
III	QM	-0.58	-.064	0.94
	MM	6.44	0.73	8.41
	Total	5.85	0.09	9.34
IV	QM	-0.41	-.037	0.27
	MM	5.11	3.02	4.60
	Total	4.69	2.65	4.87

Table 2.1 Relative IMOMM(Becke3LYP:MM3) energies (kcal/mol) of the transition states associated to each of the 12 possible reaction paths. All energies are relative to that of the lowest transition state (B-I). Reaction paths are labeled following figure 2.10.

The optimized structures of the three lower energy isomers correspond to **B-I**, **B-III** and **B-IV**. From table 2.10 it is clear that most of the energy difference between the different saddle points is in the MM part, with the QM part being quite similar. Additional calculations were carried out to analyze the different contributions to the MM energy.

The details of this analysis are collected in the text of article IX. The relevant result is that the interaction between the substrate atoms and those of the catalyst can be divided in different

blocks for the four saddle points of region **B**. These are the interaction between the styrene and the pyridazine, the two quinolines and the rest of the catalyst (see figure 2.11). This allows a quantification of the relative importance of the different regions of the catalyst in the stereoselectivity of the reaction. The first result worth remarking is how three of the considered fragments, the two quinolines and the pyridazine, account always for more than 75% of the MM interaction between the catalyst and substrate, showing the appropriateness of the analysis in terms of this fragments.

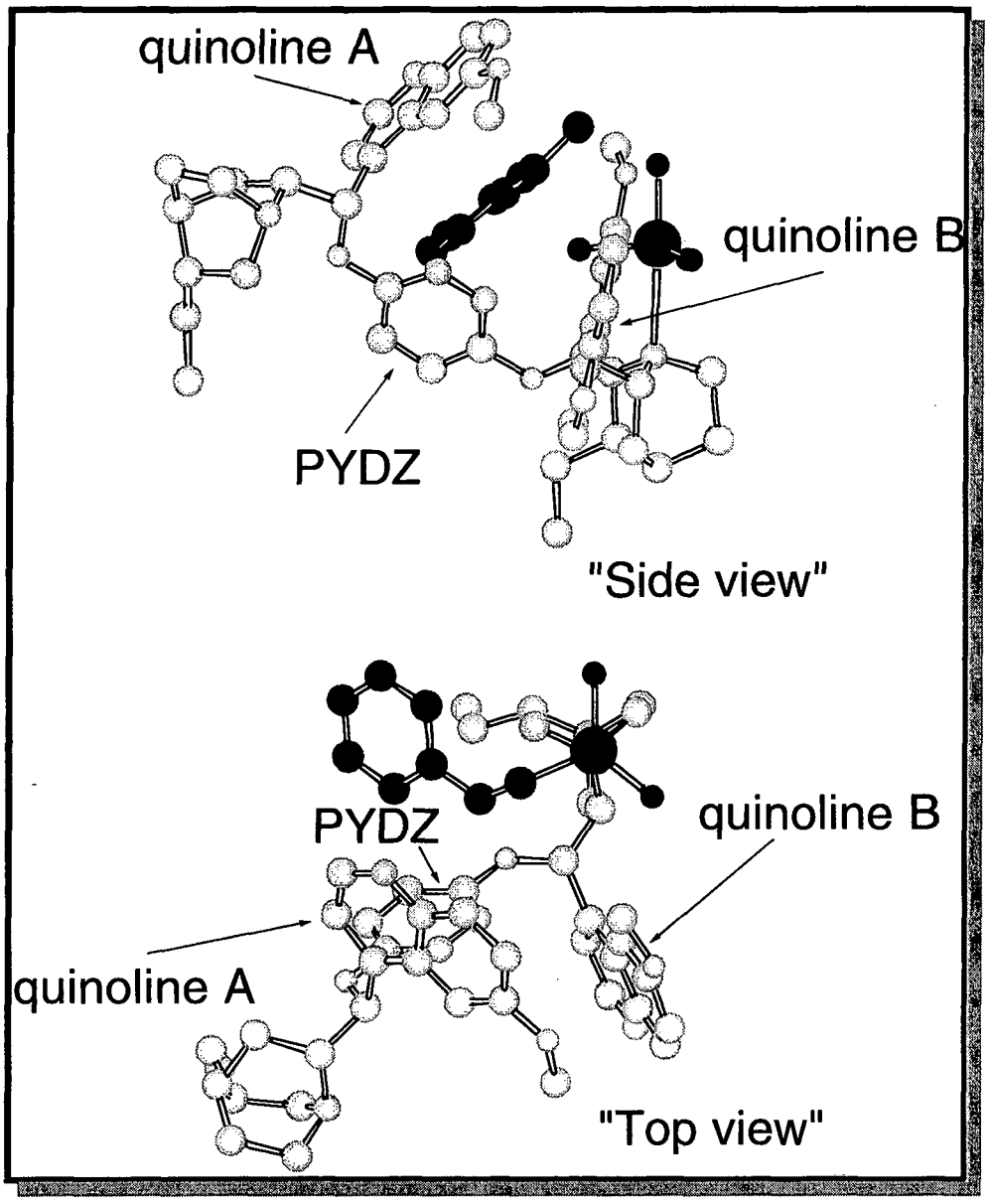

Figure 2.11 Two different views of the IMOMM(Becke3LYP:MM3) optimized transition state **B-I** (labeling the different regions of the catalyst). The styrene and the OsO4 subunit are depicted in black.

As for their relative importance, it is clear that the most important interaction for **B-I**, **B-III** and **B-IV** is the face-to-face interaction with the quinoline located most far away from the metal center.

In summary, it is clear that although experimental results can be rationalized a posteriori, it is difficult to know a priori which are the relative weights of the different factors contributing to the decision of the selectivity. In this concern, the performance of quantitative theoretical calculations can be extremely helpful.

Chapter 3

Conclusions

In this chapter the most important conclusions obtained from the work carried out in this thesis are presented. The conclusions are divided in two main blocks. In the first block there are those related with the structural part, and in the second block are those related with the reactivity part.

Structure:

FIRST: The existence of agostic interactions in the $Ir(H)_2(P^tBu_2Ph)_2^+$ complex is intimately associated to the bulkiness of the substituents in the phosphine.

SECOND: The main cause of the agostic distortion in the Mo(COCH2R)(S2CX)(CO)(PMe3)2 family of complexes is not the interaction between the metal and the β C-H bonds, but the interaction between the metal and the α C-C bond.

THIRD: The van der Waals radius for organic chloro substituents is significantly smaller than that of inorganic chloride ligands. This fact must be taken into account in the MM part of IMOMM calculations.

FOURTH: The symmetry broken distortion in the $Ir(biph)X(QR_3)_2$ (X = Cl or I, Q = P or As) family of complexes is due to the steric repulsions between the halide and phospine ligands.

Reactivity:

FIFTH: Systems involving the OsO_4 unit are not properly described by HF, CISD or MP2 methods. Instead DFT based methods provide good results.

SIXTH: The IMOMM method is able to reproduce the subtle differences in the Os-N bonding in complexes [OsO_4(quinuclidine)] and [OsO_4{dimethyl-carbamoyl)dihydroquinidine}]. Thus, it is an appropriate method for the study of

reactions involving $OsO_4(NR_3)$ systems.

SEVENTH: Theoretical calculations prove that the reaction mechanism of the osmium-catalyzed dihydroxylation of olefins cannot involve a [2+2] intermediate, whether it is base-free or base-assisted.

EIGHTH: Theoretical calculations have allowed the characterization of an intermediate for the [3+2] mechanism in the dihydroxylation of styrene catalyzed by OsO_4·(DHQD)2PYDZ. This intermediate is early in the reaction path and does not show any significant interaction between styrene and the OsO_4 subunit.

NINTH: The reaction path for the dihydroxylation of styrene catalyzed by OsO_4·(DHQD)2PYDZ goes through the **B** region of the catalyst, and with orientation **I** or **III** of the styrene, leading to the R enantiomer.

TENTH: The enantioselectivity for the dihydroxylation of styrene catalyzed by OsO_4·(DHQD)2PYDZ is governed by attractive interactions between aromatic rings in the styrene and the bis-cinchona ligand.

General:

ELEVENTH: The results collected in this work shows that the IMOMM method is a very promising tool for the study of large transition metal complexes.

Chapter 4

Articles

Article I

"Computational Evidence of the Importance of Substituent Bulk on Agostic Interactions in $Ir(H)_2(P^tBu_2Ph)_2^+$"

Gregori Ujaque, Alan C. Cooper, Feliu Maseras, Odile Eisenstein, Kenneth G. Caulton

J. Am. Chem. Soc., **120**, 361-365 (1998)

J. Am. Chem. Soc. **1998,** *120,* 361−365

Computational Evidence of the Importance of Substituent Bulk on Agostic Interactions in $Ir(H)_2(P^tBu_2Ph)_2^+$

Gregori Ujaque, Alan C. Cooper, Feliu Maseras,* Odile Eisenstein,* and Kenneth G. Caulton*

Contribution from the Department of Chemistry, Indiana University, Bloomington, Indiana 47405-4001, and LSDSMS UMR 5636, Université de Montpellier 2, 34095 Montpellier Cedex 5, France

Received August 25, 1997

Abstract: While $Ir(H)_2(P^tBu_2Ph)_2^+$ has been shown experimentally to have two agostic ^{t}Bu groups, *ab initio* B3LYP calculations on $IrH_2[P(Et)H_2]_2^+$ show that the CH_3 group of the phosphine ligand does not form any agostic bond with the strongly electron-deficient (14-valence electron) metal. In contrast, integrated molecular mechanics/molecular orbital (IMOMM) calculations on the full complex $Ir(H)_2(P^tBu_2Ph)_2^+$ duplicate the experimentally observed agostic interaction. Thus, at least in this case, the agostic interaction is due in part to the trapping of a C−H bond in the vicinity of the metal by the steric effects of the other groups of the bulky phosphine. This necessity of steric "constraint" identifies an additional influential factor for the agostic interaction.

Introduction

Following their initial discovery[1] and subsequent categorization,[2] agostic interactions have been found to be extremely common, provided a metal has a low-lying empty valence orbital. In fact, there has been little scrutiny of what factors can assist in stabilizing agostic interactions. Every complex with an empty coordination site is a candidate for an agostic bond. It is also implicit that such a bond is always due to an attraction between the electron-deficient metal center and the C−H bond acting as a weak Lewis base. Experimental[3] and computational[4] studies have revealed interaction energies in the range 10−15 kcal/mol. In addition, the few well-studied cases which show that the agostic bond forms at the expense of a significant geometrical distortion within the ligand[5,6] (e.g., bending at CH_2 and lengthening of C−H) were important landmarks. These results suggested that the agostic bond could be associated with sufficient stabilization energy to overcome geometrical distortions[7] at carbon far larger than the history of carbon chemistry could have suggested (e.g., 90° angle at acyclic four-coordinate C). Thus, the occurrence of an empty site and the presence of a C−H bond in "reasonable proximity" to the empty site could be thought to be the necessary and sufficient conditions for occurrence of an agostic interaction. In the case where no agostic bonds were observed, it was thought that the main reason was due to ancillary ligands decreasing the acidity of the metal center.

The present study suggests a more subtle situation. When the attraction between the metal and the C−H bond is not sufficiently strong to overcome the intrinsic conformation preference of the ligand bearing the potentially agostic group, substituents within this group can be "tuned" to facilitate agostic bonding.

In the course of our efforts to synthesize and characterize transition metal complexes of Ru(II) and Ir(III), d^6 configuration, with *two* empty metal valence orbitals ("14-electron complexes"), we discovered unprecedented examples where one substituent R in *each* phosphine of $L_nM(PR'_2R)_2^+$ donates to the empty orbitals (Figure 1a): the Lewis acidity of the 14-electron complex is high enough to elicit nucleophilic behavior from *two* methyl hydrogens.[8]

As we began to discover other examples of such "double agostic" complexes, we were able to establish the relative ability of ^{t}Bu, cyclohexyl, phenyl, and methyl as agostic donors. An aspect of formation of agostic interactions in $M(PR'_2R)$ which has not been adequately explored is the influence of steric pressure of the two pendent groups R′ on the ability of R to donate to an empty metal orbital. Despite accumulation of considerable experimental data on a range of doubly agostic complexes, the inevitable simultaneous introduction of several changes at a time makes it difficult to isolate single factors which

(1) Brookhart, M.; Green, M. L. H. *J. Organomet. Chem.* **1983,** *250,* 395.

(2) (a) Brookhart, M.; Green, M. L. H.; Wong, L. *Prog. Inorg. Chem.* **1988,** *36,* 1. (b) Crabtree, R. H.; Hamilton, D. G. *Adv. Organomet. Chem.* **1988,** *28,* 299.

(3) (a) Burger, B. J.; Thompson, M. E.; Cotter, W. D.; Bercaw, J. E. *J. Am. Chem. Soc.* **1990,** *112,* 1566. (b) Crabtree, R. H. *Chem. Rev. (Washington, D.C.)* **1985,** *85,* 245. (c) Gonzalez, A. A.; Zhang, K.; Nolan, S. P.; Lopez de la Vega, R.; Mukerjee, S. L.; Hoff, C. D.; Kubas, G. J. *Organometallics* **1988,** *7,* 2429. (d) Zhang, K.; Gonzalez, A. A.; Mukerjee, S. L.; Chou, S.-J.; Hoff, C. D.; Kubat-Martin, K. A.; Barnhart, D.; Kubas, G. J. *J. Am. Chem. Soc.* **1991,** *113,* 9170.

(4) (a) Lohrenz, J. C. W.; Woo, T. K.; Ziegler, T. *J. Am. Chem. Soc.* **1995,** *117,* 12793. (b) Margl, P.; Lohrenz, J. C. W.; Ziegler, T.; Blöchl, P. E. *J. Am. Chem. Soc.* **1996,** *118,* 4434. (c) Kawamura-Kuribayashi, H.; Koga, N.; Morokuma, K. *J. Am. Chem. Soc.* **1992,** *114,* 2359. (d) Thomas, J. L. C.; Hall, M. B. *Organometallics* **1997,** *16,* 2318. (e) Musaev, D. G.; Froese, R. D. J.; Svensson, M.; Morokuma, K. *J. Am. Chem. Soc.* **1997,** *119,* 367. (f) Han, Y.; Deng, L.; Ziegler, T. *J. Am. Chem. Soc.* **1997,** *119,* 5939. (g) Deng, L.; Woo, T. K.; Cavallo, L.; Margl, P. M.; Ziegler, T. *J. Am. Chem. Soc.* **1997,** *119,* 6177.

(5) Dawoodi, Z.; Green, M. L. H.; Mtetwa, V. S. B.; Prout, K. *J. Chem. Soc., Chem. Commun.* **1982,** 802.

(6) Cracknell, R. B.; Orpen, A. G.; Spencer, J. L. *J. Chem. Soc., Chem. Commun.* **1986,** 1005.

(7) (a) Jordan, R. F.; Bradley, P. K.; Baenziger, N. C.; LaPointe, R. E. *J. Am. Chem. Soc.* **1990,** *112,* 1289. (b) Jordan, R. F. *Adv. Organomet. Chem.* **1991,** *32,* 325.

(8) Cooper, A. C.; Streib, W. E.; Eisenstein, O. E.; Caulton, K. G. *J. Am. Chem. Soc.* **1997,** *119,* 9069.

S0002-7863(97)02989-2 CCC: $15.00
Published on Web 01/21/1998

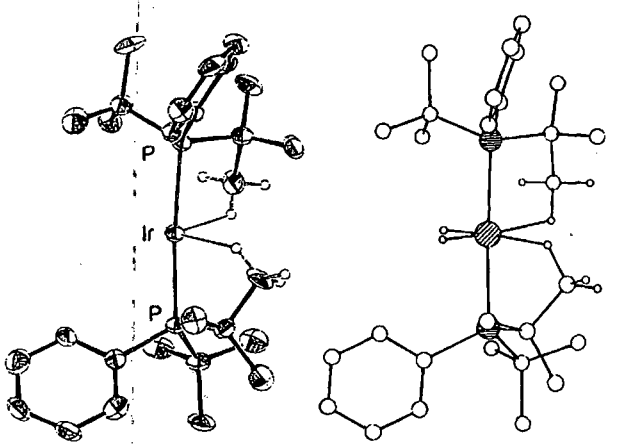

Figure 1. (a) Observed structure of $Ir(H)_2(PtBu_2Ph)_2^+$; hydrogens were not located by X-ray diffraction, and the agostic hydrogens shown were placed in idealized positions, assuming staggered conformations. (b) Optimized geometry of the same cation from the IMOMM (B3LYP: MM3) method.

influence agostic donation. This is an ideal situation to combine emerging experimental results with several "computational experiments", using integrated molecular orbital and molecular mechanics (IMOMM) methodology.[9,10,11] This is a recently proposed[9] hybrid method that uses quantum mechanics and molecular mechanics descriptions for different parts of the same system, and it has been proven to be successful in the quantification of electronic and steric effects in a number of transition metal systems.[10] In the present case, the IMOMM method enables a deeper understanding of the subtle interplay of electronic and steric factors in the occurrence of an agostic interaction.

Computational Details

Pure quantum mechanics calculations on the model systems $Ir(H)_2[P(Et)H_2]_2^+$ and $Ir(H)_2[P(Et)H(CHCH_2)]_2^+$ are carried out with Gaussian 94.[12] Two different basis sets, I and II, are used. In both of them, quasirelativistic effective core potentials replace the 60-electron core of the Ir atom[13] and the 10-electron core of the P atoms.[14] Basis set I is valence double-ζ for all atoms,[14,15] with the addition of a polarization d shell on phosphorus atoms.[16] Basis set II corresponds to a further extension including polarization shells on carbon and hydrogen atoms[17] involved in the agostic interaction.

IMOMM calculations were performed on the real system $Ir(H)_2[P^tBu_2Ph]_2^+$ with a program built from modified versions of two standard programs: Gaussian 92/DFT[18] for the quantum mechanics (QM) part and mm3(92)[19] for the molecular mechanics (MM) part. The QM part was always carried out on the $Ir(H)_2[P(Et)H_2]_2^+$ system with the computational level described in the previous paragraph. For the MM part, the MM3(92) force field was used.[20] van der Waals parameters for the iridium atom are taken from the UFF force field,[21] and torsional contributions involving dihedral angles with the metal atom in the terminal position are set to zero. All geometrical parameters are optimized without symmetry restrictions except the bond distances between the QM and MM regions of the molecules. The frozen values are 1.420 (P−H), 1.112 (C−H), 1.101 Å in the QM part and 1.843 (P−C) and 1.5247 (C−C) in the MM part. The starting point of all geometry optimizations was the X-ray structure of one of the three independent molecules of $Ir(H)_2(P^tBu_2Ph)_2^+$ present in the crystal unit cell. Therefore all comparisons with experiment are done with this particular structure, which presents only conformational differences with respect to the other two.

Results

The complex $IrH_2(P^tBu_2Ph)_2^+$ is a remarkable candidate for an agostic bond. It is a 14-electron species with two empty orbitals, a positive charge to increase the Lewis acidic character of the metal, numerous CH bonds to donate to the electron-deficient Ir, and no π-donor ligand to stabilize the high electron deficiency. It is thus not surprising that the crystal structure of the complex reveals two agostic bonds. The crystal structure shows three independent molecules in the unit cell which differ by orientation within the phosphines. The three molecules present similar agostic structures, and only one of them was computed and will be analyzed.

To theoretically characterize the agostic interaction, we initially calculated, at the DFT Becke3LYP level, a highly simplified system in which we kept only those atoms involved in the agostic interaction and the groups around the metal which are necessary to properly describe the ligand field. The calculations were thus carried out on $Ir(H)_2(PH_2Et)_2^+$. The results of the full optimization with no symmetry constraints are shown in Figure 2 and Table 1. The two phosphine ligands behave very similarly, so discussion will be limited to one of them. Satisfactorily, the geometry of the atoms directly bonded to Ir is identical with that of an even simpler model, $Ir(H)_2(PH_3)_2^+$, which confirms that the saw-horse shape of this complex is determined by the bonds to the metal (Ir−P and Ir−hydride) and the d^6 configuration at the metal and not by the presence of the agostic bonds.[8] The two empty sites are clearly apparent trans to the hydride ligands. What is highly surprising is the *lack* of any agostic interaction with the terminal CH bond of CH_3 in this purely ab initio calculation. This is evident from several structural parameters. The shortest Ir···C

(9) Maseras, F.; Morokuma, K. *J. Comput. Chem.* **1995**, *9*, 1170.
(10) (a) Matsubara, T.; Maseras, F.; Koga, N.; Morokuma, K. *J. Phys. Chem.* **1996**, *100*, 2573. (b) Ujaque, G.; Maseras, F.; Lledos, A. *Theor. Chim. Acta* **1996**, *94*, 67. (c) Barea, G.; Maseras, F.; Jean, Y.; Lledos, A. *Inorg. Chem.* **1996**, *35*, 6401. (d) Wakatsuki, Y.; Koga, N.; Werner, H.; Morokuma, K. *J. Am. Chem. Soc.* **1997**, *119*, 360. (e) Ogasawara, M.; Maseras, F.; Gallego-Planas, N.; Kawamura, K.; Ito, K.; Toyota, K.; Streib, W. E.; Komiya, S.; Eisenstein, O.; Caulton, K. G. *Organometallics* **1997**, *16*, 1979. (f) Ujaque, G.; Maseras, F.; Eisenstein, O. *Theor. Chem. Acc.* **1997**, *96*, 146.
(11) (a) Svensson, M.; Humbel, S.; Morokuma, K. *J. Chem. Phys.* **1996**, *105*, 3654. (b) Matsubara, T.; Sieber, S.; Morokuma, K. *Int. J. Quantum Chem.* **1996**, *60*, 1101.
(12) Frisch, M. J.; Trucks, G. W.; Schlegel, H. B.; Gill, P. M. W.; Johnson, B. G.; Robb, M. A.; Cheeseman, J. R.; Keith, T.; Petersson, G. A.; Montgomery J. A.; Raghavachari, K.; Al-Laham, M. A.; Zakrzewski, V. G.; Ortiz, J. V.; Foresman, J. B.; Peng, C. Y.; Ayala, P. Y.; Chen, W.; Wong, M. W.; Andres, J. L.; Replogle, E. S.; Gomperts, R.; Martin, R. L.; Fox, D. J.; Binkley, J. S.; Defrees, D. J.; Baker, J.; Stewart, J. P.; Head-Gordon, M.; Gonzalez, C.; Pople, J. A. *Gaussian 94*; Gaussian, Inc.: Pittsburgh, Pennsylvania, 1995.
(13) Hay, P. J.; Wadt, W. R. *J. Chem. Phys.* **1985**, *82*, 299.
(14) Wadt, W. R.; Hay, P. J. *J. Chem. Phys.* **1985**, *82*, 284.
(15) Hehre, W. J.; Ditchfield, R.; Pople, J. A. *J. Chem. Phys.* **1972**, *56*, 2257.
(16) Francl, M. M.; Pietro, W. J.; Hehre, W. J.; Binkley, J. S.; Gordon, M. S.; DeFrees, D. J.; Pople, J. A. *J. Chem. Phys.* **1982**, *77*, 3654.
(17) Hariharan, P. C.; Pople, J. A. *Theor. Chim. Acta* **1973**, *28*, 213.
(18) Frisch, M. J.; Trucks, G. W.; Schlegel, H. B.; Gill, P. M. W.; Johnson, B. G.; Wong, M. W.; Foresman, J. B.; Robb, M. A.; Head-Gordon, M.; Replogle, E. S.; Gomperts, R.; Andres, J. L.; Raghavachari, K.; Binkley, J. S.; Gonzalez, C.; Martin, R. L.; Fox, D. J.; Defrees, D. J.; Baker, J.; Stewart, J. J. P.; Pople, J. A. *Gaussian 92/DFT*.; Gaussian, Inc.: Pittsburgh, Pennsylvania, 1993.
(19) Allinger, N. L. *mm3(92)*; QCPE: Bloomington, IN, 1992.
(20) (a) Allinger, N. L.; Yuh, Y. H.; Lii, J. R. *J. Am. Chem. Soc.* **1989**, *111*, 8551. (b) Lii, J. H.; Allinger, N. L. *J. Am. Chem. Soc.* **1989**, *111*, 8566. (c) Lii, J. H.; Allinger, N. L. *J. Am. Chem. Soc.* **1989**, *111*, 8576.
(21) Rappé, A. K.; Casewit, C. J.; Colwell, K. S.; Goddard, W. A., III; Skiff, W. M. *J. Am. Chem. Soc.* **1992**, *114*, 10024.

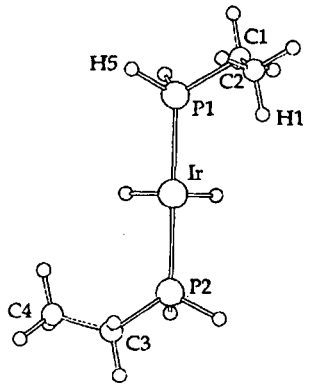

Figure 2. Optimized geometry (B3LYP) of the model complex $Ir(H)_2[P(Et)H_2]_2^+$. The H−Ir−H bond angle is 87.5°.

Table 1. Selected Geometrical Parameters (Å and deg) from Pure QM Calculations on the Model Complex $Ir(H)_2[P(Et)H_2]_2^+$ and IMOMM Calculations on the Full Complex $Ir(H)_2(P^tBu_2Ph)_2^+$[a]

	exp	QM/I	QM/II	IMOMM/I	IMOMM/II
Ir−H1		3.511	3.476	2.446	2.379
Ir−C2	2.811	4.000	3.976	3.138	3.083
C2−H1		1.097	1.097	1.109	1.111
C−H (av)[b]		1.095	1.095	1.094	1.094
Ir−P1−C1	97.0	118.8	118.4	102.6	101.7
Ir−P1−X5[c]	114.3	114.2	114.3	110.5	111.2
P1−C1−C2	102.7	112.6	112.3	106.8	106.2
C1−C2−H1		111.8	111.8	111.5	111.5
C2−C1−P1−Ir	29.7	58.5	57.8	31.7	31.2
Ir−C4	2.936	4.033	4.023	3.321	3.279
Ir−P2−C3	99.0	119.5	119.4	104.7	104.2

[a] Results are presented from calculations with two different basis sets, I and II. X-ray results for the experimental system are also provided for comparison. Atom labeling is defined in Figure 1. [b] Average of the four non-agostic C-H bonds in the two β-methyl groups. [c] X5 corresponds to H5 in the model system, and to the α-carbon of the non-agostic ^{t}Bu group in the real system.

distance is 4.0 Å (compared to 2.811 Å in the X-ray structure) leading to a Ir···H distance of 3.511 Å, which is much too long for establishing any significant interaction; this is also evident from the essentially equal distance for all CH bonds of CH_3 (1.096−1.097 Å). The structural parameters which are responsible for the longer Ir···C−H distance with respect to the experimental structure are the angle Ir−P1−C1 (118.8° in the calculation vs 97.0 in the experimental structure) and a twist of the C2−C1−P1−Ir dihedral angle (58.5° in place of 29.7°) which moves the CH_3 group away from the metal (0° dihedral angle corresponds to Ir−P1 eclipsing C1−C2). The P1−C1−C2 angle is also more open in the calculated structure (112.6°) than in the experimental system (102.7°) but the deviation is smaller than for the angle at P1. Bond distances are all unremarkable.

Improvements to the model were done in several ways. One H of PH_2Et was replaced by a vinyl group, as a model of the phenyl group. No changes in the optimized structure were obtained. This suggests that changes in the basicity of the phosphine ligand by introducing more carbon atoms at the phosphorus do not lead to sufficient electronic changes at the metal or at the C−H bonds to result in the occurrence of an agostic interaction. We also added polarization functions to C and H with no visible changes in the geometry (Table 1). It thus appears that, while the level of calculations seemed appropriate, these models are unable to describe the agostic interactions. These calculations, however, fail to represent the steric bulk of the phosphine ligands.

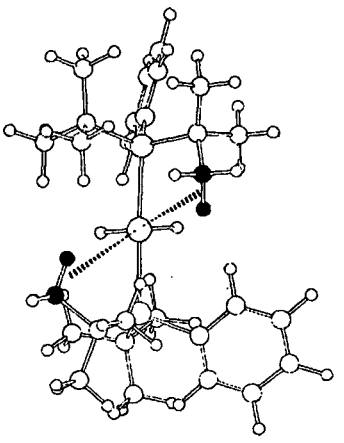

Figure 3. Optimized geometry of the complex $Ir(H)_2(PtBu_2Ph)_2^+$ with the IMOMM (B3LYP:MM3) method. The *ab initio* part is carried out on the $Ir(H)_2[P(Et)H_2]_2^+$ fragment with basis set I. C and H atoms involved in agostic interactions are highlighted in black. The H−Ir−H bond angle is 87.6°.

The entire character of the ligand was thus introduced in the calculations by using the IMOMM methodology. The results of the full optimization of $Ir(H)_2(P^tBu_2Ph)_2^+$, starting close to the experimental structure, are shown in Figure 3 and Table 1. Figure 1b shows another view, allowing direct comparison to the experimental structure. Introduction of polarization functions on C and H of the QM part gives similar results (Table 1). The saw-horse shape around the metal is again found with no major change in the position of hydride and phosphorus atoms. The ligand conformation is very similar to the experimental one, suggesting that packing forces in the solid-state structure do not greatly modify the conformation within the phosphine ligands. The striking difference with the calculation on the model systems presented above resides in the clear formation of an agostic interaction. Discussion will be limited to one phosphine ligand. The Ir···C2 nonbonding distance is now 3.138 Å (3.083 Å with polarization functions), which is still a bit longer than the experimental value of 2.811 Å, but is significantly shorter than the 4.0 Å distance calculated in $Ir(H)_2(PH_2Et)_2^+$. The corresponding Ir···H distance is also relatively short: 2.446 Å (2.379 Å with polarization). The structural parameter that has contributed most to the decrease of the Ir···C2−H1 distance is the Ir−P1−C1 angle (102.6°, 101.7° with polarization), which is only 5° larger than the experimental value of 97.0°. This is a drastic reduction from the 118.8° value in $Ir(H)_2(PH_2Et)_2^+$. There is also a change in the Ir−P1−C1−C2 dihedral angle (31.7° vs 29.7° experimentally) accompanying the change in angles at the phosphine, showing the agostic CH_3 gets closer to the metal by rotating the C1−C2 bond toward Ir. In contrast, the angles at C1 are much less perturbed by the full implementation of all substituents in the phosphine ligand. The variation in angle goes in the right direction and the calculated P1−C1−C2 angle (106.8°, 106.2° with polarization) is no more than 4° larger than the experimental values.

Although the steric bulk of the phosphine plays a central role in constraining the agostic C−H bond in proximity to the iridium, there is a real interaction of this bond with the metal. This can be seen by comparing the computed values for the two Ir−P1−C(^{t}Bu) angles of the same phosphine. That corresponding to the ^{t}Bu carrying the agostic interaction, Ir−P1−C1, is smaller by 8.9° (10.5° with polarization) than that corresponding to the other ^{t}Bu, Ir−P1−C5, again mimicking experiment. The final proof of the existence of agostic

interactions comes from the C2−H1 distances, which are stretched to 1.109 Å (1.111 Å with polarization) and are significantly longer than the other C−H bonds of the CH_3 groups (average 1.094 Å). Other bond length variations are unremarkable.

It thus appears that a simplified representation of the phosphine ligand does not lead to a structure with agostic interactions. The presence of an empty site at the metal is not by itself sufficient to maintain a C−H in bonding proximity at the expense of unfavorable deformation of the carbon chain. A more complete representation of the ligand, incorporating intraligand nonbonded interactions, leads to a structure with agostic interactions. Since the additional groups are represented at the molecular mechanics level, the basicity of the C−H of the CH_3 terminal group is not modified. Only steric factors have been changed. The motion of a CH_3 group is clearly more limited in the bulky P^tBu_2Ph than in the model PH_2Et system. The large bulk of the phosphine thus constrains the CH_3 to a small region close to the metal, in which the Ir···C−H interaction takes place. The pendent ^{t}Bu and Ph groups and the two geminal methyl groups are thus essential to forming the agostic ^{t}Bu interaction in the computation *and*, by extension of this computational experiment, *in reality*.

At this point, it must be recognized that the total number of valence electrons is not sufficient to indicate the presence of an energetically low LUMO that could lead to Lewis acid character. For example, $Ir(H)_2L_2^+$ has a saw-horse shape (**1**)

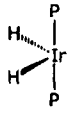

1

and an energetically low LUMO made of x^2-y^2 character (x and y pointing along the Ir−H vectors) and pointing away from the cis hydrides. The next higher empty orbital lies along the C_2 axis, but its p contribution leads to higher energy. In contrast, linear L_2Pt and R_2M (M = Zn, Hg) have a high-lying LUMO pointing along the Pt−P or M−C bonds and a next higher empty orbital made of the intrinsically high (but system-dependent) p metal orbital perpendicular to the M−P vector; they thus have only one "functional" empty orbital, and its high energy explains the absence of an agostic interaction.[22] Similarly, the LUMO of a d,[8] square-planar complex lies along the M−L bond vectors, where it is sterically unsuitable for agostic acceptance, despite its 16-electron count.[23]

Discussion

The results reported here should be viewed in a larger context. Thorpe and Ingold have identified an influence of increasing steric bulk in R of a CR_2 group on ring formation involving this CR_2: bulky R, by increasing the angle R−C−R, favors the kinetics and thermodynamics of formation of rings, especially small rings, containing the CR_2 group.[24] This effect is clearly generalizable to any ER_2 group where E is a tetrahedral atom, and indeed Shaw has elaborated the idea for PR_2R' ligands,[25] where he has been a pioneer in using bulky groups R. Bulky substituents R encourage ring closure,[26] bridging (see **2**), and *ortho* metalation[27] when R′ = C_6H_5. Agostic interaction and *ortho*-metalation have been shown to be linked.[28] Note also that the ligand $Ph_2PCH_2PPh_2$ shows a distinct aversion to be bidentate to a single metal,[29] but is most often found bridging two metals (**3**); evidently two phenyl groups lack the bulk to

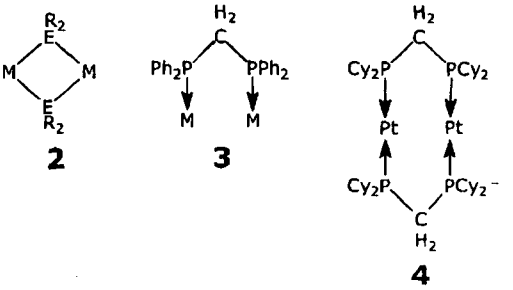

2 **3** **4**

enforce formation of the four-membered ring $M(\eta^2\text{-}Ph_2PCH_2PPh_2)$. When R = ^{t}Bu[30,31,32] or Cy,[33] the (bent) monomeric two-coordinate complexes $Pt(\eta^2\text{-}R_2PCH_2PR_2)$ are transients, highly reactive toward oxidative addition of a variety of ordinarily unreactive bonds. In the absence of suitable substrates, ring opening and transformation to long-lived, less-reactive (linear geometry at Pt) dimers **4** occurs, where a larger ring has the phosphine bridging two metals. For sterically less-demanding groups R, four-membered-ring structures apparently do not have sufficient stability to allow their experimental generation as reactive intermediates.

A number of platinum alkyl cations with β-agostic Pt−H−C bonding have been characterized by using variable-temperature ^{1}H and ^{31}P NMR spectroscopy.[34,35] For these complexes, $[Pt(CH_2CHRR')(L-L)]^+$ (L−L = $Bu_2^tP(CH_2)_3P^tBu_2$), interpretation of the chemical shifts and coupling constants suggests that the β-agostic bonding is weakest when R = R′ = H, stronger for R = H, R′ = ^{t}Bu, and strongest for R = Me, R′ = ^{t}Bu.

It is possible to work with a certain class of molecules without clear recognition of the characteristics of such molecules which confer either limitations ("boundary conditions") or benefits. This can be the case for those molecules containing at least two bulky ligands such as P^iPr_3, PCy_3, P^tBu_3, P^tBu_2R, P^iPr_2R, etc. For example, it is clearly recognized that such ligands

(22) Frederic, P.; Patt, J.; Hartwig, J. F. *Organometallics* **1995**, *14*, 3030.
(23) (a) Yao, W.; Eisenstein, O.; Crabtree, R. H. *Inorg. Chim. Acta* **1997**, *254*, 105. (b) Braga, D.; Grepioni, F.; Tedesco, E.; Biradha, K.; Desiraju, G. *Organometallics* **1997**, *16*, 1846.
(24) Eliel, E. L.; Wilen, S. H.; Mander, L. N. In *Stereochemistry of Organic Compounds*; Wiley: New York, 1994; p 682.
(25) (a) Shaw, B. L. *J. Am. Chem. Soc.* **1975**, *97*, 3856. (b) Shaw, B. L. *J. Organomet. Chem.* **1980**, *200*, 307.
(26) Al-Salem, N. A.; Empsall, H. D.; Markham, R.; Shaw, B. L.; Weeks, B. *J. Chem. Soc., Dalton Trans.* **1979**, 1972.
(27) (a) Bottomley, A. R. H.; Crocker, C.; Shaw, B. L. *J. Organomet. Chem.* **1983**, *250*, 617. (b) Mason, R.; Textor, M.; Al-Salem, N.; Shaw, B. L. *J. Chem. Soc., Chem. Commun.* **1976**, 292.
(28) (a) Albeniz, A. C.; Schulte, G.; Crabtree, R. H. *Organometallics* **1992**, *11*, 242. (b) Cooper, A. C.; Huffman, J. C.; Caulton, K. G. *Organometallics* **1997**, *16*, 1974. (c) Jiménez-Cataño, R.; Hall, M. B. *Organometallics* **1996**, *15*, 1889.
(29) (a) Gao, Y.; Holah, R. G.; Hughes, A. N.; Spivak, G. J.; Havighurst, M. D.; Magnuson, V. R.; Polyakov, V. *Polyhedron* **1997**, *16*, 2797. (b) Puddephatt, R. J. *Chem. Soc. Rev.* **1983**, *12*, 99. (c) Chaudret, B.; Delavaux, B.; Poilblanc, R. *Coord. Chem. Rev.* **1988**, *86*, 191.
(30) Hofmann, P.; Unfried, G. *Chem. Ber.* **1992**, *125*, 659.
(31) Hofmann, P.; Heib, H.; Neiteler, P.; Müller, G.; Lachmann, J. *Angew. Chem., Int. Ed. Engl.* **1990**, *29*, 880.
(32) Hofmann, P.; Heib, H.; Müller, G. *Z. Naturforsch.* **1987**, *B42*, 395.
(33) Notheis, U.; Hofmann, P. Private communication.
(34) Carr, N.; Mole, L.; Orpen, A. G.; Spencer, J. L. *J. Chem. Soc., Dalton Trans.* **1992**, 2653. Spencer, J. L.; Mhinzi, G. S. *J. Chem. Soc., Dalton Trans.* **1995**, 3819.
(35) Appleton, T. J.; Clark, H. C.; Manzer, L. E. *Coord. Chem. Rev.* **1973**, *10*, 335.

permit isolation of five-coordinate species of Ru^{II}, Os^{II}, Rh^{III}, and Ir^{III}, even when halide-bridged dimers might confer an 18-electron configuration. We have reported[36] the phosphine substituent dependence of enthalpies for addition of small ligands to such species, in an attempt to establish differences among phosphines which might otherwise all be categorized as "bulky". We have also reported the ease of *ortho*-metalation of P^tBu_2Ph to Ir^I,[37] in contrast to the rarity of *ortho*-metalation involving the smaller phosphine PMe_2Ph.[38] It is therefore important to recognize that using, among others, the bulky phosphines listed above can have the consequence of metal attack on normally inert C−H bonds (C−C or P−C bond scission might also[39] be anticipated), to give either new products or products of MD/C−H isotopic scrambling. Examples of cyclohexyl C−H oxidative addition[40] and cyclohexyl[41] and ^{i}Pr dehydrogenation are known. A rare case of conversion of PPh_3 + C_2H_4 to $PPh_2(o\text{-}C_6H_4Et)$ while attached to osmium proceeds by insertion of C_2H_4 into an *ortho*-metalated phosphine phenyl group.[42] The double agostic complexes reported here are shown to rely on bulky pendent phosphine substituents to "encourage" formation of weakly bound cycles (rings). The examples of Milstein[43] and of Shaw[44] on oxidative addition to metals of C−C and C−H bonds within the connecting unit G in $R_2P\text{−}G\text{−}PR_2$ can be attributed to this same effect. A number of the C−F oxidative additions to low-valent W involve C−F bonds of an aryl substituent on a bulky, rigid ligand.[45] In summary, it will be useful to be alert to how two of the E-substituents R′ in MER'_2R can influence the interaction of M with R (e.g., ER'_2R = $C(SiMe_3)_3$ or $C(SiMe_3)_2H$[46]), as well as cases where (at least) stabilization of unusual species can result, as in the 14-electron complexes we have sought. Finally, cases where such bond-scission or agostic interactions do *not* occur (e.g., 14-electron $Pt(P^tBu_3)_2$ or M^tBu_2 where M = Zn or Hg) are equally important for what they imply about the *lack* of strong Lewis acidity as a result of linear geometry raising the energy of the LUMO with respect to a bent situation. On the computational side, the IMOMM methodology is a potent tool for evaluating the importance of steric factors in transition metal systems, where lack of parameters for metal/ligand bonding prevents use of pure molecular mechanics methods.

Acknowledgment. This work was supported by the U.S. National Science Foundation and the Université de Montpellier 2 and French CNRS, including an international NSF/CNRS (PICS) grant for US/France collaboration. F.M. thanks the CNRS for a position of research associate. G.U. thanks the Spanish DGES for financial support under project No. PB95-0639-C02-01.

JA9729894

(36) Li, C.; Ogasawara, M.; Nolan, S. P.; Caulton, K. G. *Organometallics* **1996**, *15*, 4900.

(37) (a) Cooper, A. C.; Caulton, K. G. *Inorg. Chim. Acta* **1996**, *251*, 41. (b) Hauger, B. E.; Caulton, K. G. *J. Organomet. Chem.* **1993**, *450*, 253.

(38) Green, M. A.; Huffman, J. C.; Caulton, K. G.; Rybak, W. K.; Ziolkowski, J. *J. Organomet. Chem.* **1981**, *218*, C39.

(39) Edwards, A. J.; Esteruelas, M. A.; Lahoz, F. J.; López, A. M.; Oñate, E.; Oro, L. A.; Tolosa, J. I. *Organometallics* **1997**, *16*, 1316.

(40) Arliguie, T.; Chaudret, B.; Jalon, F.; Lahoz, F. J. *J. Chem. Soc., Chem. Commun.* **1988**, 998.

(41) (a) Heitkamp, S.; Stufkens, D. J.; Vrieze, K. *J. Organomet. Chem.* **1978**, *152*, 347. (b) Campion, B. K.; Heyn, R. H.; Tilley, T. D.; Rheingold, A. L. *J. Am. Chem. Soc.* **1993**, *115*, 5527.

(42) Desrosiers, P. J.; Cai, L.; Halpern, J. *J. Am. Chem. Soc.* **1989**, *111*, 8513.

(43) (a) Gozin, M.; Weisman, A.; Ben-David, Y.; Milstein, D. *Nature* **1993**, *364*, 699. (b) Rybtchinski, B.; Vigalok, A.; Ben-David, Y.; Milstein, D. *J. Am. Chem. Soc.* **1996**, *118*, 12406.

(44) Crocker, C.; Errington, R. J.; Markham, R.; Moulton, C. J.; Shaw, B. L. *J. Chem. Soc., Dalton Trans.* **1982**, 387.

(45) Kiplinger, J. L.; Richmond, T. G.; Osterberg, C. E. *Chem. Rev. (Washington, D.C.)* **1994**, *94*, 373.

(46) Heeres, H. J.; Meetsma, A.; Teuben, J. H.; Rogers, R. D. *Organometallics* **1989**, *8*, 2637.

Article II

"Theoretical and Synthetic Studies on Dihaptoacyl and β-Agostic Acyl Complexes of Molybdenum"

Gregori Ujaque, Feliu Maseras, Agustí Lledós, Leopoldo Contreras, Antonio Pizzano, Dieter Rodewald, Luis Sánchez, Ernesto Carmona, Angeles Monge, Caridad Ruiz

Organometallics, submitted.

1

Theoretical and Synthetic Studies on Dihaptoacyl and -Agostic Acyl Complexes of Molybdenum

Gregori Ujaque, Feliu Maseras and Agustí Lledós*

Departament de Química, Universitat Autònoma de Barcelona, 08193 Bellaterra, Barcelona, Spain

Leopoldo Contreras, Antonio Pizzano, Dieter Rodewald, Luis Sánchez* and Ernesto Carmona*

Instituto de Investigaciones Químicas-Departamento de Química Inorgánica, CSIC-Universidad de Sevilla, 41092 Sevilla, Spain

Angeles Monge and Caridad Ruiz

Instituto de Ciencia de Materiales de Madrid, CSIC, Cantoblanco, E-28049 Madrid, Spain

Abstract

Molybdenum acyl complexes of formula $Mo(C(O)CH_2SiMe_2R)(S_2CX)(CO)(PMe_3)_2$ (R = Me, Ph; X = NMe_2 (**2-Me**, **2-Ph**), N-*i*-Pr_2 (**3-Me**), NC_4H_4 (**4-Me**), O-*i*-Pr (**5-Me**, **5-Ph**), O-*t*-Bu (**6-Me**)) containing several S-donor ligands have been prepared and characterized. Compounds **2-Me** and **2-Ph** exist in solution as an equilibrium mixture between the agostic and the dihaptoacyl species. They crystallize as the isomeric mixture and as the agostic compound respectively. Complexes **3-6** show dihapto coordination both in solution and in the solid state. Confirmation of the agostic coordination of the Mo-acyl moiety has been provided by an X-Ray diffraction study of . *Ab-initio* calculations performed with the representative model species $Mo(C(O)CH_2R)(S_2CNH_2)(CO)(PH_3)_2$ (R = H (**8**), SiH_3 (**9**)) show good agreement with the structural data of the parent compounds. For **8** a value of 12.7 kcal mol^{-1} has been obtained for the agostic stabilization. Calculation of the energy profile for the CO deinsertion in **8** gives an energy barrier of 4.0 kcal mol^{-1} for the C-C breaking process, in good accordance with the available experimental data.

Introduction

The insertion of carbon monoxide into a metal-alkyl bond is a fundamental organometallic reaction.[1] The seemingly unrelated non-classical interaction, i. e. agostic interaction,[2] plays a key role in some important organometallic transformations (e. g. C-H activation[3] and olefin polymerization[4]) but also in the stabilization of unsaturated intermediates.[5] Some years ago, we reported the formation of the first agostic acyl complex of a transition metal, ,[6]a and suggested that the severely distorted **Mo-C-C** angle it presented (structure **a**) could be considered as a model for the transition state, or intermediate of

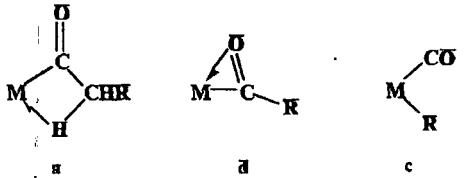

the CO insertion reaction into M-C bonds. This apparent connection between migratory CO insertion and agostic M-C-H interactions has been noted by others. Thus, time-resolved infrared and optical spectroscopy studies have considered agostic acyls as plausible alternatives to solvent stabilized- or dihapto-acyl intermediates,[7] whereas a recent theoretical investigation of the carbonylation of CH_4 by the model catalyst $RhCl(CO)(PH_3)_2$ has shown that the transition state for the migratory insertion step is stabilized by the formation of a -agostic $RhC(O)CH_3$ bond.[8]

For reasons that remain unknown to us, the experimental observation of agostic acyls is still restricted to Mo complexes of composition $Mo(\overline{C(O)CH_3})(S_2CX)CO(PMe_3)_2$, prepared and characterized in our laboratories.[6] This series of complexes has demonstrated to be particularly suitable to study the preference for the agostic coordination (**a**) over the dihaptoacyl (**d**) or the alkyl-carbonyl formulations (**c**), since the relative stabilities of these isomeric structures appear to depend in solution upon the nature of the bidentate, monoanionic S_2CX ligand. For instance, compounds that incorporate bulky and strongly electron-releasing dialkyldithiocarbamate groups exist in solution as equilibrium mixtures between the **a** and **c** type compounds while the alkylxanthate derivatives show in addition the presence of the dihapto compound of type **d**. Contrarily, the analogous complex of the less-donating 1-pyrrolyl dithiocarbamate group exists in solution as the **d** isomer only.

With the aim of improving our knowledge on the factors that govern the adoption of structure **a** we present here an extension to our previous work with the mentioned molybdenum acyls. The synthesis and characterization of silyl derivatives of composition $Mo(C(O)CH_2SiMe_2R)(S_2CX)CO(PMe_3)_2$ (R = Me, Ph; S_2CX = alkyl xanthate or dialkyldithiocarbamate) are described, as well as spectroscopic studies of their behavior in solution. Additional structural evidence for the agostic coordination is given by a new X-ray crystallographic study and most valuable complementary information is provided by the results of a theoretical analysis of the metal-acyl interaction by *ab initio* methods.

Results and Discussion

Synthesis of the Acyls $Mo(C(O)CH_2SiMe_2R)(S_2CX)(CO)(PMe_3)_2$ (R = Me, Ph). X-ray Structure of the Agostic Complex $Mo(\overline{C(O)CH_2}SiMe_3)(S_2CNMe_2)CO(PMe_3)_2$ 2a-Me. Reaction of the alkaline salts (Na^+ or K^+) of several dialkyldithiocarbamate and alkylxanthate ligands, in diethyl ether (Et_2O) or tetrahydrofuran (THF), with the chloro(acyl) complexes $Mo(\eta^2$-$C(O)CH_2SiMe_2R)Cl(CO)(PMe_3)_3$ (R = Me, **1-Me**; Ph, **1-Ph**) produces incorporation of the dithioacid ligand with concomitant release of the chloride and one of the groups PMe_3 and formation of the acyl derivatives **2-6** (Scheme 1). As shown in Scheme 1, the new acyls are

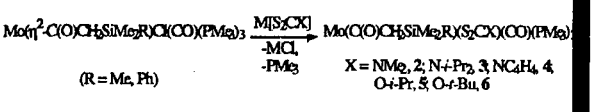

designated by numbers from **2** to **6**, according to the nature of the dithioacid ligand. Since two different R groups have been employed, they are further denoted with the appropriate **Me** or **Ph** symbol. In some instances two isomeric possibilities may be observed, namely the dihaptoacyl structure of type **d** (see above) or the agostic formulation **a**, hence these letters will additionally be used when appropriate.

With the exception of compound **5-Ph**, obtained as an oily, albeit spectroscopically pure material, complexes **3-6** are isolated as orange-red crystalline solids of the dihapto isomer. Differently, acyl **2-Me** crystallizes from its solutions in Et_2O-petroleum ether mixtures as a mixture of the agostic isomer **2a-Me** (yellow-orange) and the dihapto compound **2d-Me** (orange-red). Careful crystallization, or even manual separation of the crystalline mixture, allows the separation of the two

Formula	$MoS_2P_2SiO_2NC_{15}H_{35}$
Mr	511.5
crystal system	Orthorhombic
space group	$P2_12_12_1$
a, Å	9.338(4)
b, Å	12.480(3)
c, Å	21.103(9)
V, Å^3	2459(2)
Z	4
F(000)	1064
ρ(calcd), g cm^{-3}	1.38
temp, °C	22
μ, cm^{-1}	8.7
cryst dimens, mm	0.1 x 0.1 x 0.2
diffractometer	Enraf-Nonius CAD4
radiation	graphite-monochromated Mo Kα (λ = 0.71069 Å)
scan technique	Ω/2θ
data collected	(-11,0,0) to (11,15,26)
rflns collected	5418
unique data	2748
unique data (I) ≥ 2σ (I)	2290
R(int), %	4.1
std rflns	3 rflns
RF, %	3.7
R_wF, %	5.5
average shift/error	0.08

Table 1: Crystal and Refinement Data for **2a-Me**

Mo-P1	2.432(3)	Si-C3	1.873(11)
Mo-P2	2.413(3)	Si-C4	1.859(15)
Mo-S1	2.526(3)	Si-C5	1.868(14)
Mo-S2	2.528(3)	Si-C6	1.845(15)
Mo-C1	1.864(11)	S1-C7	1.710(11)
Mo-C2	2.045(11)	S2-C7	1.710(11)
P1-C11	1.822(14)	O1-C1	1.218(14)
P1-C12	1.785(15)	O2-C2	1.214(13)
P1-C13	1.839(14)	N-C7	1.324(13)
P2-C21	1.831(13)	N-C8	1.466(19)
P2-C22	1.815(12)	N-C9	1.460(16)
P2-C23	1.822(13)	C2-C3	1.587(15)
C1-Mo-C2	120.1(4)	Mo-P2-C21	116.7(4)
S2-Mo-C2	121.3(3)	C22-P2-C23	102.3(6)
S2-Mo-C1	108.0(3)	C21-P2-C23	100.8(6)
S1-Mo-C2	118.2(3)	C21-P2-C22	102.3(6)
S1-Mo-C1	108.6(3)	C5-Si-C6	107.2(6)
S1-Mo-S2	70.0(1)	C4-Si-C6	110.5(6)
P2-Mo-C2	74.9(3)	C4-Si-C5	109.5(6)
P2-Mo-C1	76.0(3)	C3-Si-C6	105.5(6)
P2-Mo-S2	152.7(1)	C3-Si-C5	112.8(6)
P2-Mo-S1	83.0(1)	C3-Si-C4	111.1(6)
P1-Mo-C2	75.3(3)	Mo-S1-C7	86.6(4)
P1-Mo-C1	75.7(3)	Mo-S2-C7	86.5(4)
P1-Mo-S2	86.9(1)	C8-N-C9	116.0(9)
P1-Mo-S1	156.9(1)	C7-N-C9	121(1)
P1-Mo-P2	119.7(1)	C7-N-C8	122.0(9)
Mo-P1-C13	114.5(5)	Mo-C1-O1	179.2(9)
Mo-P1-C12	116.5(5)	Mo-C2-O2	148.1(8)
Mo-P1-C11	117.5(5)	O2-C2-C3	117.2(9)
C12-P1-C13	102.5(6)	Mo-C2-C3	94.7(6)
C11-P1-C13	100.8(6)	Si-C3-C2	114.3(7)
C11-P1-C12	102.7(7)	S2-C7-N	123.1(8)
Mo-P2-C23	114.0(4)	S1-C7-N	120.7(8)
Mo-P2-C22	118.2(5)	S1-C7-S2	116.0(6)

Table 2: Selected Bond Distances and Angles for **2a-Me**

isomers. The phenyl derivative **2-Ph** seem to crystallize exclusively as the agostic form, even though the dihapto complex predominates in solution (*vide infra*). They are all moderately stable to air in the solid state, but very sensitive in solution. In particular they experiment easy C-Si heterolysis[9] in the presence of adventitious water, to generate the compounds $Mo(C(O)CH_3)(S_2CX)CO(PMe_3)_2$, previously described by our group.[6]

The coordination mode of the acyl fragment in the above complexes can be readily identified from their IR spectra (Nujol mull). Thus derivatives **3d-6d** show two bands in the carbonyl region: a strong absorption in the interval 1800-1750 cm^{-1} due to (CO) of a terminal carbonyl ligand, and a medium intensity band in the 1490-1465 cm^{-1} range, the latter being characteristic of an acyl fragment coordinated in the dihapto fashion.[10] Contrary to the above, the agostic isomers **2a-Me** and **2a-Ph**, in which back donation to the C=O fragment is absent, present the corresponding band as a fairly strong absorption at 1615 and 1598 cm^{-1} respectively.

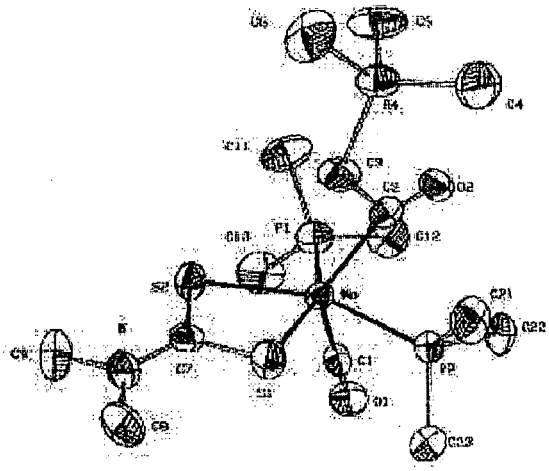

Figure 2: ORTEP diagram of $Mo(COCH_2SiMe_3)(S_2CNMe_2)CO(PMe_3)_2$ (**2a-Me**)

Further insight into the agostic nature of the interaction between the acyl fragment and the metal center in these compounds has been gained from an X-ray study carried out with the **2a-Me** derivative. Suitable crystals of this compound have been obtained by careful crystallization of its solutions in Et_2O. Figure 2 shows an ORTEP diagram of its molecules, while Tables 1 and 2 display crystallographic data and some selected bond distances and angles, respectively. The geometry of **2a-Me** clearly resembles the molecular

structure of other agostic acyls studied previously in our laboratory.[6] If the acyl group is considered to occupy a single coordination site, the geometry of **2a-Me** can be regarded as derived from a distorted octahedron, with the chelating dithioacid ligand and the two trimethylphosphine fragments occupying the equatorial plane, and the carbonyl functionalities, i. e. the terminal carbonyl ligand and the agostic acyl moiety, positioned in the axial sites. The geometry of the coordinated acyl ligand deserves specific comment. The interaction between the metal and **the terminal CH_2R group of the acyl ligand** produces a severe distortion with respect to the geometry characteristic of the monohaptoacyl fragment, M-C(O)R, clearly denoted by the value of the angle Mo-C(2)-C(3) of 94.7(6). This is significantly shorter than the value of 120.9 observed in $CpMo(^1\text{-}C(O)CH_3)(CO)_2PPh_3$.[11] Since the angle formed by the O(2) C(2) and C(3) atoms (117.2(9)) remains close to the ideal value expected for an sp^2 hybridation at C(3), the approaching of one of the -C(3)-H bonds can be envisioned as a pivotation of the acyl ligand from the monohapto coordination, to bring the carbon atom C(3) closer to the Mo atom. This originates the agostic interaction (or agostic distortion, *vide infra*) characterized by Mo-C(3) and Mo-H(32) distances of 2.69(11) and 2.65(9) Å, respectively. These values lie well in the range observed for other agostic acyls and do not require further comment. Also very characteristic of the agostic acyl interaction are the values of the Mo-C(2)-O(2) and Mo-C(2)-C(3) angles (148.1(8) and 94.7(6) respectively). They are in the intervals expected for this type of coordination but, as already discussed at length,[6] differ considerably from those corresponding to the ^{1}- and ^{2}-acyl structures.

Table 3: Relevant Structural Parameters (in Å and degrees) of $Mo(COCH_2R)(S\text{-}S)(CO)(PR_3)_2$ Agostic complexes.[a]

	7[b] X-ray	**8** Opt.	**2a-Me** X-ray	**9** Opt.	**10**[c] X-ray	**11** Opt.
Mo-C(1)	1.83(1)	1.898	1.864(11)	1.898	1.879(7)	1.888
Mo-C(2)	2.05(1)	2.048	2.045(1)	2.054	2.057(7)	2.065
Mo-S(1)	2.529(2)	2.607	2.526(3)	2.603	2.504(1)	2.571
Mo-S(2)	2.547(2)	2.607	2.528(3)	2.602	2.497(2)	2.571
Mo-P(1)	2.435(2)	2.506	2.432(3)	2.502	2.419(2)	2.510
Mo-P(2)	2.430(3)	2.506	2.413(3)	2.498	2.411(1)	2.510
C(1)-Mo-C(2)	122.7(4)	125.9	120.1(4)	126.7	118.0(3)	124.4
S(1)-Mo-S(2)	69.9(8)	71.1	70.0(1)	71.5	71.9(1)	74.0
P(1)-Mo-P(2)	120.55(9)	116.9	119.7(1)	116.5	120.2(1)	117.4
S(1)-Mo-P(1)	154.80(9)	156.4	156.9(1)	156.8	155.4(1)	157.8
S(2)-Mo-P(2)	153.50(9)	156.4	152.7(1)	157.0	157.7(1)	157.8

[a] For the atom numbering see Scheme 2. [b] Ref. 6a. [c] Ref. 6c

Table 4: Relevant Bond Distances (Å) and Angles (deg.) for the $Mo(COCH_2R)$ Fragment in Agostic Acyl Complexes.[a]

	7[b] X-ray	**8** Opt.	**2a-Me** X-ray	**9** Opt.	**10**[c] X-ray	**11** Opt.
Mo-C(2)	2.05(1)	2.048	2.045(11)	2.054	2.057(7)	2.065
Mo-C(3)	2.60(1)	2.613	2.69(11)	2.600	2.762(4)	2.671
Mo-Ha	2.06(9)	2.351	2.65(9)	2.247	2.56(6)	2.398
C(3)-Ha	1.00(9)	1.103	1.01(9)	1.108	1.00(9)	1.100
C(2)-C(3)	1.57(2)	1.595	1.587(15)	1.588	1.561(9)	1.585
Mo-C(2)-C(3)	90.9(8)	90.8	94.7(6)	90.2	98.6(4)	93.1
Mo-C(2)-O(2)	149.2(8)	147.5	148.1(8)	147.1	144.4(5)	145.7
C(3)-C(2)-O(2)	120(1)	121.7	117.2(9)	122.7	116.9(6)	121.2
C(2)-C(3)-Ha	99(5)	115.7	110(5)	114.1	116(5)	114.4

[a] For the atom numbering see Scheme 2. [b] Ref. 6a. [c] Ref. 6c

Finally, it should be noted that the formal substitution of a H atom of the $C(O)CH_3$ fragment by a $SiMe_3$ unit does not introduce any significant variation in the structural parameters of these complexes.

Structural and Electronic Features of $Mo(C(O)CH_2R)(S_2CX)(CO)(PMe_3)_2$ Agostic Complexes. Theoretical calculations were carried out on a number of model systems of experimentally reported acyl complexes. The modeling consisted always in the replacement by hydrogen atoms of substituents far away from the metal-acyl interaction. In this way, PMe_3 ligands were modeled as PH_3, and the $SiMe_3$ substituent as SiH_3. Calculations were carried out on the parent complex $Mo(COCH_3)(S_2CNMe_2)(CO)(PMe_3)_2$ (**7**)[6a] and on the species reported here $Mo(COCH_2SiH_3)(S_2CNMe_2)(CO)(PMe_3)_2$ (**2a-Me**), modeled as $Mo(C(O)CH_3)(S_2CNH_2)(CO)(PH_3)_2$ (**8**) and $Mo(C(O)CH_2SiH_3)(S_2CNH_2)(CO)(PH_3)_2$ (**9**), respectively. Additional calculations were also carried out on the phosphonium xanthate complex $Mo(C(O)CH_3)(S_2C(PMe_3)OCH_2CF_3)(CO)(PMe_3)_2$ (**10**)[6c] modeled as $Mo(C(O)CH_3)(S_2C(PH_3)OH)(CO)(PH_3)_2$ (**11**). Computed and experimental parameters concerning the coordination sphere of the metal are collected in Table 3, and those involved in the molybdenum-acyl interaction in Table 4. Atom numbering is shown in Scheme 2.

Data in Table 3 indicates a good agreement between the experimental and calculated geometrical parameters. In spite of the simplifications introduced in the theoretical study, bond distances and bond angles are well reproduced in the calculations, with differences not larger than one tenth of an Armstrong and six degrees, respectively, with respect the experimental values. The largest differences can be found for complex **11**, in which the most severe simplification of the experimental system **10** has been introduced, changing the electron-drawing CH_2CF_3 group by H. The computational level and the modelization applied look therefore suitable for dealing with this kind of systems.

In the complexes under study, six ligands are coordinated to the metal. We will attempt to classify the geometry in terms of the most frequent polyhedron geometry found in transition metal six-coordination.[12] Given that the three species adopt a very similar geometrical arrangement, we will discuss only the (**2a-Me**) structure. In this complex the two S atoms and two P atoms define a plane, and the terminal carbonyl ligand and the agostic acyl ligand are in a plane perpendicular to the former. The chelating dithiocarbamate ligand imposes a rigid angle (70.0 ° exp., 71.5 ° calc.). The S(1)-Mo-P(2) and S(2)-Mo-P(1) angles (83.0 ° exp., 85.7 ° calc. and 86.9 ° exp., 85.8 ° calc. respectively) are near the ideal octahedral value (90 °). However the P(1)-Mo-P(2) (119.7 ° exp., 116.5 ° calc.) and specially the C(1)-Mo-C(2) (120.1 ° exp., 126.7 ° calc.) angles deviate substantially from those of the octahedron (90 ° and 180 ° respectively). We must recall our compounds are d^4-six-coordinate species and substantial deformations from octahedral geometry towards a bicapped tetrahedron or a trigonal prism have been reported for this kind of complexes.[12]

Actually **2a-Me** can be described as a distorted bicapped tetrahedron in which the two sulphur atoms of the xanthate and the carbon atoms of the acyl and carbonyl ligands occupy the tetrahedron vertices whereas the two trimethyl phosphine ligands are the capping ligands that point toward two faces of the tetrahedron. The angles between the tetrahedral ligands are S(1)-Mo-C(1) = 108.0 ° exp., 101.1 ° calc., S(1)-Mo-C(2) = 118.2 ° exp., 121.1 ° calc., C(1)-Mo-C(2) = 120.1 ° exp., 126.7 ° calc., and S(1)-Mo-S(2) = 70.0 ° exp., 71.5 ° calc.

A detailed theoretical analysis of the deformations from octahedral geometry in d^4 transition-metal complexes has been performed by Kubacek and Hoffmann.[12] The electronic consequences of the deformation from the octahedral geometry toward a bicapped tetrahedron can be understood with very simple orbital arguments.[13] In Scheme 3 we have traced a qualitative picture of the energetic evolution of the block-d orbitals along the geometrical deformation. On the left side, there is the well-known orbital splitting for an octahedral ligand field. The three lower energy orbitals (d_{z2}, d_{xy} and d_{yz}) are those oriented away from the ligands, while the two higher energy orbitals (d_{x2-y2} and d_{xz}) point toward the ligands. When going towards the bicapped tetrahedron, the ligands initially in the y-axis are bent away toward negative values of the Z-coordinate. The d_{x2-y2} orbital is stabilised because its two lobes directed along the y-axis are no longer pointing toward the two ligands. The energy of the d_{yz} orbital is rised because the two ligands that have moved are now pointing toward two lobes of this orbital. The d_{xy} and d_{xz} orbitals do not have contributions from the axial ligands, so they will not be affected by the distortion. The d_{z2} orbital will be only slightly affected.

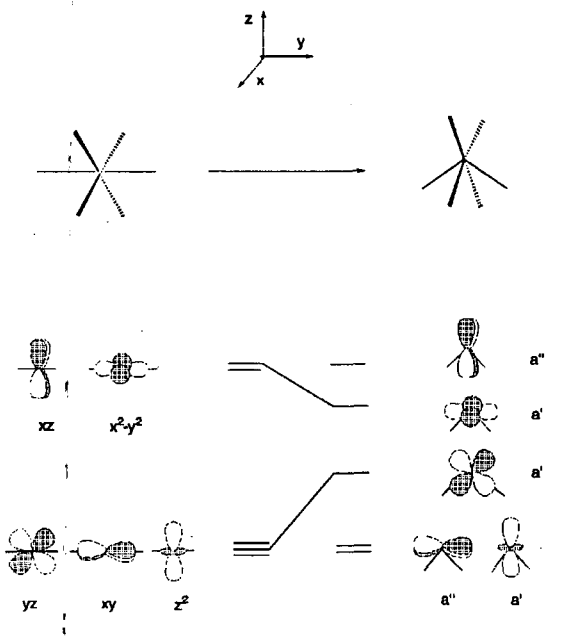

Scheme 3

The resulting orbital energy scheme for the d set of orbitals of a bicapped tetrahedron complex consists in two low energy orbital of different symmetry (a and a in the Cs group representation), two antibonding orbitals of the same symmetry (a) and a highest a antibonding orbital. In a low-spin d^4 complex the two non-bonding orbitals are filled so this is a favourable electron-counting for the bicapped tetrahedral structure.

The most noteworthy feature of complexes **2a-Me**, **7** and **10** is the strong distortion of the metal-acyl fragment with respect to the geometry expected for a monohaptoacyl coordination. This distortion, mainly reflected in the values of the Mo-C(2)-C(3) angles, causes a pivoting of the CH_2R group of the acyl ligand toward the metal. As it can be seen in Table 4 the agostic distortion is also found in the optimized geometries of the model complexes **8**, **9** and **11**. Optimized geometrical parameters of the Mo-acyl fragment agree well with the X-ray determined values.[6] The largest differences are found for the Mo-H distance, but experimental values suffer from the uncertainty in the X-ray placement of H atoms. Although calculations give -agostic structures as the most stable ones for the three systems considered, they are not able to reproduce the experimental differences between **7**, **2a-Me** and **10**. The Mo-C(2)-C(3) angle of **8** (90.8") is in excellent accord with the experimental value of **7** (90.9").[6a] However,

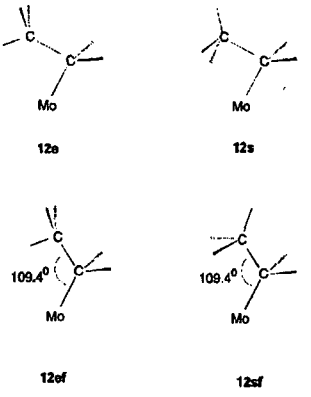

Scheme 4

Table 5: Optimized Geometrical Parameters (and degrees) for the Metal-Ethyl Fragment in $Mo(CH_2CH_3)(S_2CNH_2)(CO)(PH_3)_2$ (**12**).

	12e	12s	12ef	12sf
Mo-C(2)	2.243	2.249	2.246	2.260
Mo-C(3)	2.605	2.654	3.130	3.136
Mo-Ha[a]	2.168	2.683	2.950	3.284
C(3)-Ha[a]	1.127	1.104	1.108	1.101
C(3)-Hb	1.098	1.102	1.098	1.102
C(2)-C(3)	1.546	1.548	1.558	1.550
C(2)-H(2)	1.094	1.095	1.097	1.098
Mo-C(2)-C(3)	84.8	86.6	109.4[b]	109.4[b]
Mo-C(2)-H(2)	118.1	118.4	112.8	113.1
H(2)-C(2)-C(3)	112.7	111.6	108.6	107.9
C(2)-C(3)-Ha	114.1	111.9	113.0	111.9
C(2)-C(3)-Hb	112.0	111.2	110.9	109.5
Rel. Energy[c]	0.0	2.4	11.3	9.3

[a] Ha refers to the hydrogen atom closest to the metal. [b] Fixed value. [c] In kcal mol^{-1}.

the increase of ca. 5 ° of this angle, due to the substitution of a H atom of the acyl CH_2R group by $SiMe_3$ is not found in the model system **9**. There is also a difference for the Mo-C(1)-C(3) angle of 5" between **10** and **11**. The results indicate that the very subtle electronic differences introduced in the experimental systems by changing groups in the S-S donor ligand or the R of the acyl ligand are not accounted for in the model systems.

The origin of the agostic distortion observed in the Mo-acyl complexes can be understood with the help of the qualitative orbital picture presented in Scheme 3. These species are d^4-Mo(II) compounds with a formal valence electron count for Mo of 16. The two occupied d orbitals are d_{z2} and d_{xy}. The bonding of the monohapto C_{acyl} to the metal is mainly due to the interaction of the C_{acyl} lone pair with a lobe of the d_{yz} orbital. The agostic

7

distortion allows the involvement of the d_{x2-y2} orbital in the M-C_{acyl} bond. Both d_{yz} and d_{x2-y2} are a orbitals and mix up to reinforce the M-C_{acyl} bond. At the same time, a new bonding interaction is developed between the d_{x2-y2} orbital and the C(3) and H(2) atoms of the acyl fragment. Thus, an agostic interaction between the metal and the -CH_2R group of the acyl ligand is at work in these systems. In what follows we will analyze in detail this interaction, focusing on the $Mo(COCH_3)(S_2CNH_2)(CO)(PH_3)_2$ system **8**.

Theoretical Analysis of the ß-Agostic Interaction. To our knowledge, the only agostic acyl compounds experimentally characterized are the series of molybdenum complexes $Mo(COCH_2R)(S_2CX)(CO)(PMe_3)_2$. On the contrary several ß-agostic ethyl complexes have been reported,[2] and they are experimental and theoretical

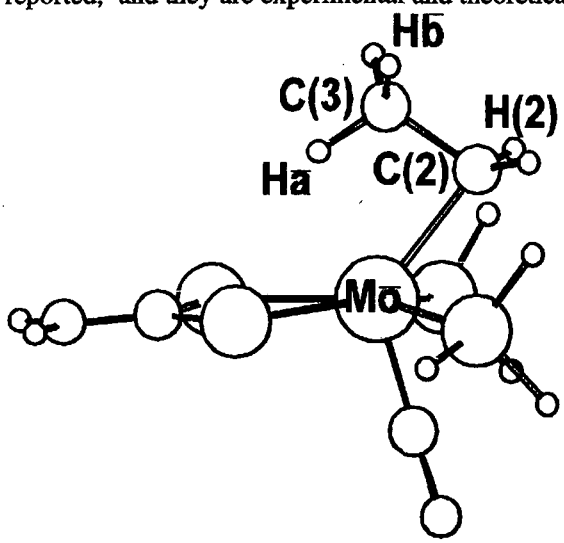

Figure 3: Optimized Geometry of the most stable structure of $Mo(CH_2CH_3)(S_2CNH_2)(CO)(PH_3)_2$ (**12e**).

benchmarks for ethyl -agostic interactions.[14] To go further into the analysis of the specificity of the agostic interaction in acyl complexes we have also analyzed theoretically the interaction of an $Mo(S_2CX)(CO)(PR_3)_2$ metal fragment with an ethyl ligand. Given the electronic structure of this d^4-metal fragment, it may be hoped that it will also develop a -agostic interaction with the ethyl. In this way, we will be able to compare acyl and ethyl -agostic interactions.

In order to analyze better this interaction, we performed for complex **12** a series of geometry optimization with different constraints. These geometries are shown in Scheme 4. The first of

Table 6: Geometrical Parameters (¯ and degrees) for the Metal-Acyl fragment in $Mo(CH_3CO)(S_2CNH_2)(CO)(PH_3)_2$ (**8**).

	8e	**8s**	**8ef**	**8sf**
Mo-C(2)	2.048	2.044	2.106	2.128
Mo-C(3)	2.613	2.661	3.180	3.198
Mo-Ha[a]	2.351	2.800	3.158	3.406
C(3)-Ha	1.103	1.098	1.100	1.101
C(3)-Hb	1.097	1.097	1.098	1.097
C(2)-C(3)	1.595	1.623	1.552	1.549
C(2)-O(2)	1.248	1.248	1.276	1.275
Mo-C(2)-C(3)	90.8	92.3	120.0[b]	120.0[b]
Mo-C(2)-O(2)	147.5	146.7	126.7	125.6
O(2)-C(2)-C(3)	121.7	121.0	113.3	114.4
C(2)-C(3)-Ha	115.7	113.4	113.9	111.1
C(2)-C(3)-Hb	107.4	101.7	107.8	107.1
Rel. Energy[c]	0	4.0	12.7	13,8

[a] Ha refers to the hydrogen atom closest to the metal.
[b] Fixed value.

them, corresponding to the absolute minimum, has no constrains, and has the C -H bond eclipsed with respect to the Mo-C_α bond. It is labeled as **12e**. A second geometry optimization, **12s**, was performed with a forced staggered conformation around the C_α-$C_\beta$bond. Both **12e** and **12s** present an important agostic distortion, with values of the Mo-C_α-$C_\beta$angle of 84.8 ° and 86.6 °, respectively. Two other geometry optimizations, **12ef** and **12sf**, were carried out with an anagostic arrangement. This was accomplished through freezing of the Mo-C_α-$C_\beta$angle to a tetrahedral value of 109.4 °. The relative energies of these four structures, together with the geometrical parameters that describe the ethyl coordination, are collected in Table 5. The optimized geometry of the most stable structure **12e** is presented in Figure 3.

12e is the minimum energy structure for **12**, indicating that a $Mo(S_2CX)(CO)(PR_3)_2$ metal fragment should establish a ß-agostic interaction with an ethyl ligand. Besides the distorted Mo-C_α-C angles, the C_β-H bond that points to the metal is significantly lengthened (1.127 Å vs. 1.10 Å of a normal C-H bond). Moreover geometrical parameters for the metal-ethyl fragment in **12e** are very similar to those of the well characterized ß-agostic EtTiCl3(dmpe) complex.[14] In particular the Mo - C_α - C_β angle is very close to the Ti-C_α-C angle (86.3(6) ° X-ray, 293 K,[14a] 84.57(9)° X-ray, 105 K[14d]). Optimization of **12** with an staggered

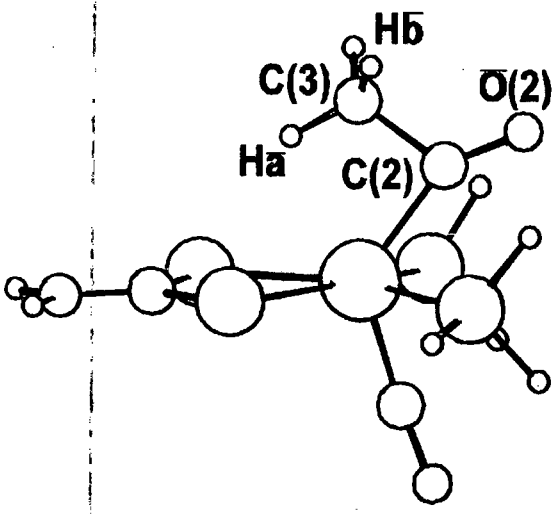

Figure 4: Optimized geometry of the most stable structure of $Mo(COCH_3)(S_2CNH_2)(CO)(PH_3)_2$ (**8e**).

ethyl group (species **12s**) gives also an agostic conformer, characterized by a Mo-C_α-C angle of 92.3 °. This conformer is calculated to lie only 2.4 kcal mol^{-1} above the minimum structure **12e**. As it has been shown very recently in a thorough study on ß-agostic interactions, these interactions do not necessarily require an ethyl group in which a C_β-H bond points toward the metal atom.[14d] In **12s** all the C_β-H bond distances have the same value, pointing to the absence of a direct M-H interaction. In agreement with the theoretical study of $EtTiCl_3(dmpe)$,[14d] methyl rotation occurs in **12** with only a small change of the Mo-C-C angle. Early EH calculations in the agostic $[Co(C_5Me_5)(Et)(PMe_2Ph)]^+$ complex indicated a different mechanism for the methyl rotation, in which the rotation about the C- Cbond takes place after cleavage of the agostic interaction.[15]

The anagostic structures **12ef** and **12sf** are not minimum in the potential energy surface and have considerably higher energies than **12e**: 11.3 kcal mol^{-1} for the eclipsed **12es** and 9.3 kcal mol^{-1} the staggered **12sf**. The energy of the agostic interaction in **12** is in the range of the interaction energiesdetermined in experimental[16] and computational[17] studies of agostic systems (10-15 kcal mol^{-1}). The pivoting of the methyl group toward the metal causes a notable stabilization of the system. The agostic interaction has been often thought as the result from the electronic donation from a C-H bond to a metal low-lying vacant orbital, to fill a vacant coordination site in an

8

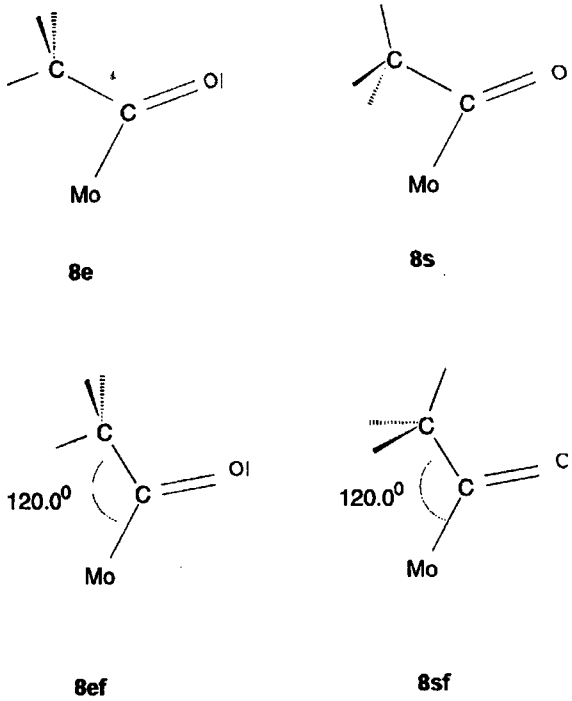

Scheme 5

electron deficient compound.[2,18] There is however a growing number of experimental and theoretical evidences pointing to the need of a more elaborate analysis of agostic interactions. On one hand, it has been recently proved that in some systems steric effects of bulky phosphines can assist in stabilizing agostic interactions.[19] On the other hand, a theoretical study of -agostic interactions in titanium ethyl derivatives has shown that the agostic distortion takes place regardless of the orientation of the C-H bond. Following that analysis, one can divide the agostic interaction in two terms, corresponding to the M-H and M-C interaction. From our calculations it is possible to roughly separate the two contributions in complex **12**. The energy difference between the two eclipsed conformations (11.3 kcal mol^{-1}) gives the total energy of the ß-agostic interaction, whereas the energy difference between the two staggered conformations (6.9 kcal mol^{-1}) approximately gives the Mo - C_β contribution. Thus, the direct M-H component of the agostic interaction in **12** can be estimated as 4.4 kcal mol^{-1}. This component is enough to invert the relative stabilities of the eclipsed and staggered conformations with respect to the anagostic situation. All these energetic values agree with the presence of a strong ß-agostic interaction between the methyl group of the ethyl ligand and the metal fragment in **12**, even stronger

than in $TiEtCl_3$(dmpe). For instance, Becke3LYP calculations in the titanium complex have produced staggered agostic and anagostic structures 0.2 and 1.8 kcal mol^{-1} respectively, above the eclipsed agostic *minimum*.[14c] A value of 8.4 kcal mol^{-1} has been calculated for the ß-agostic stablilization energy of the model $[EtTiCl_2]^+$ cation.[14c]

We have repeated the same calculations presented in the previous paragraph for the ethyl complex **12** in the case of the acyl complex **8**. In this way, in addition to the most stable conformation for the $Mo(C(O)CH_3)(S_2CNH_2)(CO)(PH_3)_2$ system, in which the $C_ß$-H bond eclipses the M-C bond (from now on **8e**), we have also optimized **8** with an staggered acyl (**8s**), and avoiding the ß-agostic interaction by fixing the Mo-$C_α$-C angle at 120 ° with an eclipsed (**8ef**) and staggered (**8sf**) acyl conformations (see Scheme 5). Geometrical parameters describing the metal-acyl fragment in the four structures, together with their relatives energies are collected in Table 6. The optimized geometries of the most stable structure is pictured in Figure 4.

At first glance, results for **8** and **12** are very similar. In the most stable conformation of both a very acute Mo-$C_α$-C angle is found and a $C_ß$-H bond of the terminal methyl eclipses the M- Cbond. So, an agostic interaction is taking place. In both the ethyl and acetyl derivatives the agostic distortion is still present in the staggered conformation (Mo-$C_α$-C angles of 86.6 ° and 92.3 ° in **12s** and **8s**, respectively). It is clear there is no need of a direct M-H interaction for the agostic distortion to take place. In **8** and **12** methyl rotation occurs with a low energy barrier and with only a small variation of the Mo-$C_α$-C angle. The energetic gain associated to the distortion is also similar (around 12 kcal mol^{-1}). However, a more detailed inspection of data shows important differences between **8** and **12**. The separation of the M-H and Mo - $C_ß$ contributions to the agostic stabilization of **8e** (12.7 kcal mol^{-1}) gives an estimation of 9.8 kcal mol^{-1} for the Mo - $C_ß$ component and only 2.9 kcal mol^{-1} for the M-H component. The Mo ··· $C_ß$ bonding plays a more important role in stabilizing the ß-agostic acyl than it does in the ethyl derivative.

Geometrical parameters of the agostic structures of **8** are in accord with this behavior. In contrast to what is found in **12**, in **8e** there is not a significant increase of the in-plane C- H bond distance. On the contrary, a remarkable lengthening of the C - C bond distance occurs in **8e** and **8s**. This fact can be seen by comparing the $C_α$-C distance in agostic and anagostic eclipsed structures (1.595 Å and 1.552 Å, respectively). The value in **8ef** is very similar to that determined by X-ray diffraction in the monohaptoacyl complex $CpMo(COCH_3)(CO)_2(PPh_3)$ (1.555 Å), in which a normal Mo-$C_α$-Cangle of 120.9 ° was found.[11] To assure that the interaction Mo - C is the responsible for the increase of the C – C distance, we have also optimized the species CH_3CONa, with a fixed Na-C-O angle of 120 °. A value of 1.563 Å was obtained for the C – C distance, confirming that our methodology furnishes acyl C – C distances not longer than 1.56 Å when a metal – C interaction is not present. A similar stretching of C – C bonds has been found in several theoretical studies[17a,17b,20] and in a very recent X-ray diffraction study.[21] In all cases it has been interpreted in terms of C – C agostic interaction. Interestingly, the variation of the $C_α$-C distance between **12e** and **12ef** although slight, is in the opposite direction. A small reduction of the C – C bond distance is obtained in going from the anagostic to the agostic structures (from 1.558 Å to 1.546 Å).

It is also worth of mentioning the shortening of the Mo-$C_α$ bond distance in forming the agostic interaction. Although this trend is observed in both the ethyl and acetyl derivatives, it becomes much more pronounced in the acyl agostic. This fact has also been proved in agostic alkylidene transition metal complexes,[22] and has been interpreted from extended Hückel by saying that the strengthening of the Mo-$C_α$ bond is the driving force for the agostic distortion.[23] It must be remarked that in **8** the strengthening of the Mo-$C_α$ bond and the weakening of the $C_α$-C in the agostic structures are also coupled with a remarkable shortening of the acyl CO distance (from 1.270 Å in **8ef** to 1.248 Å in **8e**).

Our theoretical studies on the acetyl complex indicate an important activation of the $C_α$-C in the agostic structures. To see if that is a consequence of the presence of the agostic methyl group in the acyl ligand or is a more general phenomenon we have also considered the same dithiocarbamate metal fragment but now with a formyl ligand. The optimized geometry of $Mo(HCO)(S_2CNH_2)(CO)(PH_3)_2$ model complex is similar to that found for the acetyl compound. A strong agostic distortion is taking place in the formyl system, reflected in the very acute Mo-$C_α$-HangleOther remarkable geometrical parameters are the $C_α$-H, Mo-Cand acyl C – O bond distances of 1.336 Å, 1.937 Å, and 1.334 Å, respectively. All these values, together with the Mo – H distance of 1.844 Å suggest that the structure we have obtained

is along the path of the migratory CO insertion reaction.

Comparison between ethyl and acyl - agostic molybdenum complexes has shown that, in spite of the similar structural features they present, there is an important difference between them. Whereas the agostic ethyl complex can be considered as an arrested structure on an initial step of the reaction path corresponding to elimination, the agostic acetyl complex can be seen as an arrested point in the CO insertion reaction into the Mo - C bond. In the next section we will analyze further this latter aspect.

Migratory CO Deinsertion Reaction. Our experimental results[6,9a,28] indicate that molybdenum and tungsten acyl complexes $M(COCH_2R)(S_2CX)CO(PMe_3)_2$ can easily undergo CO deinsertion to produce the seven coordinate alkyl-carbonyl isomers $M(CH_2R)(S_2CX)(CO)_2(PMe_3)_2$. In addition, we have shown in the preceeding section that an important lengthening of the acyl C-C bond is associated to the agostic distortion. To establish the relationship between such distortion and the C-C bond breaking process we have theoretically studied the reaction path for the interconversion between the -agostic acyl and alkyl-carbonyl isomers of **8**.

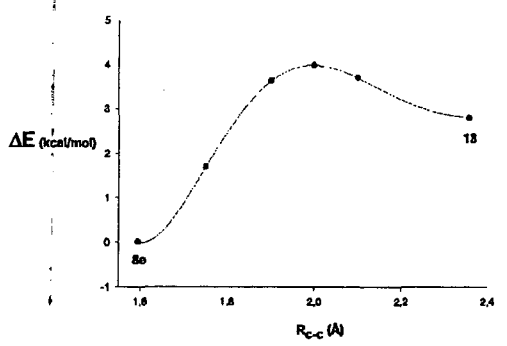

Figure 5: Energy profile for the lengthening of the C-C distance in the complex $Mo(COCH_3)(S_2CNH_2)(CO)(PH_3)_2$ (**8e**).

Starting from the minimum **8e**, we have calculated the energy profile for the CO deinsertion by optimizing the geometry of the system at several fixed values of the C-C distance. The potential energy curve obtained is presented in Figure 5. A maximum is reached at C-C = 2.0 Å. Full geometry optimization starting at the geometry with C-C = 2.1 Å leads to a stable seven-coordinate species **13** with a methyl carbonyl nature (C···C = 2.357 Å, see Figure 6).

Inspection of the geometrical changes along the reaction coordinate shows that, as expected, the C -C lengthening is accompanied by

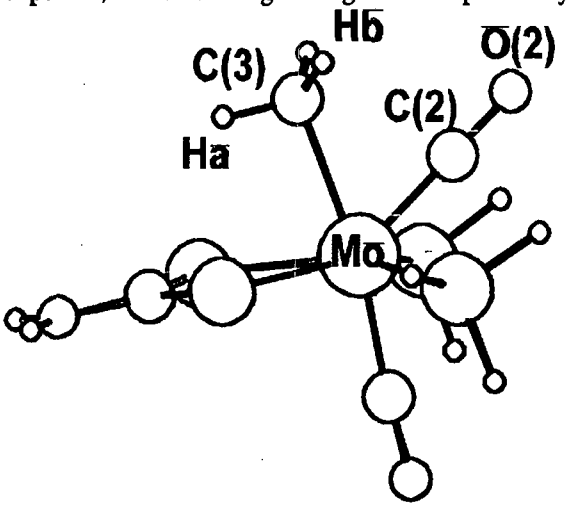

Figure 6: Optimized geometry of the $Mo(CH_3)(S_2CNH_2)(CO)_2(PH_3)_2$(**13**) complex.

CO shortening, Mo-C shortening and closure of the Mo-C-C angle. Only the geometrical parameters of the metal-acyl fragment change appreciably, the rearrangement of the other ligands in the coordination sphere of the metal being only minor. In the methyl-carbonyl structure the Mo-C and Mo-C distances have values of 1.932 Å and 2.390 Å respectively and the Mo-C-C has closed to 66.9 °. The seven-coordinate species is better described[24] as a capped octahedron, with the carbonyl CO group as capping ligand, although quite distorted because of the presence of the chelating xanthate ligand (Figure 6). We note that other heptacoordinate species may be attainable with a low energy barrier for the interconversion. We have limited the study of the methyl-carbonyl derivatives to the one directly reached by the breaking of the acyl C-C bond in the conformation it has in the minimun energy structure.

The most remarkable result of this calculation is the extremely low energy barrier (4.0 kcal mol^{-1}) found for the C-C bond breaking process in the molybdenum acyl complex **8**.

11

Moreover, the alkyl-carbonyl structure **13** lies only 2.8 kcal mol^{-1} above the acyl isomer. So that, the reverse reaction, the migratory CO insertion takes place with an energy barrier of only 1.2 kcal mol^{-1}. This value is much lower than those previously calculated for the migratory CO insertion in $Rh(PH_3)_2Cl(H)(CH_3)(CO)$ (27.4 kcal mol^{-1})[8] and in $CH_3Mn(CO)_5$ (18 kcal mol^{-1}).[25] The energy barriers for the C-C bond forming and breaking processes in **8** are of the same order than those of the methyl rotation. Interestingly, this result is fully consistent with our previous experimental observation of a fluxional behavior of leading to the equivalence of the two carbonyl groups. This process is likely to go also through a 7-coordinate methyl species, and its free energy of activation was estimated to be 9.4 kcal mol^{-1}. The difference between this value and the 4.0 kcal mol^{-1} computed here is likely associated to the fact that **8e** does not seem the most appropriate isomer for the fluxionality process, which probably requires more severe rearrangements and the involvement of higher energy 7-coordinate isomers. For comparative purposes, we have also computed the energy profile for the -elimination in **8**. In this case the C-H bond is broken. Optimization of several points at fixed values of the C-H distances gives a monotonous energy raising: 9.0 kcal mol^{-1} at C-H= 1.30 Å, 25.7 kcal mol^{-1} at C-H = 1.50 Å, 42.5 kcal mol^{-1} at C-H = 1.75 Å and 46.3 kcal mol^{-1} at C-H = 1.90 Å. There is not a minimum for the system in this direction.

It is clear that the -agostic interaction between the terminal methyl group of the acyl ligand and the metal is able to stabilize a very advanced structure in the reaction path that leads to the alkyl-carbonyl species. Besides this interaction assists the C-C bond breaking process. The small energy difference between the acyl and alkyl-carbonyl isomers of 8 justifies that subtle changes in the basicity of the metal, in the donating power of the ancillary ligands or in the steric requirements could shift significantly the acyl/alkyl-carbonyl equilibrium.

Solution behavior of Compounds 2-6. Multinuclear (^1H, $^{13}C\{^1H\}$ and $^{31}P\{^1H\}$) NMR studies of solutions prepared from crystalline samples of **2a-Me** or **2a-Ph** in $C_6D_5CD_3$, C_6D_6 or CD_2Cl_2 clearly show the existence of two sets of resonances. By comparison with the data already available for dihapto and agostic acyls of composition $Mo(C(O)CH_3)(S_2CX)CO(PMe_3)_2$,[6] the spectra can inequivocally be assigned to a mixture of the two kind of complexes, that is, the agostic (R = Me, **2a-Me**; Ph, **2a-Ph**) and the dihapto Mo(2-C(O)CH_2SiMe_2R)(S_2CNMe_2)$CO(PMe_3)_2$ (R = Me, **2d-Me**; Ph, **2d-Ph**) isomers, the latter being predominant. In the mentioned solvents the **2d/2a** ratio does not change appreciably, either with time or temperature, once the values of 6.6 (R = Me) and 3.4 (R = Ph) are attained. The agostic-to-dihapto acyl isomerization is favourable even at low temperatures. Thus when a crystalline sample of **2a-Me** is dissolved at -40 °C and the NMR spectra recorded at that temperature, a **2d/2a**-Me ratio of ca. 1 is already observed and this value quickly increases to ca. 6 upon warming at room temperature. Further cooling of the mixture does not cause any observable variation. Interestingly, an identical isomeric composition is obtained when a crystalline sample of **2d-Me** is dissolved. It seems therefore clear that the agostic acyls **2a** readily evolve in solution to their dihaptoacyl isomers **2d** until the equilibrium is achieved (Scheme 6). This behaviour parallels prior observations for the acetyl compounds $Mo(C(O)CH_3)(S_2COR')CO(PMe_3)_2$ (R' = Me, Et, *i*-Pr) which cristallize as the agostic form but exist in solution mostly as mixtures of the **A** and **D** structures (Scheme 7). At variance with the above, compound **3** exists in solution as the dihapto isomer predominantely, with only minor signals due to the agostic species.

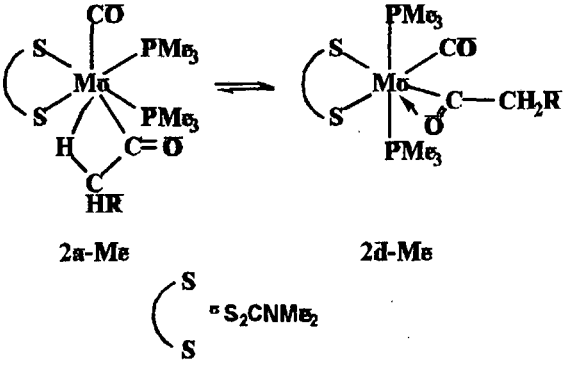

Scheme 6

In contrast with their acetyl-dithiocarbamate counterparts, the xanthate compounds **5** and **6** occur in solution in the form of the dihaptoacyl isomer only. The same applies to the pyrrolyl dithiocarbamate derivative **4**. It is worth mentioning at this point that the dihaptoacyls **2d-6d** display dynamic properties in solution. For instance the two ^{31}P nuclei of complex **2a-Me** appear at -90 °C as an AB spin system with $^2J_{PP}$ = 115 Hz. This pattern of lines coallesces upon warming and finally gives a singlet at room temperature. As described previously, this fluxional

behavior is due to a libration motion of the ^{2}-acyl moiety, which converts the equatorial into an effective plane of symmetry.[26]

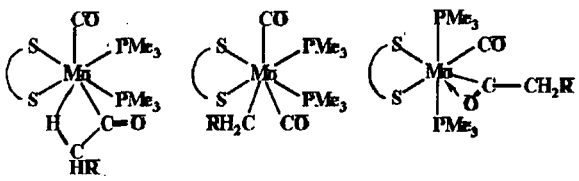

A C D

Scheme 7

With regards to the relative stability of the isomeric acyl structures, the silyl derivatives **2-6** follow the trend already described for the corresponding acetyl complexes (R = H). For the latter compounds, strongly donating chelating ligands favour the agostic coordination, whereas less electron releasing ligands enhance the dihapto structure. Thus, in our case the dimethyl dithiocarbamate derivatives **2** exist in solution as isomeric mixtures, while the complex **4d-Me**, which contains the less donating pyrrol dithiocarbamate[27] exists in solution exclusively as the dihapto isomer.

The avaibility of the silyl derivatives **2-6** allows in addition to establish a sequence of reactivity in what concerns the tendency of compounds of composition $Mo(C(O)CH_2R)(S_2CNMe_2)CO(PMe_3)_2$ to undergo exchange between the isomeric agostic acyl (**A**), dihaptoacyl (**D**) and alkyl carbonyl (**C**) structures (Scheme 7). The molybdenum acyl complex $Mo(C(O)CH_2CMe_3)(S_2CNMe_2)CO(PMe_3)_2$ derived from the neopentyl group, i. e. with R = CMe_3, exists only as the dihapto isomer, while the corresponding acetyl derivative (R = H) occurs as the agostic complex. In this case, however, variable temperature NMR studies have shown[9b,c] that the two degenerate ground-state structures possible for this compound (and its analogous) interconvert fastly at room-temperature through the undetected alkyl(carbonyl) isomer **C**. When R = $SiMe_3$, an intermediate situation is found because, as described above, the solutions of these complexes contain mixtures of the agostic and the dihapto acyl isomers. These differences appear to be mostly steric in origin.[28]

Some final comments will be devoted to the interconversion of structures of type **A** and **D**. Obviously, the proposed mechanism should take into account the different stereochemistry of the two isomers. Thus, simple releasing of the -CH interaction and re-coordination of the acyl through the oxygen atom would not be satisfactory. As mentioned both throughout this article and in previous publications[6,9a,29] molybdenum and tungsten acyl complexes of composition $M(C(O)CH_2R)(S_2CX)CO(PMe_3)_2$ can readily undergo deinsertion to produce the corresponding seven coordinate alkyl-carbonyl isomers $M(CH_2R)(L\text{-}L)(CO)_2(PMe_3)_2$. Since seven-coordinate species can easily undergo ligand rearrangements, a plausible mechanism for the isomerization process could involve CO deinsertion from the agostic complexes to give the corresponding alkyl-carbonyls, followed by ligand redistribution and subsequent CO insertion to generate the dihaptoacyl compounds with their preferred stereochemistry (Scheme 8). Similar seven-coordinate intermediates have been proposed for the irreversible transformation of [Mo](^{2}-C(O)R)(CNR') complexes into their isomeric dihaptoiminoacyl-carbonyl compounds [Mo](^{2}-C(NR')R)(CO).[29] In addition we have demonstrated that tungsten alkyls of composition $W(CH_2R)(S_2CNMe_2)(CO)_2PMe_3$ show fluxional behaviour at room temperature due to ligand mobility around the coordination sphere of the metal.[30]

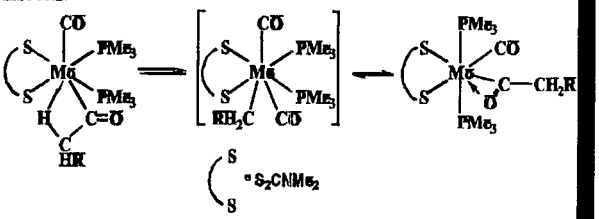

Conclusions

Small energy differences have been observed between the agostic and the dihapto coordination modes of the acyl ligand in $Mo(C(O)CH_2SiMe_2R)(S_2CX)(CO)(PMe_3)_2$ complexes. As previously observed in the analogous acetyl derivatives, strongly electron-releasing ligands appear to favour the agostic interaction, but the preference is not however very pronounced so that small changes in the steric effects around the metal, or in the nature of the co-ligands can unbalance the situation in favour of any of the two isomers.

Ab initio calculations show that the agostic interaction between the acyl ligand and the Mo atom observed in the $Mo(C(O)CH_2R)(S_2CNH_2)(CO(PH_3)_2$ models, is significant and lie well in the range observed for other M-H-C non-classical interactions that exist in metal alkyls. Separation between the M-H and M-C contributions indicates an stronger importance of the latter (9.8 vs. 2.9 kcal mol^{-1}), thus allowing the

rotation around the C-C bond without cleavage of the agostic interaction. By comparing with the monohapto situation, the interaction between the $C(O)CH_3$ fragment and the metal center proximates the Mo and C atoms, shortens the C-O and Mo- C bonds, and lengthens the C-C bond. This scenario can be viewed as an advanced intermediate along the reaction path of the CO deinsertion process in a monohapto acyl. An Energy profile of the agostic acyl to the alkyl-carbonyl carried out by optimization of the molecular geometries at different C-C bond distance values indicates a low energy barrier for the deinsertion process, in excellent accord with the behavior observed in solution for the $Mo(C(O)CH_3)(S_2CX)CO(PMe_3)_2$ complexes.

Experimental Section

Microanalyses were carried out either by the Analytical Service of the University of Sevilla or by Pascher Microanalytical Laboratory, Remagen (Germany). IR spectra were recorded both as nujol mulls or in an appropriate solvent on a Perkin-Elmer 684 instrument. ^1H, ^{13}C and ^{31}P NMR spectra were adquired on a Varian XL-200 spectrometer. $^{31}P\{^1H\}$ NMR shifts were referenced to external 85 % H_3PO_4, while $^{13}C\{^1H\}$ and ^1H shifts referenced to the residual protio signals of deuterated solvents. All data are reported in ppm downfield from $MeSi_4$. All manipulations were performed under oxigen-free nitrogen or argon following conventional Schlenk techniques or by using a Vacuum Atmospheres drybox. Solvents were dried under an appropriate dessicant, deoxigenated and freshly distilled prior to use. $Mo(^2\text{-}C(O)CH_2SiMe_3)Cl(CO)(PMe_3)_3$[6a] and $ZnCl_2(PMe_3)_2$[6c] were prepared as described previously. Dithiocarbamate and xanthate salts as well as PMe_3 were synthesized according to literature procedures. Sodium dimethyldithiocarbamate was dried by heating at 90 °C at 10^{-2} torr for three days. All other reagents were purchased from commercial suppliers.

$Mo(^2\text{-}C(O)CH_2SiMe_2Ph)Cl(CO)(PMe_3)_3$ (1-Ph). Over a yellow suspension of $MoCl_2(CO)_2(PMe_3)_3$ (0.45 g, 1.0 mmol) and $ZnCl_2(PMe_3)_2$ in diethyl ether was slowly added 1.2 mmol of $MgClCH_2SiMe_2Ph$ (1.4 mL, 0.86 M solution). On addition colour progresively turns orange-red. The mixture is stirred for 5 h and volatiles removed under vacuo. Extraction in a 1:1 petroleum ether:diethyl ether mixture followed by centrifugation and concentration of the resulting red liquor afforded 0.37 g of **1-Ph** as red crystals (65 % yield). Anal. Calcd. for $C_{20}H_{40}O_2P_3SiClMo$: C, 42.5; H, 7.1. Found: C, 42.8; H, 7.4. IR (Nujol mull cm^{-1}): 1794 (s), 1507 (m) (CO). ^1H NMR (20 °C, C_6D_6): 0.52 (s, $SiMe_2$), 1.04 (t, J_{HP} = 3.0 Hz, PMe_3), 1.20 (d, J_{HP} = 8.0 Hz, 2 PMe_3), 3.20 (s, CH_2), 7.20, 7.58 (m, Ph). $^{31}P\{^1H\}$ NMR (20 °C, C_6D_6): 23.3 (d, J_{PP} = 23 Hz), 37.5 (t, J_{PP} = 23 Hz). $^{13}C\{^1H\}$ NMR (20 °C, CD_3COCD_3): -1.7 (s, $SiMe_2$), 15.5 (t, J_{CP} = 10 Hz, PMe_3), 20.3 (d, J_{CP} = 25 Hz, PMe_3), 39.4 (s, CH_2), 128.5, 129.9, 134.3, 138.7 (s, Ph), 251.4 (dt, J_{CP} = 31, 10 Hz, CO), 271.4 (q, J_{CP} = 12 Hz, COR).

Preparation of $Mo(C(O)CH_2SiMe_2R)(L\text{-}L)CO(PMe_3)_2$ complexes. L-L = S_2CNMe_2; R = Me (2a-Me, 2d-Me), Ph (2a-Ph); $S_2CN(i\text{-}Pr)_2$ R = Me (3d-Me); $S_2CNC_4H_4$, R = Me (4d-Me); $S_2CO\text{-}i\text{-}Pr$, R = Me (5d-Me), Ph (5d-Ph); $S_2CO\text{-}t\text{-}Bu$, R= Me (6d-Me). All these compounds were prepared in a similar way by treating the chloroacyl $Mo(^2\text{-}C(O)CH_2SiMe_2R)Cl(CO)(PMe_3)_3$ with 1.2 equivalents of the sodium or potassium salts of the bidentate ligands in diethyl ether or tetrahydrofuran at room temperature. The synthesis of **2-Ph** is presented as representative example.

A crystalline sample of **1-Ph** (0.56 g, 1.0 mmol) was dissolved in 40 mL of THF and cooled in an ice bath. Anhydrous NaS_2CNMe_2 (0.17 g, 1.2 mmol) was added to the reaction mixture producing a colour change from deep red to orange. The resulting suspension was stirred at room temperature for 2h at 0-10 °C after what volatiles were removed and the resulting residue was extracted with a 1:1 petroleum ether:diethyl ether mixture. Centrifugation followed by concentration and cooling at -10 °C of the liquour afforded **2a-Ph** as orange crystals in 80 % yield. From the corresponding chloro-acyl complexes and the appropriate dithiocarbamate or xanthate salts the following compounds were obtained in similar yields. These compounds were isolated as orange-red crystalline solids, except **4d-Me** which is purple, by crystallization of their solutions in petroleum ether-diethylether mixtures.

Although some spectroscopic data for the complex $Mo(C(O)CH_2SiMe_3)(S_2CNMe_2)(CO)(PMe_3)_2$ (**2a-Me** and **2d-Me**) have already been reported, for the sake of completeness, their most relevant spectroscopic data are indicated below.

$Mo(C(O)CH_2SiMe_3)(S_2CNMe_2)CO(PMe_3)_2$ (2a-Me). IR (Nujol mull cm^{-1}): 1760 (s), 1615 (m) (CO), 1515 (m) (CN). ^1H NMR (20 °C, C_6D_6): 0.28 (s, $SiMe_3$), 1.42 (d, J_{HP} = 8.8 Hz, PMe_3), 2.56 (brs, CH_2), 2.60 (s, NMe_2). $^{31}P\{^1H\}$ NMR

(20 °C, C_6D_6): 26.7 (brs). $^{13}C\{^1H\}$ NMR (20 °C, C_6D_6): 0.5 (s, SiMe3), 15.8 (d, J_{CP} = 28 Hz, PMe3), 38.6 (s, NMe_2). Other carbon resonances were not observed due probably to the low concentration of this compound in solution.

Mo(^{2}-C(O)CH$_2$SiMe3)(S$_2$CNMe$_2$)(CO)(PMe3)$_2$ (2d-Me). IR (Nujol mull cm^{-1}): 1750 (s), 1490 (m) (CO), 1515 (m) (CN). ^1H NMR (20 °C, C_6D_6): 0.14 (s, SiMe3), 1.56 (t, J_{HP} = 3.6 Hz, PMe3), 3.08 (s, CH_2), 2.77, 2.83 (s, NMe_2). $^{31}P\{^1H\}$ NMR (20 °C, C_6D_6): 2.5 (s). $^{13}C\{^1H\}$ NMR (20 °C, C_6D_6): -0.7 (s, SiMe3), 15.7 (t, J_{CP} = 11 Hz, PMe3), 37.7 (s, CH_2), 39.2, 39.8 (s, NMe_2), 210.3 (s, S_2C), 238.2 (t, J_{CP} = 16 Hz, CO), 275.5 (t, J_{CP} = 16 Hz, *C*OR).

Mo(C(O)CH$_2$SiMe$_2$Ph)(S$_2$CNMe$_2$)(CO)(PMe$_3$)$_2$ (2a-Ph). Anal. Calcd. for $C_{20}H_{37}NO_2P_2S_2SiMo$: C, 41.9; H, 6.4; N 2.4. Found: C, 42.2; H, 6.8; N, 1.6. IR (Nujol mull cm^{-1}): 1785 (s), 1615 (w) (CO). ^1H NMR (20 °C, C_6D_6): 0.58 (s, $SiMe_2$), 1.37 (d, J_{HP} = 8.9 Hz, PMe3), 2.58 (s, $N(CH_3)_2$), 2.69 (brs, CH_2), 7.25, 7.70 (m, Ph). $^{31}P\{^1H\}$ NMR (20 °C, C_6D_6): 27.9 (brs). $^{13}C\{^1H\}$ NMR (20 °C, C_6D_6): -0.8 (s, $SiMe_2$), 15.5 (d, J_{CP} = 28 Hz, PMe3), 38.8 (s, $N(CH_3)_2$), 128.3, 129.0, 134.5, 140.2 (s, Ph). Other carbon resonances were not observed due probably to the low concentration of this compound in solution.

Mo(^{2}-C(O)CH$_2$SiMe$_2$Ph)(S$_2$CNMe$_2$)(CO)(PMe3)$_2$ (2d-Ph). IR (THF cm^{-1}): 1775 (s) (CO). ^1H NMR (20 °C, C_6D_6): 0.46 (s, SiMe3), 1.52 (t, J_{HP} = 3.6 Hz, PMe3), 2.77, 2.82 (s, $N(CH_3)_2$), 3.28 (s, CH_2), 7.19, 7.50 (m, Ph). $^{31}P\{^1H\}$ NMR (20 °C, C_6D_6): 3.6 (s). $^{13}C\{^1H\}$ NMR (20 °C, C_6D_6): -1.8 (s, $SiMe_2$), 15.9 (t, J_{CP} = 11 Hz, PMe3), 37.1 (s, CH_2), 39.5, 40.1 (s, $N(CH_3)_2$), 128.2, 129.6, 134.1, 138.1 (s, Ph), 210.5 (s, S_2C), 238.7 (t, J_{CP} = 14 Hz, CO), 275.9 (t, J_{CP} = 16 Hz, *C*OR).

Mo(^{2}-C(O)CH$_2$SiMe3)(S$_2$CN-*i*-Pr$_2$)(CO)(PMe3)$_2$ (3d-Me). Anal. Calcd. for $C_{19}H_{43}NO_2P_2S_2SiMo$: C, 40.2; H, 7.6, N, 2.5. Found: C, 40.5; H, 7.6, N, 2.7. IR (Nujol mull cm^{-1}): 1760 (s), 1475 (m) (CO), 1490 (m) (CN). ^1H NMR (20 °C, C_6D_6): 0.12 (s, SiMe3), 1.19 (brs, $CH(CH_3)_2$), 1.56 (t, J_{HP} = 3.5 Hz, PMe3), 3.05 (s, CH_2), 4.60 (brs, CH). $^{31}P\{^1H\}$ NMR (20 °C, C_6D_6): 4.8 (s). $^{13}C\{^1H\}$ NMR (20 °C, C_6D_6): -0.6 (s, SiMe3), 15.7 (t, J_{CP} = 11 Hz, PMe3), 19.3, 19.7 (s, $CH(CH_3)_2$), 38.0 (s, CH_2), 50.0, 50.8 (s, CH), 209.7 (t, J_{CP} = 7 Hz, S_2C), 237.9 (t, J_{CP} = 14 Hz, CO), 276.0 (t, J_{CP} = 16 Hz, *C*OR).

Mo(^{2}-C(O)CH$_2$SiMe3)(S$_2$CNC$_4$H$_4$)(CO)(PMe3)$_2$ (4d-Me). Anal. Calcd. for $C_{17}H_{33}NO_2P_2S_2SiMo$: C, 38.3; H, 6.2, N, 2.6. Found: C, 37.8; H, 5.9, N, 2.6. IR (Nujol mull cm^{-1}): 1780 (s), 1465 (m) (CO), 1485 (m) (CN). ^1H NMR (20 °C, C_6D_6): 0.08 (s, SiMe3), 1.39 (t, J_{HP} = 3.7 Hz, PMe3), 3.00 (s, CH_2), 6.10, 7.80 (t, CH). $^{31}P\{^1H\}$ NMR (20 °C, C_6D_6): 5.8 (s). $^{13}C\{^1H\}$ NMR (20 °C, C_6D_6): -0.6 (s, SiMe3), 15.8 (t, J_{CP} = 12 Hz, PMe3), 37.8 (s, CH_2), 112.9, 117.9 (s, CH), 208.7 (t, J_{CP} = 8 Hz, S_2C), 237.1 (t, J_{CP} = 15 Hz, CO), 276.0 (t, J_{CP} = 16 Hz, *C*OR).

Mo(^{2}-C(O)CH$_2$SiMe3)(S$_2$CO-*i*-Pr)(CO)(PMe3)$_2$ (5d-Me). Anal. Calcd. for $C_{16}H_{36}NO_2P_2S_2SiMo$: C, 35.5; H, 6.8. Found: C, 35.3; H, 6.8. IR (Nujol mull cm^{-1}): 1795 (s), 1485 (m) (CO). ^1H NMR (20 °C, C_6D_6): 0.21 (s, SiMe3), 1.07 (d, J_{HP} = 6.2 Hz, $CH(CH_3)_2$), 1.44 (t, J_{HP} = 3.6 Hz, PMe3), 3.02 (s, CH_2), 5.34 (h, J_{HH} = 6.2 Hz, CH). $^{31}P\{^1H\}$ NMR (20 °C, C_6D_6): 5.2 (s). $^{13}C\{^1H\}$ NMR (20 °C, C_6D_6): 1.0 (s, SiMe3), 15.7 (t, J_{CP} = 11 Hz, PMe3), 21.4 (s, $CH(CH_3)_2$), 37.8 (s, CH_2), 74.5 (s, CH), 222.3 (t, J_{CP} = 6 Hz, S_2C), 236.7 (t, J_{CP} = 15 Hz, CO), 276.7 (t, J_{CP} = 16 Hz, *C*OR).

Mo(^{2}-C(O)CH$_2$SiMe$_2$Ph)(S$_2$CO-*i*-Pr)(CO)(PMe3)$_2$ (5d-Ph). Satisfactory elemental analysis was precluded by its thermal instability. IR (Nujol mull cm^{-1}): 1800 (s), 1465 (m) (CO). ^1H NMR (20 °C, C_6D_6): 0.40 (s, SiMe3), 1.10 (d, J_{HP} = 6.2 Hz, $CH(CH_3)_2$), 1.44 (t, J_{HP} = 3.7 Hz, PMe3), 3.23 (s, CH_2), 5.40 (h, J_{HH} = 6.2 Hz, CH), 7.20, 7.46 (m, Ph). $^{31}P\{^1H\}$ NMR (20 °C, THF/CD_3COCD_3): 9.7 (s). $^{13}C\{^1H\}$ NMR (20 °C, C_6D_6): -2.3 (s, $SiMe_2$), 15.5 (t, J_{CP} = 11 Hz, PMe3), 21.3 (s, $CH(CH_3)_2$), 36.9 (s, CH_2), 74.5 (s, CH), 127.9, 129.4, 133.7, 137.4 (s, Ph), 222.3 (t, J_{CP} = 7.8 Hz, S_2C), 237.1 (t, J_{CP} = 13 Hz, CO), 276.6 (t, J_{CP} = 15 Hz, *C*OR).

Mo(^{2}-C(O)CH$_2$SiMe3)(S$_2$CO-*t*-Bu)(CO)(PMe3)$_2$ (6d-Me). Anal. Calcd. for $C_{17}H_{38}NO_2P_2S_2SiMo$: C, 37.8; H, 7.0. Found: C, 38.0; H, 7.1. IR (Nujol mull cm^{-1}): 1760 (s), 1485 (m) (CO). ^1H NMR (20 °C, C_6D_6): 0.12 (s, SiMe3), 1.56 (t, J_{HP} = 3.7 Hz, PMe3), 1.63 (s, CMe_3), 3.20 (s, CH_2). $^{31}P\{^1H\}$ NMR (20 °C, C_6D_6): 5.4 (s). $^{13}C\{^1H\}$ NMR (20 °C, C_6D_6): -0.7 (s, SiMe3), 15.7 (t, J_{CP} = 11 Hz, PMe3), 21.4 (s, $C(CH_3)_3$), 37.8 (s, CH_2), 86.9 (s, $C(CH_3)_3$), 222.1 (t, J_{CP} = 6 Hz, S_2C), 236.9 (t, J_{CP} = 14 Hz, CO), 276.5 (t, J_{CP} = 15 Hz, *C*OR).

Computational Details. All calculations were performed with the GAUSSIAN 94 series of programs.[31] A molecular orbital *ab initio* method with introduction of correlation energy through the

Moller-Plesset (MP) perturbation approach,[32] excluding excitations concerning the lowest energy electrons (frozen core approach), was applied. Effective core potentials (ECP) were used to represent the 28 innermost electrons of the metal atom[33a] as well as the 10 electron core of the phosphorus, sulfur and silicon atoms.[33b] Geometry optimizations were carried out at the second level of the Moller-Plesset theory (MP2) with a basis set of valence double- quality for all the atoms. It has been already proved that the computed MP2 geometries in agostic complexes are in excellent agreement with experimental neutron diffraction data.[34] The basis set used for the metal and the phosphorus, sulfur and silicon atoms was that associated with the pseudopotential[32] with a standard LANL2DZ (Mo) and LANL1DZ (P, S, Si) contraction schemes.[31] For the other atoms the 6-31G basis set was used.[35]

All the geometrical parameters were optimized to find the most stable structure for each compound. In order to evaluate the energy differences between agostic and anagostic geometries, optimizations were performed for the least stable structures keeping fixed the value of the Mo-C-C at 109.4° in **12** and 120 ° in **8**. Symmetry restrictions (Cs) were introduced in the optimizations when possible.

X-ray Structure Determination of 2a-Me. A summary of the fundamental crystal data is given in Table 1. A crystal of **2a-Me** was coated with an epoxy resin and mounted in a Kappa diffractometer. The cell dimensions were refined by least-squares fitting of the values of 25 reflections. The intensities were corrected for Lorentz and polarization effects. Scattering factors for neutral atoms and anomalous dispersion corrections for Mo, P and S were taken from ref 36. The structures were solved by Patterson and Fourier methods. An empirical absorption correction[37] was applied at the end of the isotropic refinement. Final mixed refinement with unit weights and fixed isotropic factors and coordinates for H atoms except for H(31) and H(32) for which the corresponding coordinates were refined, led to final values of R = 0.037 and R_w = 0.055. The final values of the positional parameters are given in Table 2. Most of the calculations were carried out with the X-ray 80 system.[38]

Acknowledgment. We acknowledge financial support from the DGES (Project No PB95-0639-CO2-01) and the DGICYT (grant No. PB94-1436). We also acknowledge Junta de Andalucía for the award of research fellowships. The use of computational facilities of the Centre de Supercomputació i Comunicacions de Catalunya (C^4) is gratefully appreciated. Prof. O. Eisenstein (Montpellier) is acknowledged for fruitful discussions.

Supporting Information Available. Tables of atomic and thermal parameters for **2a-Me** (3 pages). Ordering information is given on any current masthead paper.

16

References

1.() Parshall, G. W.; Ittle, S. D. *Homogeneous Catalysis*, 2nd ed.; Wiley-Interscience: New York 1992. (b) Collman, J. P.; Hegedus, L. S.; Norton, J. R.; Finke, R. G. *Principles and Applications of Organotransition Metal Chemistry;* University Science Books: Mill Valley, CA, 1987.

2.() (a) Brookhart, M.; Green, M. L. H. *J. Organomet. Chem.* **1983**, *250*, 395. (b) Brookhart, M.; Green, M. L. H.; Wong, L. -L. *Prog. Inorg. Chem.* **1988**, *36*, 1.

3.() (a) Gleiter, R.; Hyla-Kryspin, I.; Niu, S.; Erker, G. *Organometallics* **1993**, *12*, 3828. (b) Crabtree R. H. *Angew. Chem. Int. Ed. Engl.* **1993**, *32*, 789.

4.() (a) Grubbs, R. H.; Coates, G. W. *Acc. Chem. Res.* **1996**, *29*, 85. (b) Brintzinger, H. H.; Fischer, D. F.; M lhaupt, R.; Rieger, B.; Waymouth, R. *Angew. Chem. Int. Ed. Engl.* **1995**, *34*, 1143. (c) Tanner, M. J.; Brookhart, M.; DeSimone, J. M. *J. Am. Chem. Soc.* **1997**, *119*, 7617. (b) Schmidt, G. F.; Brookhart, M. *J. Am. Chem. Soc.* **1985**, *107*, 1443. (d) Han, Y.; Deng, L.; Ziegler, L. *J. Am. Chem. Soc.* **1997**, *119*, 5939.

5.() (a) Jordan, R. F.; Bradley, P. K.; Baenzinger, N. C.; Lapointe, R. E. *J. Am. Chem. Soc.* **1990**, *112*, 1289. (b) Brookhart, M.; Lincoln, D. M.; Bennett, M. A.; Pelling, S. *J. Am. Chem. Soc.* **1990**, *112*, 2691. (c) Conroy-Lewis, F. M.; Mole, L.; Redhouse, A. D.; Litster, S. A.; Spencer, J. L. *J. Chem. Soc., Chem. Comm.* **1991**, 1601. (d) Cracknell, R. B.; Orpen, A. G.; Spencer, J. L. *J. Chem. Soc., Chem. Comm.* **1984**, 326. (e) Turner, H. W.; Schrock, R. R. *J. Am. Chem. Soc.* **1983**, *105*, 4942. (f) Feng, S. G.; White, P. S.; Templeton, J. L. *J. Am. Chem. Soc.* **1990**, *112*, 8192.

6.() (a) Carmona, E.; SÆnchez, L.; Mar n, J. M.; Poveda, M. L.; Atwood, J. L.; Priester, R. D.; Rogers, R. D*J. Am. Chem. Soc.* **1984**, *106*, 3214. (b) Carmona, E.; Contreras, L.; Poveda, M. L.; SÆnchez, L*J. Am. Chem. Soc.* **1991**, *113*, 4322. (c) Contreras, L.; Monge, A.; Pizzano, A.; Ruiz, C.; SÆnchez, L.; Carmona, E*Organometallics* **1992**, *11*, 3971.

7.() Boese, W. T.; Ford, P. C. *J. Am. Chem. Soc.* **1995**, *117*, 8381. (b) Boese, W. T.; Lee, b.; Ryba, D. W.; Belt, S. T.; Ford, P. C. *Organometallics* **1993**, *12*, 4739.

8.() (a) Margl, P.; Ziegler, T.; Bl chl *J. Am. Chem. Soc.* **1996**, *118*, 5412.

9.() For other C-Si heterolysis see for example: (a) Carmona, E.; Contreras, L.; GutiØrrez-Puebla, E.; Monge, A.; SÆnchez, L. J*Organometallics* **1991**, *10*, 71. (b) Allen, S. R.; Green, M.; Orpen, A. G.; Williams, I. D. *J. Chem. Soc., Chem. Comm.* **1982**, 826.

10.() Although the value of (CO) cannot be taken as diagnostic of dihapto coordination, confident assignament can be made along a series of similar compounds: Durfee, L. D.; Rothwell, I. P. *Chem. Rev.* **1988**, *88*, 1059.

11.() Churchill, M. R.; Fennessey, J. P. *Inorg. Chem.* **1968**, *7*, 953.

(12) Kubacek, P.; Hoffmann, R. *J. Am. Chem. Soc.* **1981**, *103*, 4320.

(13) Albright, T.A.; Burdett, J.K.; Whango, M.H. *Orbital interactions in Chemistry*; Wiley: New York, USA, **1985**, pp. 289-294.

(14) (a) Dawoodi, Z.; Green, M.L.H.; Mtetwa, V.S.B.; Prout, K.; Schult, A.J.; Williams, J.M.; Koetzle, T.F. *J. Chem. Soc., Dalton Trans.* **1986**, 1629. (b) McGrady, G.S.; Downs, A.J.; Haaland, A.; Scherer, W.; Mckean, D.C. *Chem. Commun.* **1997**, 1547. (c) Popelier, P.L.A.; Logothetis, G. *J. Organomet. Chem.* **1998**, *555*, 101. (d) Haaland, A.; Scherer, W.; Rund, K.; McGrady, G.S.; Downs, A.J.; Swang, O. *J. Am. Chem. Soc.* **1998**, *120*, 3762.

(15) Cracknell, R.B.; Orpen, A.G.; Spencer, J.L. *J. Chem. Soc, Chem. Commun.* **1986**, 1005.

(16) (a) Crabtree, R.H. *Chem. Rev.* **1985**, *85*, 245. (b) GonzÆlez, A.A.; Zhang, K.; Nolan, S.P.; L pez de la Vega, R.; Mukerjee, S.L.; Hoff, C.D.; Kubas, G.L. *Organometallics* **1988**, *7*, 2429. (c) Burger, B.J.; Thompson, M.E.; Cotter, W.D.; Bercaw, J.E. *J. Am. Chem. Soc.* **1990**, *112*, 1566. (d) Zhang, K.; GonzÆlez, A.A.; Mukerjee, S.L.; Chou, S.-J.; Hoff, C.D., Kubat-Martin, K.A.; Barnhart, D.; Kubas, G.J. *J. Am. Chem. Soc.* **1991**, *113*, 9170.

(17) (a) Kawamura-Kuribayashi, H.; Koga, N.; Morokuma, K. *J. Am. Chem. Soc.* **1992**, *114*, 2359. (b) Lohrenz, J.C.W.; Woo, T.K.; Ziegler, T. *J. Am. Chem. Soc.* **1995**, *117* 12793. (c) Margl, P.; Lohrenz, J.C.W.; Ziegler, T.; Bl chl, P.E. *J. Am. Chem. Soc.* **1996**, *118*, 4434. (d) Thomas, J.L.C.; Hall, M.B. *Organometallics* **1997**, *16*, 2318. (e) Musaev, D.G.; Froese, R.D.J.; Svensson, M.; Morokuma, K. *J. Am. Chem. Soc.* **1997**, *119*, 367. (f) Han, Y.; Deng, L.; Ziegler, T. *J. Am. Chem. Soc.* **1997**, *119*, 5939. (g) Deng, L.; Woo, T.K.; Cavallo, L.; Margl, R.M.; Ziegler, T. *J. Am. Chem. Soc.* **1997**, *119*, 6177.

(18) (a) Crabtree, R.H. *Angew. Chem. Int. Ed. Engl.* **1993**, *32*, 789. (b) Shilov, A.E.; Shul pin, G.B. *Chem. Rev.* **1997**, *97*, 2879.

(19) Ujaque, G; Cooper, A.C.; Maseras, F; Eisenstein, O.; Caulton, K.G. *J. Am Chem. Soc* **1998**, *120*, 361.

17

(20) Koga, N.; Morokuma, K. *J. Am. Chem. Soc.* **1988**, *110*, 108.
(21) Tomaszewski, R.; Hyla-kryspin, I.; Mayre, C.L.; Arif, A.M.; Gleiter, R.; Ernst, R.D. *J. Am. Chem. Soc.* **1998**, *120*, 2959.
(22) Schultz, A.J.; Brown, R.K.; Williams, J.W.; Schrock, R.R. *J. Am. Chem. Soc.* **1981**, *103*, 169.
(23) (a) Goddard, R.J.; Hoffmann, R.; Jemmis, E.D. *J. Am. Chem. Soc.* **1980**, *102*, 7667. (b) Eisenstein, O.; Jean, Y. *J. Am. Chem. Soc.* **1985**, *107*, 1177. (c) Demolliens, A.; Jean, Y.; Eisenstein, O. *Organometallics* **1986**, *5*, 1457.
(24) Maseras, F.; Eisenstein, O. *New J. Chem.* **1997**, *21*, 961.
(25) Versluis, L.; Ziegler, T. *Organometallics* **1990**, *9*, 2985.
(26) Curtis, M. D.; Shiu, K. B.; Butler, W. M. *J. Am. Chem. Soc.* **1986**, *108*, 1550.
(27) (a) Herrick, R. S.; Templeton, J. L. *Inorg. Chem.* **1986**, *25*, 1270. (b) Kellner, R.; Prokopwoski, P.; Malissa, H. *Anal. Chim. Acta.* **1974**, *68*, 401.
(28) Strong influence of steric effects have been found to favour six-coordinated dihaptoacyl coordination over the seven-coordinated alkyl-carbonyl formulation in related tungsten compounds: see Ref. 30.
(29) Pizzano, A.; SÆnchez, L.; Altmann, M.; Monge, A.; Ruiz, C.; Carmona, E*J. Am. Chem. Soc.* **1995**, *117*, 1759.
(30) Carmona, E.; Contreras, L.; Poveda, M. L.; SÆnchez, L. J.; Atwood, J. L.; Rogers, R. D*Organometallics* **1991**, *10*, 61.
(31) Frisch, M.J.; Trucks, G.W.; Schlegel, H.B.; Gill, P.M.W.; Johnson, B.G.; Robb, M.A.; Cheeseman, J.R.; Keith, T.A.; Petersson, G.A.; Montgomery, J.A.; Raghavachari, K.; Al-Laham, M.A.; Zakrzewski, V.G.; Ortiz, J.V.; Foresman, J.B.; Cioslowski, J.; Stefanov, B.B.; Nanayakkara, A.; Challacombe, M.; Peng, C.Y.; Ayala, P.Y.; Chen, W.; Wong, M.W.; Andr s, J.L.; Replogle, E.S.; Gomperts, R.; Martin, R.L.; Fox, D.J.; Binkley, J.S.; De Frees, D.J.; Baker, J.; Stewart, J.P.; Head-Gordon, M.; Gonzalez, C.; Pople, J.A. *Gaussian 94*; Gaussian Inc.: Pittsburgh PA, 1995.
(32) Moller, C.; Plesset, M.S. *Phys. Rev.* **1934**, *46*, 618.
(33) a)Hay, P.J.; Wadt, W.R. *J. Chem. Phys.* **1985**, *82*, 299. (b) Wadt, W.R.; Hay, P.J. J. *Chem. Phys.* **1985**, *82*, 284.
(34) Weiss, H.; Haase, F.; Ahlrichs, R. *Chem. Phys. Letters* **1992**, *194*, 492.
(35) Hehre, W.J.; Ditchfield, R.; Pople, J. A. *J. Chem. Phys.* **1972**, *56*, 2257.
(36) *International Tables for X-ray Crystallography*; Kynoch Press: Birmingham, U. K., 1974; vol. IV, pp 72-98.
(37) Walker, N.; Stuart, D. *Acta Crystallogr.* **1983**, *A39*, 158.
(38) Stewart, J. M. The X-ray 80 System; Computer Science Center, University of Maryland: College Park, MD, 1985.

Article III

"Different van der Waals Radii for Organic and Inorganic halogen atoms: a Significant Improvement in IMOMM Performace"

Gregori Ujaque, Feliu Maseras, Odile Eisenstein

Theor. Chem. Acc., **96**, 146-150 (1997)

Theor Chem Acc (1997) 96:146-150

Theoretical Chemistry Accounts

Regular Papers

Different van der Waals radii for organic and inorganic halogen atoms: a significant improvement in IMOMM performance

Gregori Ujaque*, Feliu Maseras, Odile Eisenstein

Laboratoire de Structure et Dynamique des Systèmes Moléculaires et Solides, U.M.R. 5636, Université de Montpellier II, F-34095 Montpellier Cedex 5, France

Received: 25 February 1997 / Accepted: 7 April 1997

Abstract. The discrepancies between X-ray and integrated molecular orbital molecular mechanics computed geometries for $Os(H)_2Cl_2(P^iPr_3)_2$ and $Ir(H)_2Cl(P^tBu_2Ph)_2$ are explained by the inadequacy of the default molecular mechanics van der Waals radii for halogen elements. A simple procedure is proposed for the calculation of corrected van der Waals radii, and the application of the corrected radius for chloride is shown to improve substantially the results for the systems under test.

Key words: Van der Waals radii – Organic and inorganic halogen atoms – Integrated molecular orbital molecular mechanics

1 Introduction

Integrated molecular orbital molecular mechanics (IMOMM) is a recently proposed computational scheme [1], that has been already applied successfully to a number of cases [2–5]. It uses two different methodological levels for different parts of the same chemical system, quantum mechanics for the part harder to describe, and molecular mechanics (MM) for the rest, in a way not very different from other proposed schemes [6, 7]. Its accuracy depends on the performance of each one of its two components, the quantum mechanics description must be precise enough to evaluate accurately all interactions within the quantum mechanical region of the system, and the molecular mechanics description must be precise enough to evaluate accurately all the other interactions.

IMOMM implemented with the MM3(92) force field [8] appears to be well suited for the quantification of steric effects in transition metal complexes with bulky ligands [2–4]. There appears to be, however, a systematic error in complexes containing sterically active halide ligands, their steric effects seeming to be underestimated. One of the possible sources of this error is the inadequacy of the default van der Waals radii used in the force field. They are fitted essentially for organic systems, and one may expect that inorganic, more anionic, halogen atoms would have larger radii.

This work proves the validity of this hypothesis and proposes solutions to the problem. In the following sections, the problem is presented, the possible solution is outlined, and its validity is tested on the model systems.

2 The $Os(H)_2Cl_2(P^iPr_3)_2$ and $Ir(H)_2Cl(P^tBu_2Ph)_2$ systems

Tests on two different systems are carried out. The first of them is $Os(H)_2Cl_2(P^iPr_3)_2$ (system **1a** Fig. 1). The chemical characteristics of this particular hexacoordinated species have been discussed in detail elsewhere [5]. It suffices to say that the defining parameter of the steric effect is the X-Os1-P2-C14 dihedral angle, roughly defining the angle between the Os1-P2-P3 and Os1-C14-C15 planes. This dihedral angle has a value of 41.9° in the X-ray structure [9, 10] and a value of 0.0° in a geometry optimization at the restricted Hartree-Fock (RHF) level on the model system $Os(H)_2Cl_2(PH_3)_2$ (**1b**) [11].

This result (0.0°) for the $Os(H)_2Cl_2(PH_3)_2$ model system is confirmed by a more sophisticated ab initio calculation at the BECKE3LYP level [12]. In contrast, a geometry optimization of Fig. **1a** at the IMOMM (BECKE3LYP:MM3) computational level using the aforementioned model system for the quantum mechanical part and the default MM3(92) parameters [8], yielded a dihedral angle of 27.2°. This is a remarkable improvement from the 0.0° obtained on the model system, but still lower than the experimental value of 41.9°. At any rate, the previous proposal of a steric origin for the distortion [11] is qualitatively confirmed.

The second test system is $Ir(H)_2Cl(P^tBu_2PH)_2$ (system **2a** Fig. 2). The geometry of this pentacoordinated complex is better seen as derived from a trigonal

**Permanent address*: Unitat de Quimica Fisica, Department de Química, Universitat Autònoma de Barcelona, E-08193 Bellaterra, Barcelona, Spain
e-mail: maseras@lsd.univ-montp2.fr
Correspondence to: F. Maseras

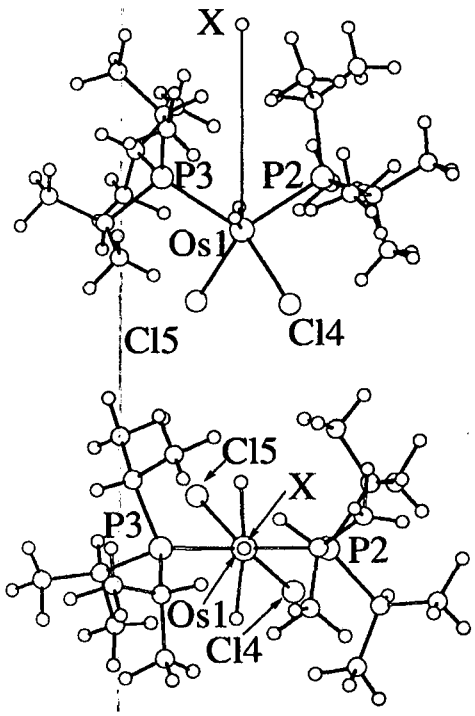

Fig. 1. X-ray structure of $Os(H)_2Cl_2(P^iPr_3)_2$ [9,10]. X is a dummy atom on the bisector of the P2-Osl-P3 angle. Two different views are shown for clarity

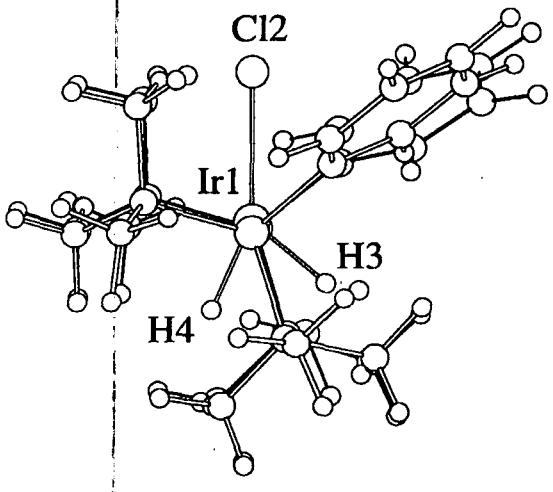

Fig. 2. X-ray structure of $Ir(H)_2Cl(P^tBu_2Ph)_2$ [10,13]

bipyramid with the phosphine ligands in the axial positions. The metal centre and the other three ligands (Cl2, H3, H4) lie essentially in a plane. The X-ray structure shows a remarkable asymmetry between the two Cl—Ir—H bond angles: Cl2—Ir1—H3 is 131.1°, while Cl2—Ir1—H4 is 156.2° [13], an asymmetry that is maintained in solution [14]. This asymmetry is not reproduced in the geometry optimization at the RHF level of the model system $Ir(H)_2Cl_2(PH_3)_2$ (**2b**) that gives a C_{2v} structure with two identical Cl—Ir—H values [15].

This unsatisfactory result could not be corrected when calculations on the same $Ir(H)_2Cl(PH_3)_2$ model system were carried out at the more sophisticated BECKE3LYP level [12]. The resulting geometry was again C_{2v}, with a Cl—Ir—H angle of 145.3°. A geometry optimization of **2a** at the IMOMM(BECKE3LYP:MM3) level using $Ir(H)_2Cl(PH_3)_2$ for the quantum mechanical part and the default MM3(92) parameters [8] did not produce any significant improvement. The molecule was no longer C_{2v} because of the asymmetry of the P^tBu_2Ph ligand, but the two Cl—Ir—H bond angles were still essentially identical: 147.1° and 146.0°. This result was in contrast to the previous proposal of a steric origin for this distortion [13].

If the discrepancy between calculations on model systems and X-ray structures is related to steric effects, it ought to have been corrected by IMOMM, as has been proven in previous studies [2–4]. The fact that the improvement was only partial for **1** and non-existent for **2** hints at the existence of a methodological problem in these particular systems. One peculiarity of both systems is that the steric repulsion is mostly caused by interactions between the anionic Cl^- and H^- ligands attached to the metal and the organic alkyl substituents of the phosphine ligands. Interactions of this type are essentially controlled by the van der Waals interaction between the atoms. It is hard to argue on the accuracy of MM3 parameters for alkyl substituents, since the force field is especially designed for this kind of atoms [16]. On the other hand, the quality of the van der Waals parametrization of the inorganic ligands Cl^-, H^- is much less reliable, since the MM3 force field considers them to be in an organic environment. The accuracy of this parametrization is analysed in detail in the following section. Another well-known limitation of the MM3 force field, the lack of electrostatic interactions, must be discarded as the source of this systematic error. Electrostatic interactions between ionic and neutral fragments must be weakly binding, through the interaction of the charge with dipoles and induced dipoles, and not the repulsive interaction missing in these IMOMM calculations.

3 Improved van der Waals radii for halide atoms

In the MM3 force field, the main contribution to the direct interaction between two non-bonded atoms i,j comes from the so-called van der Waals energy, defined in the following way [16c]

$$E_{ij} = \varepsilon\,[184000\exp(-12.0d_{ij}/D_{ij}) - 2.25(D_{ij}/d_{ij})^6]$$

with

$$D_{ij} = r_i + r_j$$

$$\varepsilon = \sqrt{\varepsilon_i \cdot \varepsilon_j}$$

where d_{ij} is the interatomic distance, and r_i and ε_i correspond to the van der Waals radius and hardness of atom i. Our goal is to determine whether the default parameters, defined for organic substituents, are appropriate for inorganic ligands, and if not, how they should be modified.

The problem of the assignment of parameters for the description of nonbonding interactions has a long his-

148

tory of its own, with approaches based both on experimental [17] and theoretical methods [18]. It is not the focus of this paper to discuss the validity of the different approaches, but just to apply a reasonable method to obtain a crude estimate of the difference between organic substituents and inorganic ligands. With this idea in mind, we chose to concentrate on the parameters of chloride, that is bulkier and more negatively charged than hydride. Of the two van der Waals parameters corresponding to chloride, the radius seems to be more critical to the steric effects in this type of hindered systems than the hardness. Therefore, our efforts will concentrate on determining what value should be assigned to the van der Waals radius of chloride within the MM3(92) force field.

The van der Waals radius for chlorine atoms in organic and in inorganic environments is computed with a method that has been deemed to be appropriate for the calculation of the van der Waals surface of molecules in a recent publication [19]. It consists of using the helium atom as a probe in geometry optimizations at the Møller-Plesset (MP3) level with a 6-311 ++ G(3*d*, 3*p*) basis set.

One simple model is chosen for each of the two different environments considered. The model organic system is H_3C—Cl···He, and the model inorganic system is Na—Cl···He. For further simplification, the helium atom is restricted to a head-on approach on the chlorine atom, as shown in Fig. 3. The resulting optimized Cl—He distances for the two systems are significantly different: 3.31 Å for the organic system and 3.71 Å for the inorganic system. The radius for helium is found from a calculation on the helium dimer to be 1.58 Å. According to this, the van der Waals radius for organic chlorine is 1.73 Å, and the van der Waals radius for inorganic chlorine, 2.13 Å. The inorganic chlorine ligand, more negatively charged than the organic chlorine substituent, has a significantly larger radius, as should be expected.

These values are remarkably similar to those that can be obtained through the application of completely different approaches used in the field of solvation models [20]. The following formula has been proposed for the atomic radius (Å) of chlorine [20a]:

$$\rho_{Cl} = 1.65 + 0.559\{-(1/\pi)\arctan[(q + 0.75)/0.1] + 1/2\}$$

with q corresponding to the partial charge on the chlorine atom. Using a charge of −0.21 a.u. for organic chlorine [20b] and a nominal value of −1.00 a.u. for inorganic chlorine, the corresponding atomic radii would be 1.68 and 2.14 Å, respectively.

In contrast, the agreement of our computed value for organic chlorine with the MM3 van der Waals radius for this element (2.07 Å) is unexpectedly poor. The MM3 value is actually much closer to that of inorganic chlorine! In order to understand this discrepancy, the standard experimental van der Waals radii [21] that can be found in textbooks [22], were examined. The value for chlorine, determined essentially for organic systems, is 1.75 Å [21] . This is in good agreement with our computed value and far from the MM3 standard value. The discrepancy between standard and MM3 van der Waals radii is by no means restricted to chlorine. The standard value for carbon in methane, ethane and ethylene is 1.70 Å [21, 22] while the MM3 value for sp^3 carbon is 2.04 Å. This apparent contradiction is simply a problem of terminology. What MM3 calls the van der Waals radius is a parameter inserted in a mathematical expression, the value of which is adjusted to reproduce properly the overall experimental properties, like crystal parameters and heat of sublimation [16c, 23]. It probably incorporates corrections to other errors in the force field. As a result, it does not correspond exactly to the van der Waals radius, although it is directly related to it.

Therefore, it would not be appropriate to input directly the van der Waals radius that we have computed for inorganic chlorine into the MM3 force field. On the other hand, the sophisticated fitting procedure used in the definition of the MM3 force field is out of reach because of the scarceness of experimental data and the prohibitive computing effort. Instead, we make the assumption that the relationship between the "real" and the MM3 van der Waals radius for organic chlorine is conserved for inorganic chlorine. That is, since the difference between the two values for the organic molecule is 0.34 Å, we will assume that the MM3 radius for inorganic chlorine is 2.13 + 0.34 = 2.47 Å. The validity of this approximation is tested in the following section.

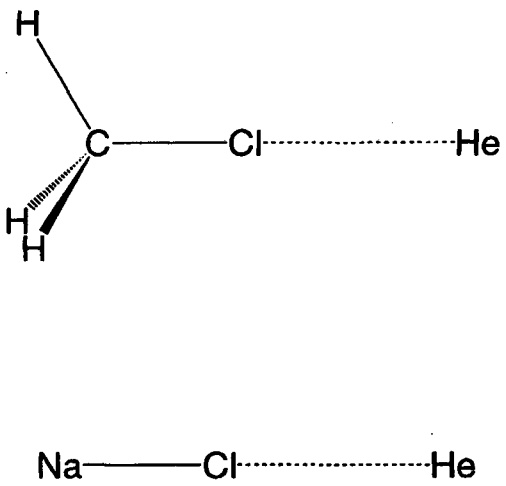

Fig. 3. Orientation used in the geometry optimizations of the H_3C—Cl··· He and Na—Cl··· He systems

4 Return to the $Os(H)_2Cl_2(P^iPr_3)_2$ and $Ir(H)_2Cl(P^tBU_2\ Ph)_2$ systems

The geometry optimization of **1a** is repeated at the same IMOMM(BECKE3LYP:MM3) computational level mentioned above with an MM3 van der Waals radius of 2.47 Å for chlorine. The resulting value for the X-Os1-P2-Cl4 dihedral angle is 35.7°. This is substantially closer to the experimental value of 41.9° than the 27.2° obtained when the default radius of 2.07 Å was used, and much better than the 0.0° obtained in the pure ab initio calculation on the model system. This result proves

in the first place that the steric effects in this molecule are primarily related to the chlorine atoms, as could indeed be expected [11]. More to the point of this work, it also proves that modification of the MM3 van der Waals radius in the form proposed in the previous section improves significantly agreement with the experiment.

The geometry optimization of **2a** is also repeated at the same IMOMM(BECKE3LYP:MM3) level with the modified van der Waals radius for chlorine. As a result, the symmetry of the two Cl—Ir—H bond angles is broken, with resulting values of 122.0° and 162.6°. Again, this is in much better agreement with experiment (131.1° and 156.2°) than the results obtained with the standard MM3 radius for chlorine (147.1° and 146.0°). In this case, however, the relationship of the increase in the steric effects of chlorine with the distortion is not so obvious. There is no van der Waals interaction between the chlorine and the hydride ligands. Furthermore, the direct interaction with a single chlorine atom could hardly break the equivalence between two hydride ligands in principle equivalent. The answer is in the steric interactions of chlorine with the phosphine ligands. The bulkier chlorine produces a larger repulsion with the phosphine ligands, as exemplified by the Cl—Ir—P angles. Their average is 89.4° in the BECKE3LYP calculation on model system **1b**, 89.4° in the IMOMM calculation with the standard van der Waals radius for chlorine, 92.3° in the IMOMM calculation with the corrected van der Waals radius for chlorine, and 93.8° in the X-ray structure. The introduction of the corrected van der Waals radius forces an increase of the Cl—Ir—P angle, pushing the phosphines towards the hydride ligands, and increasing the phosphine–hydride repulsions, which are direct responsible of the asymmetry of the complex [13].

Therefore, the use of a corrected van der Waals radius for chloride improves dramatically the agreement of IMOMM computed structures with experimental data. Finer tuning of the van der Waals radii for chloride and hydride and of the hardness of both elements would probably account for most of the remaining discrepancies.

5 Computational details

IMOMM calculations on systems **1** and **2** are performed with a program built from modified versions of two standard programs: GAUSSIAN 92/DFT [24] for the quantum mechanics part and MM3(92) [8] for the molecular mechanics part. Ab initio calculations use the BECKE3LYP method [12], with a valence double-ζ basis set [25] supplemented with a polarization *d* shell on P and Cl [25d]. The molecular mechanics part uses the MM3(92) force field [8]. Van der Waals parameters for osmium and iridium atoms are taken from the UFF force field [26], and torsional contributions involving dihedral angles with the metal atom in terminal position are set to zero. Geometry optimizations are full except for the P—H (1.42 Å) distances in the ab initio part and the P—C_{sp^2} (1.843 Å), P—C_{sp^3} (1.828 Å) distances in the MM part.

Calculations for the determination of the van der Waals radii on the NaCl···He and CH_3Cl···He systems were carried out with the GAUSSIAN 94 package [27] at the MP3 level [28] with a 6-311++G(3*d*, 3*p*) basis set [29].

6 Conclusions

MP3/6-311++G(3*d*, 3*p*) calculations on simple models with helium probes demonstrate that the van der Waals radius for organic, essentially neutral, chloro substituents, is significantly different from that of inorganic, essentially anionic, chloride ligands. Use of a corrected van der Waals radius for inorganic chlorine in the MM part of IMOMM(BECKE3LYP:MM3) calculations leads to significant improvements in the agreement with experimental X-ray structures for the $Os(H)_2Cl_2(P^iPr_3)_2$ and $Ir(H)_2Cl(P^tBu_2Ph)_2$ systems. Further development of specific parameters for the MM description of non-bonded interactions involving inorganic ligands appears as a major venue of improvement for the performance of the IMOMM method.

Acknowledgements. We thank one referee for making us aware of the relationship of this subject with recent developments in the field of solvation models. F. M. thanks the C.N.R.S. for a position of Research Associate. G. U. acknowledges financial support from the Spanish "Dirección General de Enseñanza Superior" under project no. PB95-0639-C02-01.

References

1. Maseras F, Morokuma K (1995) J Comput Chem 9:1170
2. (a) Ujaque G, Maseras F, Lledós A (1996) Theor Chim Acta 94:67; (b) Barea G, Maseras F, Jean Y, Lledós A (1996) Inorg Chem 35:6401
3. (a) Matsubara T, Maseras F, Koga N, Morokuma K (1996) J Phys Chem 100:2573; (b) Svensson M, Humbel S, Morokuma K (1996) J Chem Phys 105: 3654; (c) Matsubara T, Sieber S, Morokuma K (1996) Int J Quantum Chem 60:1101; (d) Froese RDJ, Morokuma K (1996) Chem Phys Lett 263:393
4. Ogasawara M, Maseras F, Gallego-Planas N, Kawamura K, Ito K, Toyota K, Streib WE, Komiya S, Eisenstein O, Caulton KG (1997) Organometallics 16:1979
5. Maseras F, Eisenstein O N J Chem (1997) vol 20 (in press)
6. (a) Humbel S, Sieber S, Morokuma K (1996) J Chem Phys 105:1959; (b) Svensson M, Humbel S, Froese R, Matsubara T, Sieber S, Morokuma K (1996) J Phys Chem 100:19357; (c) Coitiño EL, Truhlar DG, Morokuma K (1996) Chem Phys Lett 259:159
7. (a) Warshel A, Karplus M (1972) J Am Chem Soc 94:5612; (b) Singh UC, Kollman PA (1986) J Comput Chem 7:718; (c) Field MJ, Bash PA, Karplus M (1990) J Comput Chem 11:700; (d) Luzhkov V, Warshel A (1991) J Am Chem Soc 113:4491; (d) Stanton RV, Hartsough DS, Merz KM Jr. (1995) J Comput Chem 16:113; (e) Tuñon L, Martins-Costa MTC, Millot C, Ruiz-López MF, Rivail JL (1996) J Comput Chem 17:19; (e) Gao J (1996) Acc Chem Res 29:298; (f) Noland M, Coitiño EL, Truhlar DG (1997) J Phys Chem A 101:1194
8. Allinger NL (1992) MM3(92). QCPE, Bloomington IN
9. Aracama M, Esteruelas MA, Lahoz FJ, Lopez JA, Meyer U Oro LA, Werner H (1991) Inorg Chem 30:288
10. Allen FH, Kennard O (1993) Chem Des Autom News 8:31
11. Gusev DG, Kuhlman R, Rambo JR, Berke H, Eisenstein O, Caulton KG (1995) J Am Chem Soc 117:281

12. (a) Becke AD (1993) J Chem Phys 98:5648; (b) Lee C, Yang W, Parr RG (1988) Phys Rev. B 37:785; (c) Stephens PJ, Devlin FJ, Chabalowski CF, Frisch MJ (1994) J Phys Chem 98:11623
13. Albinati A, Bakhmutov VI, Caulton KG, Clot E, Eckert J, Eisenstein O, Gusev DG, Grushin VV, Hauger BE, Klooster WT, Koetzle TF, McMullan RK, O'Loughlin TJ, Pélissier M, Ricci JS, Sigalas MP, Vymenits AB (1993) J Am Chem Soc 115:7300
14. Hauger BE, Gusev DG, Caulton KG (1994) J Am Chem Soc 116:208
15. Riehl J-F, Jean Y, Eisenstein O, Pélissier M (1992) Organometallics 11:729
16. (a) Allinger NL, Yuh YH, Lii JH (1989) J Am Chem Soc 111:8551; (b) Lii JH, Allinger NL (1989) J Am Chem Soc 111:8566; (c) Lii JH, Allinger NL (1989) J Am Chem Soc 11:8576
17. (a) Nesbitt DJ (1988) Chem Rev. 88:843; (b) van der Avoirdd A, Wormer PES, Moszynski R (1994) Chem Rev 94:1931
18. (a) Buckingham AD, Fowler PW, Hutson JM (1988) Chem Rev 88:963; (b) van Duijneveldt FB, van Duijneveldt-van de Rijdt J GCM, van Lenthe JH (1994) Chem Rev 94:1873; (c) Chalasinski G, Szczesniak MM (1994) Chem Rev 94: 1723
19. Yin D; MacKerell AD Jr (1996) J Chem Phys 100:2588
20. (a) Cramer CJ, Truhlar DG (1992) J Comput Chem 13:1089; (b) Storer JW, Giesen DJ, Cramer CJ, Truhlar DG (1995) J Comput Aided Mol Des 9:87
21. Bondi A (1964) J Phys Chem 68:441
22. Huheey JE, Keiter EA, Keiter RL (1993) Inorganic chemistry. Principles of structure and reactivity, 4th edn. HarperCollins, NewYork
23. Allinger NL; Hirsch JA, Miller MA, Tyminski IR, Van-Catledge FA (1968) J Am Chem Soc 90:1199
24. Frisch MJ, Trucks GW, Schlegel HB, Gill PMW, Johnson BG, Wong MW, Foresman JB, Robb MA, Head-Gordon M, Replogle ES, Gomperts R, Andres JL, Raghavachari K, Binkley JS, Gonzalez C, Martin RL, Fox DJ, Defrees DJ, Baker J, Stewart JJP, Pople JA (1993) GAUSSIAN 92/DFT, Gaussian Inc., Pittsburgh, Pa
25. (a) Hehre WJ, Ditchfield R, Pople JA (1972) J Chem Phys 56:2257–2261; (b) Wadt WR, Hay PJ (1985) J Chem Phys 82:284; (c) Hay PJ, Wadt WR (1985) J Chem Phys 82:299; (d) Francl MM, Pietro WJ, Hehre WJ, Binkley JS, Gordon MS, DeFrees DJ, Pople JA (1982) J Chem Phys 77:3654–3665
26. Rappé AK, Casewit CJ, Colwell KS, Goddard WA, III, Skiff WM (1992) J Am Chem Soc 114:10024
27. Frisch MJ, Trucks GW, Schlegel HB, Gill PMW, Johnson BG, Robb MA, Cheeseman JR, Keith T, Petersson GA, Montgomery JA, Raghavachari K, Al-Laham MA, Zakrzewski VG, Ortiz JV, Foresman JB, Peng CY, Ayala PY, Chen W, Wong MW, Andres JL, Replogle ES, Gomperts R, Martin RL, Fox DJ, Binkley JS, Defrees DJ, Baker J, Stewart JP, Head-Gordon M, Gonzalez C, Pople JA (1995) GAUSSIAN 94, Gaussian Inc., Pittsburgh, Pa
28. (a) Møller C, Plesset MS (1934) Phys Rev 46:618; (b) Pople JA, Seeger R, Krishnan R (1977) Int J Quantum Chem Symp 11: 149
29. (a) Krishnan R, Binkley JS, Seeger R, Pople JA (1980) J Chem Phys 72:650; (b) McLean AD, Chandler GS (1980) J Chem Phys 72:5639; (c) Clark T, Chandrasekhar J, Spitznagel GW, Schleyer PVR (1983) J Comput Chem 4:294; (d) Frisch MJ, Pople JA, Binkley JS (1984) J Chem Phys 80:3265

Article IV

"Breaking an Electronically Preferred Symmetry by Steric Effects in a Series of [Ir(biph)X(QR_3)$_2$] Compounds (X = Cl, Q = P or As)"

Gregori Ujaque, Feliu Maseras, Odile Eisenstein

New J. Chem., **22**, 1493-1498 (1998)

Breaking an electronically preferred symmetry by steric effects in a series of [Ir(biph)X(QR_3)$_2$] compounds (X = Cl or I, Q = P or As)

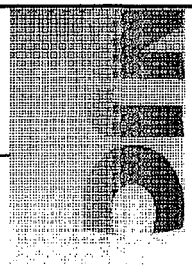

Gregori Ujaque,[a] Feliu Maseras,*,†,[a] Odile Eisenstein,*,[a] Louise Liable-Sands,[b] Arnold L. Rheingold,*,[b] Wenbin Yao[c] and Robert H. Crabtree*,[c]

[a] *LSDSMS (UMR 5636) Case Courrier 14, Université de Montpellier 2, 34095, Montpellier, Cedex 5, France*

[b] *Department of Chemistry, University of Delaware, Newark, DE, 19716, USA*

[c] *Department of Chemistry, Yale University, New Haven CT, 06520-8107, USA*

A hybrid quantum mechanical/molecular mechanics IMOMM (B3LYP : MM3) method has been applied to a series of five-coordinate 16-electron d^6 ML_5 Ir^{III} compounds having a relatively flat potential for a distortion from Y to T geometry and for which crystal structures have been obtained. In this series of type [Ir(biph)X(QPh_3)$_2$] (biph = biphenyl-2,2′-diyl; Q = P, X = Cl, **2a**; Q = As, X = Cl, **2b**; Q = P, X = I, **2c**), the halide is found to lie in the (biph)Ir plane but off the C_2 axis of the {Ir(biph)Q_2} fragment by a variable angular distortion ϕ. While $\phi = 0$ is preferred electronically for [Ir(C_4H_4)Cl(PH_3)$_2$], the steric bulk of the real systems **2a–2c** leads to ϕ taking experimental values of 8.2–17.2°. The observed deviation of the halide from the C_2 axis is shown by IMOMM to be the result of a direct interaction of the phenyl substituents of the axial ligands with the equatorial ligands and not to an electronic effect. The crystal structures for **2b** and **2c** have been determined.

Quantum chemical calculations have attained an impressive level of reliability in recent years and quantitative studies are possible even on reasonably large molecules. To save computational time, it is nevertheless still usually necessary to simplify the ligand set by replacing PR_3 by PH_3, for example. This means that when there is a significant deviation between the quantum chemical and experimental results on a given system, one cannot immediately tell whether the deviation is due to the steric effects of the real PR_3 ligand or to some nonsteric electronic effect that has not been well represented in the calculations.

Hybrid quantum mechanics–molecular mechanics (QM/MM) methods have recently become available that can help resolve such ambiguities. In these, the core of the molecule, consisting of the metal and the immediate ligand sphere, is represented by quantum chemical methods, and the exterior part, comprising the substituents on the ligands, is represented by molecular mechanics. In this way a large molecule can be treated realistically without requiring prohibitive amounts of computer time. Here, we report application of a combined (QM/MM) hybrid method IMOMM (B3LYP : MM3) to the title complexes. This particular hybrid method[1] has already proved successful in computing steric effects in several transition-metal complexes.[2]

Following the original experimental discovery,[3a] various theoretical studies have clearly established that five-coordinate d^6 16-electron complexes with one equatorial π-donor ligand (labeled L'_{eq} in diagram **1a**), show a preference for a Y structure, **1a**, This resembles a trigonal bipyramidal structure but has one small angle (<90°) between two equatorial ligands.[3b–d] In such a Y structure, the M—L'_{eq} bond defines the mirror plane which necessarily bisects the angle between the two identical equatorial ligands. A T structure **1b** is not very different in energy, however, and in certain cases can be the ground state. This structure is octahedral with one missing vertex and the π-donor ligand is located in the basal site.

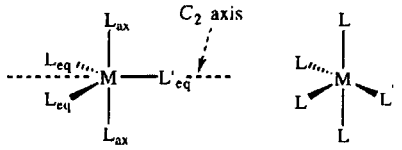

1a Y-type **1b** T-type

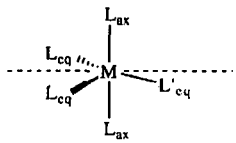

1c Y/T-type

Two experimental examples, discovered almost simultaneously in the groups of Crabtree and of Caulton,[4–8] showed that in certain circumstances it is possible to break the symmetry in what would otherwise be a pure Y-type molecule. In spite of having two identical ligands in the equatorial plane these compounds adopt structure **1c** intermediate between Y and T geometries, denoted Y/T. For [$IrH_2Cl(P\{Bu^t\}_2Ph)_2$] (**1d**) the Y/T structure is found in the solid state by neutron diffraction[4] and is maintained in solution as shown by ^1H NMR studies at low temperature.[5] IMOMM (B3LYP : MM3) calculations revealed that the observed deviation from Y geometry is a result of steric interactions between the phosphine substituents and the equatorial ligands.[6] The potential energy surface linking Y and T geometries is known to be flat[3d] and it is no doubt this factor that permits the existence of structures with a geometry intermediate between the two pure forms.

This paper probes the generality of these distortions and reports a series of 16-electron Ir^{III} complexes where the IrH_2

* E-mail: odile.eisenstein@lsd.univ-montp2.fr; arnrhein@udel.edu; robert.crabtree@yale.edu

† Present address: Unitat de Química Física, Edifici C.n., Universitat Autònoma de Barcelona, 08193, Bellaterra, Catalonia, Spain; feliu@klingon.uab.es

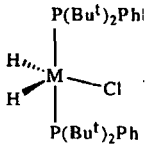

1d

group of the above system is replaced by an iridium diaryl. This new system shows the same types of distortions and provides a good quantitative test of the hybrid methods mentioned above. The new series of complexes has the advantage that only non-hydride ligands are present, permitting definitive structural study without recourse to neutron diffraction.

Results and Discussion

We showed[7] in 1993 that biphenylene undergoes a C—C bond activation reaction with $[Ir(cod)Cl]_2$ (cod = 1,5-cyclooctadiene) to give a biphenyl-1,2-diyl (=biph) complex, $[Ir(cod)(biph)Cl]_2$, where the biph ligand is the organometallic analogue of 2,2'-bipyridine [eqn. (1)]. The complex was found to react readily [eqn. (1)] with PPh_3 to give a 16-electron five-coordinate Ir^{III} species, $[Ir(biph)Cl(PPh_3)_2]$ (**2a**) which was structurally characterized. Five-coordinate Ir^{III} species like **2**

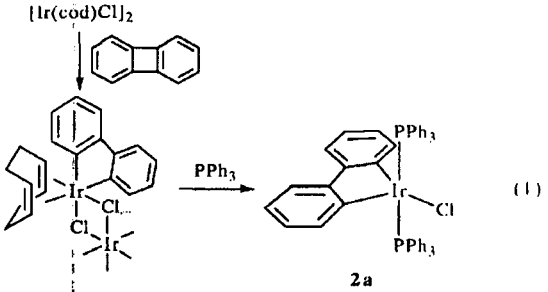

(1)

2a
Y/T geometry

are expected to have a pure Y structure owing to the presence of only one equatorial π-donor ligand, a halide.

At the time of its discovery, it was surprising to find that in **2a** the experimental structure was neither Y nor T but intermediate between the two situations, as shown in diagram **3c**. This was initially thought to be an electronic effect but work

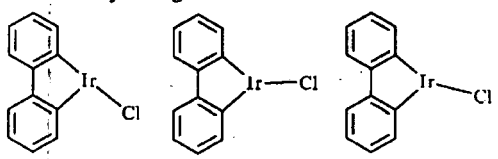

3a
pure T

3b
pure Y

3c
experimental
Y/T structure

to be described below now makes clear that we are seeing a steric effect. As a test, we wanted to compare a series of complexes of type **2** to see if the deviation from the ideal Y geometry changes with the steric effects of the ligands.

Synthesis and structural study

In the present work, we have synthesized and structurally characterized two related species of type **2** with ligands of slightly different steric size: $[Ir(biph)Cl(AsPh_3)_2]$ (**2b**) and $[Ir(biph)I(PPh_3)_2]$ (**2c**). These have now been prepared in good yield as air-stable orange (**2b**) or red (**2c**) crystals by the standard routes shown in eqns. 2 and 3.

$$[Ir(cod)Cl(biph)]_2 \xrightarrow{AsPh_3} [Ir(biph)Cl(AsPh_3)_2] \quad (2)$$

$$[Ir(biph)Cl(PPh_3)_2] \xrightarrow[acetone]{LiI} [Ir(biph)I(PPh_3)_2] \quad (3)$$

The five-coordinate, 16-electron species **2a–2c** are not readily converted to the corresponding six-coordinate species $[Ir(biph)X(QPh_3)_3]$. In more recent work[9] we find that the reaction of $[Ir(biph)Cl(cod)]$ with $SbPh_3$ gives a six-coordinate product, $[Ir(biph)Cl(SbPh_3)_3]$, presumably because $SbPh_3$ is a slightly less sterically bulky ligand largely as a result of its longer Ir—Sb bond. The sterically unencumbered PMe_3 also gives a six-coordinate $[Ir(biph)Cl(PMe_3)_3]$.[9] This suggests that the formation of the five-coordinate compounds **2a–2c** is at least in part the result of steric effects, although the presence of the high *trans*-influence biph ligand no doubt also encourages five-coordination.

Crystals suitable for crystallographic study were grown from CH_2Cl_2 solution by slow evaporation. The crystallographic work (Table 1) gave the distance and angular data of Table 2. The corresponding ORTEP diagrams are shown in Fig. 1 and 2. The crystal of compound **2b** contained two independent molecules having very similar but not identical metric parameters.

Both **2b** and **2c** have similar structures to that of $[Ir(biph)Cl(PPh_3)_2]$ (**2a**) which was determined previously.[8] In all cases, the $(biph)IrQ_2$ fragment has near C_{2v} symmetry but the halide, while remaining in the equatorial biph plane (the sum of the three equatorial L—Ir—L angles is 359.87–360°), lies significantly off the C_2 axis so that one biph carbon, denoted C_{trans}, becomes more *trans* than *cis*, and the other, denoted C_{cis}, becomes more *cis* than *trans* to the halide group. Fig. 3 illustrates the situation by showing the equatorial ligands. All the molecules of type **2** studied to date therefore have essentially the same geometry, lying between the ideal Y and T forms, but they show different deviations from pure Y geometry. We have used the angles ω_1, ω_2 and ϕ shown in Fig. 3 as a measure of this deviation in the following discussion. The fact that C_{cis}, C_{trans}, Ir and X are always in the same plane allows the value of ϕ to be derived from ω_1 and ω_2 by eqn. 4.

$$\phi = |\tfrac{1}{2}(\omega_1 + \omega_2) - \omega_1| \quad (4)$$

A pure Y geometry should correspond to a ϕ value of zero and a pure T geometry should lead to a ϕ value close to 45°. The values found in the present work lie between 8.2 and 17.2° and therefore indicate a geometry closer to Y than T.

Table 1 X-Ray crystallographic data for **2b** and **2c**[a]

Compound	**2b**	**2c**
Formula	$C_{48}H_{38}As_2ClIr$	$C_{48}H_{38}P_2IIr$
Space group	$P2_1/c$	$P2_1/n$
a/Å	23.5757(3)	14.5086(2)
b/Å	19.10520(10)	10.92350(8)
c/Å	19.1809(2)	25.52790(10)
β/°	113.2260(10)	103.6310(10)
V/Å^3	7939.30(19)	3931.83(6)
MW	992.27	995.82
ρ(calc)/g cm^{-3}	1.660	1.682
Z	8	4
θ Range/°	1.42–28.17	1.48–28.26
No. of data used	14939	6706
No. of parameters refined	937	467
$R[I > 2\sigma(I)]$[b]	3.28%	3.15%
$R_w[I > 2\sigma(I)]$[b]	8.22%	7.87%

[a] Details in common: T = 173(2) K, scan type ω–2θ, λ = 0.71069 Å, largest shift/error = 0.2, empirical DIFABS absorption correction. [b] Function minimized: $R = \Sigma||F_o| - |F_c||/|F_o|$ and $R_w = [\Sigma w(|F_o| - |F_c|)^2/\Sigma wF_o^2]^{1/2}$, where $w = 4F_o^2/\sigma^2(F_o)^2$.

Table 2 Selected bond distances (Å) and angles (°) for **2b** and **2c**; X = halide, Q = P or As

	2b (1st molecule)[a]	**2b** (2nd molecule)[a]	**2c**
Ir—X	2.3950(10)	2.3967(10)	2.7197(3)
Ir—Q(1)	2.4359(4)	2.4350(4)	2.3374(12)
Ir—Q(2)	2.4362(4)	2.4332(4)	2.3509(12)
Ir—C_{trans}[b]	2.041(4)	2.050(4)	2.051(4)
Ir—C_{cis}[b]	2.035(4)	2.034(4)	2.024(5)
X—Ir—Q(1)	92.99(3)	88.83(3)	91.92(3)
X—Ir—Q(2)	90.37(3)	93.35(3)	91.77(3)
X—Ir—C_{trans}	149.27(12)	151.21(12)	158.1(2)
X—Ir—C_{cis}	132.93(13)	130.96(14)	123.75(14)
Q(1)—Ir—Q(2)	173.28(2)	174.04(2)	172.62(5)
C_{cis}—Ir—C_{trans}	77.8(2)	77.7(2)	78.1(2)
ϕ	8.2(4)	10.1(4)	17.2(4)

[a] The crystal of **2b** contained two independent molecules; the atom numbering of the first has been given unmodified [*e.g.* C(1)] and the second in primes [*e.g.* C(1')]. [b] The carbon atoms of the biph bound directly to Ir are labeled as being *cis* or *trans* with reference to the halide because of the slightly different numbering system in the two compounds. C_{cis} is C(1) in the first molecule of **2b**, C(12') in the second molecule of **2b** and C(7) in **2c**; similarly, C_{trans} is C(12) in the first molecule of **2b**, C(1') in the second molecule of **2b** and C(1) in **2c**.

We find that both the ligand conformations and the ϕ values in the two molecules of **2b** are essentially the same, suggesting that packing forces have only a minor role in determining the distortion. This is a rare case in which an organometallic molecule with a relatively flat bending potential (see below) has been studied in two independent forms. The low influence of packing forces on the distortion suggested by the present work may not be general, however, because ionic solids in particular might be expected to have a much higher effective internal pressure and could therefore show a greater structural variability depending on the details of the packing.

Theoretical study

Previously reported calculations[8] at the extended Hückel theory level seemed to indicate an electronic origin for the deviation, ϕ. The structure of the simplified system [Ir(C_4H_4)Cl(PH_3)$_2$] was thus optimized at the B3LYP level. The results show that the geometry of the complex is close to that of the full biph system with the exception of the presence of a C_2 symmetry which is present in the calculated structure and lacking in the experimental system. The computed geometry had C_2 symmetry despite the fact that the geometry optimization was carried out with no symmetry restrictions and

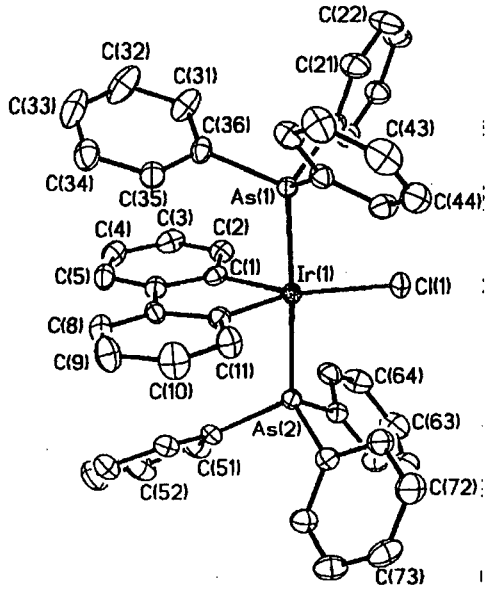

Fig. 1 ORTEP diagram of **2b**. Only one of the two independent but chemically equivalent molecules is shown. The other has essentially the same conformation. The thermal ellipsoids are plotted at 50% probability and the hydrogen atoms are omitted for clarity

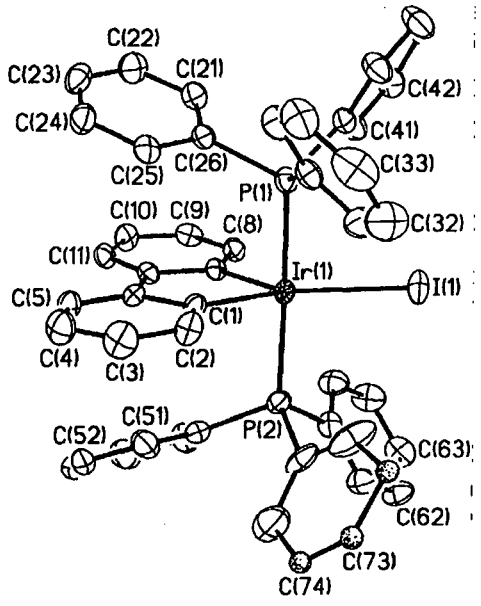

Fig. 2 ORTEP diagram of **2c**. Carbons C(72)–C(74) are disordered over two positions and were refined isotropically. Thermal ellipsoids are plotted at 50% probability and the hydrogen atoms are omitted for clarity

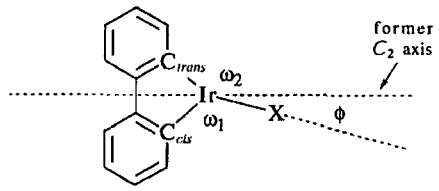

Fig. 3 Ligands in the equatorial plane of complex **2**, showing the deviation of the halide from the ideal C_2 axis (dotted) of a pure Y structure. QR_3 ligands are located above and below the equatorial plane. Angle ϕ is the deviation of the X group from the C_2 axis, ω_1 is the C_{cis}—Ir—X angle and ω_2 is the C_{trans}—Ir—X angle. X always lies in the C_{cis}, C_{trans}, Ir plane

started from a non-symmetrical structure. The Ir—C distances are reasonably well represented (calcd., 2.06 Å; exptl. average, 2.00 Å), the alternating long and short distances within the metallacycle are also well reproduced (calcd., 1.355, 1.459 Å; exptl. 1.415, 1.440 Å). The significant difference between theory and experiment for the C=C of the metallacycle is clearly due to it being part of a phenyl ring in the biph complex, in which case the double bond is delocalized. The calculated Ir—Cl distance of 2.449 Å is reasonably close to the experimental value of 2.380 Å as is also the case for the Ir—P distances (calcd., 2.331 Å; exptl., 2.345 Å). As in the experimental system, the metallacycle is planar. A pure Y structure for $[Ir(C_4H_4)Cl(PH_3)_2]$ agrees with the expectations based on the presence of one equatorial π donor (Cl).[3] Our previous proposal[8] that the geometrical constraint of the biph ligand helps cause the distortion has therefore been discarded.

Having established that **2** has an electronic preference for a Y structure with $\phi = 0°$, the observed deviation in **2a–2c** seemed likely to be a steric effect. This makes the series of compounds of type **2** suitable for study by the hybrid combined IMOMM (B3LYP:MM3) method. Examination of the experimental structures of **2a–2c** showed that in each case the same ligand conformation is adopted. This conformation was therefore taken as the departure point for the IMOMM study so as to minimize the potential problem of falling into a series of local minima of no relevance to the experimental solid-state conformation. The minimization was carried out with the object of seeing how well the ϕ value that emerged in each case matched the experimental value and if the trend of the values matched the experimental trend.

The IMOMM calculations on $[Ir(biph)X(QR_3)_2]$ always reproduce the experimental conformation, indicating that this is a local minimum for the isolated complex and that the crystal packing is not a determining factor. The calculations also show a displacement of the halide from its electronically preferred position on the C_2 axis in a direction which allows the Ir—X bond to stay coplanar with the metallacycle. However, as in the case of the IMOMM calculation on $[IrH_2ClL_2]$, the geometrical results are not quantitatively satisfactory if the radius of Cl is maintained at its standard value contained in the MM3 program because this is the value appropriate for organic chlorides. With the standard radius, $[Ir(biph)Cl(PPh_3)_2]$ shows only a slight distortion away from C_{2v} symmetry ($\phi = 1.4°$). If the Cl radius is increased to account for its ionic nature using the procedure described in a previous paper,[6] the optimized structure now comes remarkably close to the experimental one (calc. $\phi = 11.4$; exptl., 10.15°). For all Q and X studied, the displacement, as measured by ω_1, ω_2 and ϕ, is given in Table 3. The same distorted geometry was obtained from calculations starting both from the experimental non-symmetrical arrangement and starting from a symmetrical C_{2v} arrangement. The latter arrangement was tested specifically in the case of $[Ir(biph)Cl(PPh_3)_3]$ to ensure that no other local minimum is present. In spite of the potential energy surface for the displacement of the Cl from the axis being very flat, good agreement with experiment was obtained.

On going from PH_3 to PPh_3 (X = Cl), all the calculated metal–ligand distances increase slightly, probably as a consequence of the increased steric bulk around the metal. The C—C bond of the metallacyclopentadiene is not changed on moving from the IrC_4H_4 to the Ir(biph) model since the adjacent phenyl rings of biph are represented only at the MM3 level and therefore delocalization of the electrons of the C=C bond is not possible.

The calculated value of ϕ increases on going from Cl to I (L = PPh_3) as is also the case for the experimental results (calc., 14.6; exptl., 17.2°). The increased distortion is clearly associated with a bigger steric interaction with the larger halide. Changing Q from P to As (X = Cl) diminishes the experimental distortion by only one degree [$\phi = 9.15°$(av.)]; the calculations show no change (calc., 11.3°). The longer Ir—Q distance presumably causes the ligand cone angle to decrease.

The calculations thus closely mimic the experimental system, even though the substituents on QR_3 are represented in a purely MM (steric) manner; this suggests that the interactions between the substituents and the other ligands are essentially controlled by steric factors. Previous work in this area[2b,9] has shown that steric effects in organometallic compounds tend to be dispersed over numerous centers and no particular atom or group can be considered as the dominant contributor. Compound **2** has even more atoms than the complexes studied previously and so the possibilities for dispersal of steric effects are even greater. For this reason, we did not conduct any analysis to attempt to estimate the relative size of the interatomic repulsions. It is also very satisfying that the IMOMM hybrid method is able to reproduce subtle structural changes from Y to T even on a potential energy surface known from *ab initio* calculations to be very flat.[3b–d]

Experimental

Syntheses

General procedures and materials. All manipulations were performed under a dry nitrogen atmosphere using standard Schlenk techniques. Solvents were dried by standard procedures. All the reagents were used as received without further purification. $[Ir(cod)Cl(biph)]_2$ and $[Ir(biph)Cl(PPh_3)_2]$ were prepared by literature methods.[7]

^1H and ^{31}P NMR spectra were recorded on a GE Omega 300 spectrometer. Elemental microanalyses were performed by Robertson Microlit Laboratories.

Chloro(biphenyl-2,2′-diyl)bis(triphenylarsine)iridium(III) (2b). A suspension of $[Ir(cod)Cl(biph)]_2$ (0.20 g, 0.21 mmol) and triphenylarsine (0.28 g, 0.92 mmol) in CH_2Cl_2 (10 mL) was stirred at room temperature for 5 h under N_2. The resulting red-orange product was filtered off, washed with Et_2O (2 × 10 mL), and dried *in vacuo*. Yield: 0.28 g (0.28 mmol, 67%). ^1H NMR (CD_2Cl_2, 298 K): δ 7.49 (2H, d,

Table 3 Results of the IMOMM and (B3LYP : MM3) calculation on $[Ir(biph)XL_2]$

			Calc.			Exptl.		
Compound	L	X	ω_1	ω_2	ϕ	ω_1	ω_2	ϕ
2a[a]	PPh_3	Cl	130.6	153.4	11.4	131.3	151.4	10.15
2b	$AsPh_3$	Cl	130.7	153.3	11.3	132.93	149.27	8.2
2b′[b]	$AsPh_3$	Cl	130.7	153.3	11.3	130.96	151.21	10.1
2c	PPh_3	I	128.0	155.3	14.6	123.75	158.1	17.2
2d[c]	PH_3	Cl	142	142	0	—	—	—

Angles in degrees. $\omega_1 = C_{cis}—Ir—X$; $\omega_2 = C_{trans}—Ir—X$; $\phi = |\frac{1}{2}(\omega_1 + \omega_2) - \omega_1|$. [a] With the standard MM3 value of the Cl radius (adapted for organic chlorides) ω_1 and ω_2 are 140.4 and 143.2° ($\phi = 1.4°$). [b] Data for the second molecule in unit cell. [c] Theoretical value only; compound not synthesized.

$J = 7.2$ Hz), 7.2–7.4 (36H, br, Ph), 6.47 (2H, t, $J = 7.2$ Hz, biph), 6.33 (2H, t, $J = 7.2$ Hz, biph), 6.31 (2H, d, $J = 7.2$ Hz, biph). Anal. Calcd. (found) for $C_{48}H_{38}As_2ClIr$: C, 58.10 (57.88); H, 3.86 (4.00%).

Iodo(biphenyl - 2,2' - diyl) bis (triphenylphosphine) iridium (III) (2c). A mixture of $[Ir(biph)Cl(PPh_3)_2]$ (0.10 g, 0.11 mmol) and LiI (0.14 g, 1.0 mmol) in acetone (20 mL) was stirred at ambient temperature for 12 h, during which time the color changed from red-orange to red. The solvent was removed under reduced pressure, and CH_2Cl_2 (20 mL) was added to dissolve the red precipitate. The solution was filtered through Clite, the filtrate was reduced to 5 mL *in vacuo*, followed by addition of Et_2O (15 mL) to precipitate a red product, which was filtered off, washed with Et_2O (2 × 10 mL), and dried *in vacuo*. Yield: 78 mg (0.078 mmol, 71%). ^1H NMR (CD_2Cl_2, 298 K): δ 7.2–7.4 (38H, br, Ph and biph), 6.46 (2H, t, $J = 7.3$ Hz, biph), 6.34 (2H, dt, $J = 1.1$, 7.3 Hz, biph), 6.21 (2H, dd, $J = 1.1$, 7.3 Hz, biph). Anal. Calcd. (found) for $C_{48}H_{38}P_2IIr$: C, 57.90 (58.08); H, 3.84 (3.80%).

Crystallographic structural determination

Crystal, data collection and refinement parameters are given in Table 1. Data was collected on a Siemens P4/CCD diffractometer. The systematic absences in the diffraction data are uniquely consistent with the space groups reported. The structures were solved by direct methods, completed by subsequent difference Fourier synthesis and refined by full-matrix least-squares procedures. An empirical absorption correction was applied, based on a Fourier series in the polar angles of the incident and diffracted beam paths and was used to model an absorption surface for the difference between the observed and calculated structure factors.[10] The asymmetric unit of **2b** consists of two independent molecules. Three carbon atoms of both of the biph rings of **2c**, equally disordered over two positions, were refined isotropically, and the corresponding hydrogen atoms were ignored owing to this disorder. All other non-hydrogen atoms were refined with anisotropic displacement coefficients and all other hydrogen atoms were treated as idealized contributions. Five of the remaining peaks in the final difference map of **2b** (1.06 to 1.54 e $Å^{-3}$) were in chemically unreasonable positions 1.18–1.44 Å from the Ir and were considered as noise.

All software and sources of the scattering factors are contained in the SHELXTL (5.3) program library.[11]

CCDC reference number 440/062.

Computational details

Pure quantum mechanical calculations on the model systems $[Ir(C_4H_4)X(QH_3)_2]$ were carried out with Gaussian 94.[12] Pseudo potentials were used for representing the 60-electron core of Ir,[13] the 10-electron core of P and Cl, the 18-electron core of As and the 26-electron core of I.[13b]

The associated double-ζ basis set with a LANL2DZ contraction[12] was used for the Ir, P, As, Cl and I atoms. A polarization d shell was added for the P,[14] Cl,[14] I[15] and As[15] atoms. The C and H atoms had a valence double-ζ basis set.[16] Full geometry optimizations were carried out at the B3LYP level.[17]

IMOMM calculations were performed on $[Ir(biph)X(QPh_3)_2]$ (X = Cl, I; Q = P, As) with a program built from modified versions of two standard programs: Gaussian 92/DFT[18] for the quantum mechanics (QM) part and MM3 (92) for the molecular mechanics[19a] (MM) part. The QM part was always carried out for $[Ir(C_4H_4)X(QH_3)_2]$ at the computational level described in the previous paragraph. For the MM part, the MM3(92) force field was used.[19b] Van der Waals parameters for the iridium atom were taken from the UFF force field.[20] Parameters for bending contributions involving As—C—C bond angles and torsional contributions involving As-C-C-R dihedral angles were taken from the values assigned to P-C-C and P-C-C-R. Torsional contributions involving dihedral angles with the metal atom in terminal position were set at zero. The values of the radii of Cl and I in the MM3 program were modified to take into account their greater negative charge when bonded to a transition-metal center according to the procedure described previously:[6] radii for Cl and I were 2.47 Å and 2.71 Å, respectively. All geometrical parameters were optimized without symmetry restrictions except for the bond distance between the QM and MM regions of the molecules. These were frozen at 1.420 (P–H). 1.532 (As–H), 1.101 Å (C–H) in the QM part; and 1.828, 1.943 (As–C), and 1.434 Å (C–C) in the MM part. The starting point of all geometry optimizations was the crystal structure coordinates for the iridium complexes.

Acknowledgements

We thank NSF for support (R.H.C.) and for their support (A.L.R.) of the purchase of a CCD-based diffractometer. We thank the CNRS for a research associate position (F.M.) and the UAB for supporting G.U.'s stay in Montpellier.

References

1 F. Maseras and K. Morokuma, *J. Comput. Chem.* 1995, **16**, 1170.
2 (*a*) T. Matsubara, F. Maseras, N. Koga and K. Morokuma, *J. Phys. Chem.* 1996, **100**, 2573; (*b*) Y. Wakatsuki, N. Koga, H. Werner and K. Morokuma, *J. Am. Chem. Soc.*, 1997, **119**, 360; (*c*) G. Ujaque, A. C. Cooper, F. Maseras, O. Eisenstein and K. G. Caulton, *J. Am. Chem. Soc.*, 1998, **120**, 361; (*d*) F. Maseras and O. Eisenstein, *New. J. Chem.*, 1998, **22**, 5.
3 (*a*) H. Werner, A. Hohn and M. Dziallas, *Angew. Chem., Int. Ed. Engl.*, 1986, **25**, 1090; (*b*) Y. Jean and O. Eisenstein, *Polyhedron*, 1988, **7**, 405; (*c*) I. E.-I. Rachidi, O. Eisenstein and Y. Jean, *New J. Chem.*, 1990, **14**, 671; (*d*) J.-F. Riehl, Y. Jean, O. Eisenstein and M. Pélissier, *Organometallics*, 1992, **11**, 729.
4 A. Albinati, V. I. Bakhmutov, K. G. Caulton, E. Clot, J. Eckert, O. Eisenstein, D. G. Gusev, V. V. Grushin, B. E. Hauger, W. Kloosster, T. F. Koetzle, R. K. McMullan, T. J. O'Loughlin, M. Pélissier, J. S. Ricci, M. P. Sigalas and A. B. Vymenits, *J. Am. Chem. Soc.*, 1993, **115**, 7300.
5 B. E. Hauger, D. G. Gusev and K. G. Caulton, *J. Am. Chem. Soc.*, 1994, **116**, 208.
6 G. Ujaque, F. Maseras and O. Eisenstein, *Theor. Chem. Acc.*, 1997, **96**, 146.
7 Z. Lu, C.-H. Jun, S. de Gala, M. Sigalas, O. Eisenstein and R. H. Crabtree, *J. Chem. Soc., Chem. Commun.*, 1993, 1877.
8 Z. Lu, C.-H. Jun, S. de Gala, M. Sigalas, O. Eisenstein and R. H. Crabtree, *Organometallics*, 1995, **14**, 1168.
9 G. Barea, F. Maseras, Y. Jean and A. Lledòs, *Inorg. Chem.*, 1996, **35**, 6401.
10 N. Walker and D. Stuart, *Acta Crystallogr., Sect. A*, 1983, **39**, 158.
11 G. Sheldrick, Siemens XRD, Madison, WI, 1996.
12 M. J. Frisch, G. W. Trucks, H. B. Schlegel, P. M. W. Gill, B. G. Johnson, M. A. Robb, J. R. Cheeseman, T. Keith, G. A. Peterson, J. A. Montgomery, K. Raghavachari, M. A. Al-Laham, V. G. Zakrzewski, J. V. Ortiz, J. B. Foresman, J. Cioslowski, B. B. Stefanov, A. Nanyakkara, M. Challacombe, C. Y. Peng, P. Y. Ayala, W. Chen, M. W. Wong, J. L. Andres, G. S. Replogle, R. Gomperts, R. L. Martin, D. J. Fox, J. S. Binkley, D. J. Defrees, J. Baker, J. P. Stewart, M. Head-Gordon, C. Gonzalez and J. A. Pople, Gaussian 94: Revision, D. I. Gaussian, Inc., Pittsburgh, PA, 1995.
13 (*a*) P. J. Hay and W. R. Wadt, *J. Chem. Phys.*, 1985, **82**, 299 (*b*) P. J. Hay and W. R. Wadt, *J. Chem. Phys.*, 1985, **82**, 284.
14 M. M. Francl, W. J. Pietro, W. J. Hehre, J. S. Binkley, M. S. Gordon, D. J. Defrees and J. A. Pople, *J. Chem. Phys.*, 1982, **77**, 3654.
15 A. Höllwarth, M. Böhme, S. Dapprich, A. W. Ehlers, A. Gobbi, V. Jonas, K. F. Köhler, R. Stegmann, A. Veldkamp and G. Frenking, *Chem. Phys. Lett.*, 1993, **208**, 237.
16 W. J. Hehre, R. Ditchfield and J. A. Pople, *J. Chem. Phys.*, 1972, **56**, 2257.
17 (*a*) A. D. Becke, *J. Chem. Phys.*, 1993, **98**, 5468; (*b*) C. Lee, W. Yang and R. G. Parr, *Phys. Rev. B*, 1988, **37**, 785; (*c*) P. J. Stephens, F. J. Devlin, C. F. Chabalowski and M. J. Frisch, *J. Phys. Chem.*, 1994, **98**, 11623.

18 M. J. Frisch, G. W. Trucks, H. B. Schlegel, P. M. W. Gill, B. G. Johnson, M. W. Wong, J. B. Foresman, M. A. Robb, M. Head-Gordon, G. S. Replogle, R. Gomperts, J. L. Andres, K. Raghavachari, J. S. Binkley, C. Gonzalez, R. L. Martin, D. J. Fox, D. J. Defrees, J. Baker, J. P. Stewart and J. A. Pople, Gaussian 92/DFT, Gaussian, Inc., Pittsburgh, PA, 1993.
19 (*a*) N. L. Allinger, MM3(92), QCPE, Indiana University, 1992; (*b*) N. L. Allinger, Y. H. Yuh and J. H. Lii, *J. Am. Chem. Soc.*, 1989, **111**, 8551; (*c*) J. H. Lii and N. L. Allinger, *J. Am. Chem. Soc.*, 1989, **111**, 8566; (*d*) J. H. Lii and N. L. Allinger, *J. Am. Chem. Soc.*, 1989, **111**, 8576.
20 A. K. Rappé C. J. Casewit, K. S. Colwell, W. A. Goddard III and W. M. Skiff, *J. Am. Chem. Soc.*, 1992, **114**, 10024.

Received in Cambridge, UK, 25th June 1998; *Paper* 8/04840A

Article V

"A Comparative Study of DFT and Traditional ab initio Methodologies on the OsO_4 Molecule"

Gregori Ujaque, Feliu Maseras, Agustí Lledós

Int. J. Quant. Chem., submitted.

A comparative study of DFT and traditional ab initio methodologies on the OsO_4 molecule.

Gregori Ujaque, Feliu Maseras and Agustí Lledós

Unitat de Química Física, Edifici C.n., Universitat Autònoma de Barcelona, 08193 Bellaterra, Catalonia, Spain

Abstract

The performance of different conventional ab initio methodologies and density functional procedures is compared through its application to the theoretical calculation of bond distance and harmonic vibrational frequencies of the OsO_4 molecule. The problem of the basis set is first considered, with up to 9 different basis sets being tested in calculations using the hybrid Becke3LYP density functional, and the most appropriate basis set is used in the comparison of Hartree-Fock, post Hartree-Fock and density functional methods. The post-Hartree-Fock methods analyzed are MP2, CISD and CCSD(T), and the density functionals tested are SVWN, BLYP, BPW91 and Becke3LYP. The results show that for this particular system, density functional methods perform better than HF-based methods with the exception of CCSD(T), which gives the best overall results.

Keywords: density functional methods, ab initio methods, osmium tetraoxide, vibrational frequencies, inorganic chemistry.

Introduction

The theoretical characterization of inorganic compounds is by no means an easy task. This problem has attracted strong interest within the community of theoretical chemists. The first developments came within the extended Hückel formalism [1], which brought about satisfactory results by providing a qualitative explanation to experimental data for a large number of transition metal systems [2,3]. This method, being inexpensive from the computational point of view, is however unable to explain certain aspects of the experimental behavior of a number of chemical systems. These must be explained through ab initio molecular orbital-based methods. Methods, based on density functional theory (DFT) are also emerging as very powerful tools for carrying out theoretical calculations involving metals. More and more studies are appearing testing the performance of different methodologies in the determination of the structures and energetics of organic [4] and inorganic (both main group and transition metal) [5] compounds. Although this kind of studies are numerous, little work exists dealing with transition metal compounds. In this paper we will compare the performance of Hartree-Fock, post Hartree-Fock and DFT methodologies in the description of a number of experimental parameters, including IR spectra, of one particular transition metal compound: OsO_4.

OsO_4 is one of the most important compounds of osmium. It can be prepared by oxidation of the metal or of simple Os salts, and its high volatility allows its easy sublimation. It is a yellow solid which is soluble in water and CCl_4 to give pale yellow solutions. It is industrially important both in biological chemistry for the "fixation" of biological tissue, and in medicine [6]. Another application of this compound is in the fine organic chemicals industry because it can be used stoichiometrically or catalytically in the cis-dihydroxylation of alkenes to cis-diols [7,8]. A very wide range of alkenes and unsaturated organic substrates has been oxidized using OsO_4. By using OsO_4 in presence of chiral auxiliaries (like tertiary amines) the asymmetric dihydroxylation of a range of organic substrates has been achieved [8,9,10].
In OsO_4, the distribution of the oxygen ligands around the metal gives a tetrahedral arrangement, with T_d symmetry. O-Os-O angles are 109.471° , and dihedral angles between O-Os-O planes are 120°. Hence, only one geometrical parameter (the Os-O bond distance) is needed to characterize the present compound.

When a theoretical study is done, one typical problem is the choice of the basis set [11,12]. It is well known that the use of large basis sets leads to better results. Normally, reactivity studies involve building up a potential energy surface (PES) and hence optimizing geometries. This fact prevents the use of a large basis set and imposes a small or medium-sized basis set, so that geometry optimization calculations will be computationally feasible. One of the goals of the present paper is to compare different commonly used basis sets in order to establish a classification regarding their quality.

Computational details

All the calculations presented in this paper are carried out using the Gaussian 94 package of programs [13]. The different HF and post-HF methods used are: RHF, Restricted Hartree-Fock; CISD, Configuration Interactions with all simple and double substitutions from the Hartree-Fock reference determinant [14,15,16]; MP2, a perturbational Moller-Plesset calculation introducing correlation energy correction up to the second order [17,18,19]; and CCSD(T), Coupled Cluster calculations with full introduction of both Single and Double substitutions including Triple excitations non-iteratively [20].
For DFT calculations both functional of the density (local) and the density gradient (nonlocal) have been used. On the first category (LDA) [21], calculations have been performed with the correlation functional of Vosko, Wilk and Nusair [22], with the Slater exchange functional (SVWN). In the more sophisticate nonlocal density approximation, pure Becke [23] or hybrid Becke's 3 parameter exchange functional [24] with the Lee-Yang-Parr correlation functional [25] (B3LYP and BLYP), and with Perdew and Wang's correlation functional [26] (BPW91), have been used.
Table 1 collects the description of the basis sets used. In all the cases effective core potential (ECP) are used on the metal atom. The pseudopotentials used are those defined by Hay and Wadt [27] in most cases (**A**, **B**, **C**, **D**, **E**, **H**, **I**) and those defined by Stevens, Krauss, Bash and Jasien [28] in two cases (**F**, **G**). The basis set for the metal is always double-ζ, with one set of f polarization functions [27] being added in the case of basis sets **H** and **I**. The basis set for oxygen starts with a valence double-ζ quality in the **A** set (basis 6-31G) [29]. Then the effect of the addition of diffuse [30] (basis set **C**) and polarization [31] (basis set **B**) functions is evaluated, as well as that of a shift to valence

triple-ζ quality [32] (basis set **D**). The use of the alternative basis set of Dunning - Huzinaga [33], of similar size, is also evaluated in basis sets **E**, **F** and **I**.

Table 1. Basis sets used. LANL2DZ* corresponds to the addition of an f shell to the LANL2DZ set.

Basis set	Basis set description		N° of basis functions
	Os	O	
A	LANL2DZ	6-31G	58
B	LANL2DZ	6-31G*	78
C	LANL2DZ	6-31+G	74
D	LANL2DZ	6-311G*	94
E	LANL2DZ	D95V*	78
F	SKBJ	D95V*	87
G	SKBJ	6-31G*	87
H	LANL2DZ *	6-31G*	85
I	LANL2DZ *	D95V*	85

Results and discussions

The results and discussion are divided in different subsections. First of all, the problem of the basis set is considered. Afterwards, the different theoretical HF, post-HF, and DFT methodologies are evaluated. Finally, the last subsection contains some considerations on the stability of the wavefunction and the importance of non dynamic correlation.

A) Choice of the basis set.

In this section the different basis set are tested using the density functional theory, particularly the hybrid Becke3LYP functional. The results of the geometry optimization are compared between them. Afterwards, the better basis sets found are tested again using CCSD(T), one of the bests ab initio methods available at this moment, and the resulting geometry are compared with experimental values.

Table 2 shows the Becke3LYP optimized value of the Os-O bond distance for the nine basis set considered, and the experimental value. No angles are considered because this molecule is a perfect tetrahedron, and the optimizations have been made within the T_d symmetry. Os-O distances emerging from the Becke3LYP geometry optimizations with the nine different basis sets considered (Table 2) can be grouped in three different blocks. The first group is constituted by basis sets **A** and **C**, with distances of 1.742 Å and 1.739 Å, respectively. The second group includes basis sets **B**, **D**, **E**, **F** and **G**, with distances between 1.712 Å and 1.719 Å. Finally, the third group is defined by basis sets **H** and **I**, with values of 1.695 Å and 1.696 Å, respectively. These results are quite informative if we put them together with the definition of the basis sets presented in Table 1.

Table 2. Comparison of optimized Os-O distance using differents basis sets and methodologies. The experimental value is also provided for comparison.

Method	Basis set	d_{Os-O}
Exptl.		1.711[a]
	A	1.742
	B	1.712
	C	1.739
Becke3LYP	D	1.719
	E	1.712
	F	1.712
	G	1.712
	H	1.695
	I	1.696
CCSD(T)	B	1.736
	H	1.710

[a] Ref 34.

The peculiarity of **A** and **C** is that they are the only basis sets where no d polarization functions on the oxygen atoms are included. Therefore, inclusion of these polarization functions, which represent an increase of 20 basis functions, seems necessary. The difference is well exemplified by the results of basis sets **A** and **B**. Basis set **B** is basically the same as basis set **A**, with the only difference of one d shell per oxygen atom. This change brings the Os-O distance from 1.742 Å (basis set **A**) to 1.712 Å (basis set **B**), a decrease of 0.03 Å. The importance of polarization functions of atoms involved on π-bonding to the metal atom is not unprecedented [12], and was therefore to be expected.

The peculiarity of the third group of basis sets, **H** and **I**, is again the presence of polarization functions, in this case of the metal atom. The addition of a set of f functions on the osmium atom

brings the Os-O distance down by an extra 0.02 Å. This is well shown by the difference between the results with basis sets **B** and **H**, differing by only this set of polarization functions, and having Os-O distances of 1.712 Å and 1.695 Å, respectively; or by the difference between basis sets **E** and **I**, with the same relationship, and yielding values of 1.712 Å and 1.696 Å respectively. The importance of f functions on metal atoms is not so usual.

The fact that the results can be grouped by the presence of polarization functions on the oxygen and osmium atoms proves that the other parameters that have been varied in the definition of the basis sets have little effect on the geometry optimization. The addition of diffuse functions on the oxygen atoms brings little change, as can be seen from the comparison of basis sets **A** and **C**, with a difference of only 0.003 Å. The shift from valence double-ζ to valence triple-ζ in oxygen brings only a change of 0.007 Å between **B** (6-31G*) and **D** (6-311G*). Another factor that has been considered is the replacement of the basis set by another of similar quality published by a different group. The 6-31G* basis set, from Pople's group, has been replaced by another valence double-ζ basis set including a polarization shell, D95V*, developed by Dunning, Huzinaga and coworkers. The comparison between the optimized geometries with basis sets **B** (6-31G*) and **E** (D95V*) is clear-cut, they give exactly the same value of 1.712 Å up to the thousandth of Å. A change in the pseudopotential and the associated basis set for the osmium atom has also been considered. The LANL2DZ pseudopotential of Hay and Wadt has been replaced by the SKBJ pseudopotential of Stevens, Basch, Krauss and Jasien. The four combinations between basis set for metal (LANL2DZ, SKBJ) and oxygen (6-31G*, D95V*) have been considered in basis sets **B, E, F, G**. The optimized value for the Os-O distance is in the four cases the same: 1.712 Å.

Once established that the hierarchy between the basis sets for this complex is ruled by the presence of polarization functions on the oxygen and osmium atoms, a comparison with the experimental result must be carried out. It is quite clear from Table 2 that the best agreement with the experimental values of 1.711 Å in the Becke3LYP geometry optimization corresponds to the second group of basis sets, those with polarization functions only on the oxygen atoms. This fact is in contradiction with the expectation that the larger basis set, with polarization on the oxygen and the osmium atoms should provide the best result. In order to clarify this point, a geometry optimization was carried out at the CCSD(T) level with a basis set representative of each of the best groups of basis sets. The basis sets chosen were **B** and **H**, and the results are also included in Table 2. The best agreement corresponds in this case to the **H** basis set, with a result of 1.710 Å, only 0.001 Å shorter than the experimental value of 1.711 Å. The result with the **B** basis set is slightly worse, 1.736 Å, 0.025 Å longer than experiment. Therefore, we must attribute the better agreement with experiment of Becke3LYP optimization with the **B** basis set to an accidental correlation of errors, the **H** basis set being actually better for this system.

Therefore, and as a summary of this subsection, we can say that the addition of polarization functions on both the osmium and the oxygen atoms have a sensible effect on the geometry optimization of OsO_4. The best basis set is that including both sets of polarization functions, and f shell on osmium and a d shell on oxygen. However, because of the fact that the program we

Table 3: Optimized value (Å) for the Os-O bond distance of the OsO_4 molecule, computed using different methods.

Method	d_{Os-O}
Expt.[a]	1.711
HF and post-HF	
RHF	1.664
CISD	1.681
MP2	1.728
CCSD(T)	1.736
CCSD(T)[b]	1.710
DFT	
Becke3LYP	1.712
BPW91	1.727
BLYP	1.737
SVWN	1.710

[a] Ref. 34. [b] All calculations are made using the **B** basis

have been using is not able to compute analytical gradients for systems including f functions, we propose that a good compromise can be obtained with **B** basis set (LANL2DZ for Os, 6-31G* for O); and basis set **H** (LANL2DZ* for Os, 6-31G* for O) should be used only for calculations requiring especially high accuracy. Because of this, results on next subsection will use these two basis sets.

B) Comparison of computational methods.

The performance of different methods in the computation of optimal geometries and harmonic frequencies is compared in this subsection. The basis set used in most of the calculations presented in the section is **B**. In the case of the CCSD(T) method the **H** basis set is also used. The comparison is made between methods

Table 4: Vibrational frequencies (in cm^{-1}) corresponding to the normal modes of OsO_4, computed using different methods.

	T_2	E	A_1	T_2	Average discrepancy (%)
Expt.[a]					
Raman	322.7	333.1	965.2	960.1	
HF and post-HF					
RHF	378.0	384.3	1186.7	1120.3	14.0
CISD	362.2	369.8	1135.0	1104.9	13.9
MP2	313.7	313.0	862.6	1136.7	9.5
CCSD(T)	325.3	323.5	942.9	977.6	1.7
CCSD(T)[b]	333.6	333.7	986.3	1011.3	2.8
DFT					
Becke3LYP	327.9	332.3	1025.6	1014.2	3.4
BPW91	314.9	319.6	979.5	976.4	2.4
BLYP	309.5	312.5	959.4	957.6	2.8
SVWN	320.8	326.0	1021.2	1017.6	3.6

[a] Ref. 35. [b] All calculations are made using the **B** basis set, except for this one, where the **H** basis set is used.

based on Hartree-Fock and post-HF theory, and methods based on Density Functional Theory.

As far as the Os-O bond distances are concerned, computed values using the different methods are gathered in Table 3. Among the different methods tested, CCSD(T) is considered the best one. This method gives a value for the bond distance of 1.736 Å. This value is 0.025 Å larger than the experimental one, but the discrepancy is due to the lack of f orbitals on Os, as discussed above. Because of this, 1.736 Å ought to be considered the optimal value with this basis set **B**.

Bond distances obtained by HF and post-HF methods, are systematically shorter than the CCSD(T) value, with the RHF and CISD methods yielding unacceptable discrepancies of more than 0.05 Å. The MP2 calculation gives a bond distance of 1.728 Å, only 0.008 Å shorter than the CCSD(T) distance. In the DFT calculations, the values of the bond distances are close to the CCSD(T) target. Discrepancies are always smaller than 0.03 Å, with the BLYP value being only 0.001 Å off the CCSD(T) value.

Now we will discuss the harmonic vibrational frequencies. Symmetry labels corresponding to each normal mode, together with the corresponding values, are collected in Table 4. In the OsO_4 molecule there are four normal modes of vibration, of A_1, E and T_2 symmetries. All the normal modes of vibration are active in the Raman spectrum, and only two of them (the two T_2 modes) are active in the infrared spectrum.

The RHF vibrational frequencies calculated are always larger than the experimental values, the largest difference corresponding to the normal mode with A_1 symmetry. The average discrepancy of the vibrational frequencies calculated by this method with the experimental values is 14.0%. Some post-HF methods have also been used to calculate the vibrational frequencies. The CISD method gives an average error of 13.9%, which is almost the same as the RHF method. For CISD, all of the frequencies are also larger than the experimental values. The MP2 method changes this trend, the frequencies corresponding to E, A_1 and one of the two T_2, are smaller than the experimental value, and the other T_2 frequency is larger. The average error for MP2 is smaller (9.5%) than for RHF and CISD. The last post-HF method that has been used in this test, is the CCSD(T) method. This is considered one of the best quantum mechanical methods. The average error obtained with this method is 1.4%, which represent a significant improvement. The two frequencies corresponding to T_2 symmetry are larger than the experimental values, and the two other frequencies (corresponding to E and A_1 symmetries) are shorter than the experimental ones. We tried to get a further improvement by testing the **H** basis set in the CCSD(T) calculation, but there was no improvement. The error was 2.8%, still quite good, but worse than with the **B** basis set. The problem seems to be in the two higher frequencies. Experimental values are 965.2 cm^{-1} for A_1 and 960.1 cm^{-1} for T_2, while the computed values are 986.3 cm^{-1} for A_1 and 1011.3 cm^{-1} for T_2.

Table 4 also contains the computed vibrational frequencies using different methods based on the Density Functional Theory. The first one used, the Becke3LYP method, give an average discrepancy of 3.4%, with respect to the experimental values. The computed frequencies for the two normal modes with less energy are smaller than the experimental ones, while the computed frequencies for the two higher energy normal modes are larger than the experimental ones. Things are similar with the BeckePW91 method, though the average discrepancy is a little smaller, 2.4%. This method gives the smallest value for the average error among the DFT methods. At the BeckeLYP level all of the computed frequencies are lower in energy than the experimental values, and the average error is 2.8%. The last DFT method tested, the local density SVWN, gives similar results than Becke3LYP and BeckePW91, though with a slightly larger average discrepancy of 3.6%.

A general view of Table 4 shows that errors are never very large, but that a classification can be done among the different methods. The larger error is given by the RHF, CISD and MP2 methods, with errors larger than 9%. The other calculations, CCSD(T) and DFT, provide always discrepancies with experiment smaller than 4%. The success of the CCSD(T) method is not surprising, since this is a very accurate, and computationally demanding, method. The fact that all DFT methods (including SVWN, without gradient corrections) beat so clearly the CISD and MP2 methods for this particular system is however more unexpected. We will briefly analyze in the next subxection the reason of this result.

C) The wave function. A stability test.

The fact that the CISD and MP2 methods cannot improve significantly the poor results of the RHF calculation on OsO_4 suggests a problem with

non dynamic correlation. CISD and MP2 are certainly efficient in the introduction of dynamic correlation, correction to the lowest energy states determinant of the system; but they are not appropriate in cases of near degeneracy of the ground state. The appropriate consideration of non dynamic correlation would require the performance of multiconfigurational calculations. However, one simple way to ascertain the existence of non dynamic correlation is the performance of stability test on the wavefunction.

The program Gaussian 94 has the ability to test the stability of a single-determinant wavefunction with respect to relaxing various constraints. In this case, we studied the instability allowing the RHF determinant to become UHF. The calculation, carried out with the **B** basis set, proves that the RHF function is not stable. In particular, there are three negative eigenvalues, and all of them involve transfer from the three higher energy occupied orbitals to the two lower energy unoccupied orbitals. The three occupied orbitals involved have T_1 symmetry, and are linear combination of p orbitals of the oxygen atoms involved in π bonding with the metal. The only orbitals in the metal belonging to this symmetry group are of f nature. The importance of these oxygen t_1 orbitals is probably the reason for the large effect of f polarization functions on the metal for this system. The two unoccupied orbitals involved are the formally non-bonding d orbitals on osmium. The optimization of the wavefunction within the UHF formalism leads to a broken symmetry solution with an energy 26.3 kcal/mol below the RHF solution.

This results shows that the restricted determinant used is not a local minimum when the specified degrees of freedom are taken into consideration. This is especially serious, because MP2 calculations are only valid when the wavefunction has no internal instabilities [36]. Therefore, results presented in the previous section with this method have no real value.

We used the same Gaussian 94 code to test the stability of the DFT Becke3LYP "wavefunction". Although we are aware that there is not such a thing as a wavefunction in the density functional theory, we expect that a study on the orbitals defining the α and β spin densities could be informative. The result of this stability test was that the restricted single determinant was stable with respect to instabilities leading to an unrestricted solution. We performed also an additional unrestricted Becke3LYP calculation starting from the orbitals of the broken symmetry UHF solution. This calculation converged to the restricted Becke3LYP solution. There is therefore a sharp difference between the HF and Becke3LYP calculation. In both cases there is only one solution, but it is unrestricted at the HF level, and restricted at the Becke3LYP level.

Results in this subsection prove that non dynamic correlation is important in OsO_4, and that HF itself or HF based methods like CISD or MP2 are not valid, because they focus on only one Slater determinant. On the other hand, DFT methods, even if they are also single-determinant, are able to provide a satisfactory description because they somehow succeed in the introduction of non-dynamic correlation.

Conclusions

The theoretical study of the OsO_4 system with a number of different basis sets, as well as different HF-based and DFT methods, allows a classification of the requirements for an appropriate reproduction of experimental data. The basis set must be of valence double-ζ nature, and include a polarization d shell on oxygen. Addition of polarization f shell on osmium is also recommended, although it can be neglected if there are problems in computation of analytic gradients. The addition of diffuse functions on oxygen, as well as the shift from valence double-ζ to valence triple-ζ seems to have no effect. Similarly, replacement of the tested basis set by others of similar quality from other groups brings very minor changes.

Comparison of different theoretical methods shows that the best agreement with experiment, both in geometry and frequencies, is provided by the CCSD(T) method. A good agreement is also obtained when the DFT based methods are applied, the functionals Becke3LYP, BPW91, BLYP and SWVN having been tested. The worst results are provided by the HF, CISD and MP2 methods. This failure of HF and HF-based methods introducing dynamic correlation can be explained through the importance of non dynamic correlation in this system, which is proved through stability calculations.

Acknowledgment. Financial support from the Spanish DGES through Project No. PB95-0639-CO2-01 is acknowledged. The use of computational facilities of the Centre de Supercomputació de Catalunya (C^4) is appreciated.

References

1.[] R. Hoffmann. J. Chem. Phys., 39, 1397 (1963); R. Hoffmann, Acc. Chem. Res. 4, 1 (1971)
2.[] T. A. Albright, J.K. Burdett and M. H. Whangbo, *Orbital Interactions in Chemistry*, Wiley, New York, 1985.
3.[3] R. W. Grimes and D. Onwood, J. Chem. Soc., Faraday Trans. 86, 233 (1990).
4.[] See for example: D. C. Sorescu, C. M. Bennet and D. L. Thompson J. Phys. Chem. A 102, 10348 (1998); V. Branchadell, E. Muray, A. Oliva, R. M. Ortuño and C. Rodríguez-García J. Chem. Phys. A **102,** 10106 (1998); A. Bottoni J. Chem. Phys. A **102,** 10142 (1998).
5.[] See for example: C. Van Wullen Int. J. Quantum Chem. 58, 147 (1996); M. R. Bray, R. J. Deeth, V. J. Paget and P. O. Sheen Int . J. Quantum Chem. **61,** 85 (1997); M. Torrent, P. Gili, M. Duran and M. Solà, Int. J. Quantum Chem. **61,** 405 (1997); P. J. Hay and R. L. Martin **109,** 3075 (1998); A. Kovaer, G. I. Csonka and G. M. Keseru, J. Comp. Chem. **19,** 308 (1998); I. Bytheway and M. W. Wong, Chem. Phys. Lett. **282,** 219 (1998); G. Sandrone and D. A. Dixon, J. Phys. Chem. A **102,** 10310 (1998); M. Sodupe, J. Bertrán, L. Rodríguez-Santiago and E. J. Baerends, J. Phys. Chem. A **103,** 166 (1999).
6.[] J. S. Hanker, D. K. Romanovicz and H. Padykula, J. Histochem., 49, 263 (1976).
7.[] M. Schröder, Chem. Rev. 80, 187 (1980); W. P. Griffith, Transition Met. Chem. 15, 251 (1990).
8.[] H. C. Kolb, M. S. VanNieuwenhze and K. B. Sharpless, Chem. Rev. 94, 2483 (1994) and cites therein.
9.[] E. J. Corey and M. Noe, J. Am. Chem. Soc., 115, 12579 (1993); E. J. Corey and M. Noe, J. Am. Chem. Soc. 118, 11038 (1996).
10.[] S. Dapprich, G. Ujaque, F. Maseras, A. Lledós, D. G. Musaev and K. Morokuma, J. Am . Chem. Soc. 118, 11660 (1996); G. Ujaque, F. Maseras and A. Lledós, J. Org. Chem,. **62,** 7892 (1997).
11.[] F. Maseras, A. Lledós, M. Duran and J. Bertrán, J. Chem. Soc. Faraday Trans. 88, 1111 (1992).
12.[] G. Barea, G. Ujaque, F. Maseras and A. Lledós, J. Mol. Struct. (Theochem), 371, 59 (1996).
13.[] Gaussian 94, Revision E.1, M. J. Frisch, G. W. Trucks, H. B. Schlegel, P. M. W. Gill, B. G. Johnson, M. A. Robb, J. R. Cheeseman, T. Keith, G. A. Petersson, J. A. ontgomery, K. Raghavachari, M. A. Al-Laham, V. G. Zakrzewski, J. V. Ortiz, J. B. Foresman, J. Cioslowski, B. B. Stefanov, A. Nanayakkara, M. Challacombe, C. Y. Peng, P. Y. Ayala, W. Chen, M. W. Wong, J. L. Andres, E. S. Replogle, R. Gomperts, R. L. Martin, D. J. Fox, J. S. Binkley, D. J. Defrees, J. Baker, J. P. Stewart, M. Head-Gordon, C. Gonzalez, and J. A. Pople, Gaussian, Inc., Pittsburgh PA, 1995.
14.[] J. A. Pople, R. Seeger and R. Krishnan, Int. J. Quant. Chem. Symp. 11, 149 (1977).
15.[] R. Krishnan, H. B. Schlegel and J. A. Pople, J. Chem. Phys. 72, 4654 (1980).
16.[] K. Raghavachari and J. A. Pople, Int. J. Quant. Chem 20, 167 (1981).
17.[] M. Head-Gordon, J. A. Pople and M. J. Frisch, Chem. Phys. Lett. 153, 503 (1988); M. J. Frisch, M. Head-Gordon and J. A. Pople, Chem. Phys. Lett **166,** 275 (1990); M. J. Frisch, M. Head-Gordon and J. A. Pople, Chem. Phys. Lett. **166,** 281 (1990).
18.[] M. Head-Gordon and T. Head-Gordon, , Chem Phys. Lett. 220, 122 (1994).
19.[] S. Saebo and J. Almlof, Chem. Phys. Lett. 154, 83 (1989).
20.[] J. A. Pople, M. Head-Gordon and K. Raghavachari, J. Chem. Phys. 90, 3700 (1989).
21.[] J. C. Slater, Quantum Theory of Atomic Structure McGraw-Hill, New York, 1960; O. Gunnarson and I. Lundqvist, Phys. Rev. B 10, 1319 (1974).
22.[] S. H. Vosko, L. Wilk and M. Nusair, Can. J. Phys. 58, 1200 (1980).
23.[] A. D. Becke, Phys. Rev. A 38, 3098 (1988).
24.[] A. D. Becke, J. Chem. Phys. 98, 5648 (1993).
25.[] C. Lee, W. Yang and R. G. Parr, Phys. Rev. B 37, 785 (1988).
26.[] J. P. Perdew and Y. Wang, Phys. Rev. B 45, 13244 (1992).
27.[] P. J. Hay and W. R. Wadt, J. Chem. Phys. 82, 270 (1985); W. R. Wadt and P. J. Hay, J. Chem. Phys **82,** 284 (1985); A. W. Ehlers, M. Böme, S. Dapprich, A. Gobbi, A. Höllwarth, V. Jonas, K. F. Köhler, R. Stegmann, A. Veldkamp and G. Frenking, Chem. Phys. Lett. **208,** 111 (1993).
28.[] W. J. Stevens, M. Krauss, H. Bash and P. G. Jasien, Can. J. Chem. 70, 612 (1992).
29.[] J. S. Binkley, J. A. Pople and W. J. Hehre, J. Amer. Chem. Soc. 102, 939 (1980); M. S. Gordon, J.

S. Binkley, J. A. Pople, W. J. Pietro and W. J. Hehre, , "Self-Consistent Molecular Orbital Methods. 22. Small Split-Valence Basis Sets for Second-Row Elements", J. Amer. Chem. Soc. **104**, 2797 (1988).
30.[] T. Clark, J. Chandrasekhar, G. W. Spitznagel and P. v. R. Schleyer, J. Comp. Chem. 4, 294 (1983).
31.[] M. J. Frisch, J. A. Pople and J. S. Binkley, J. Chem. Phys. 80, 3265 (1984).
32.[] A. D. McLean and G. S. Chandler, J. Chem. Phys. 72, 5639 (1980); R. Krishnan, J. S. Binkley, R. Seeger and J. A. Pople, J. Chem. Phys. **52**, 1033 (1970).
33.[] T. H. Dunning, Jr. and P. J. Hay, in Modern Theoretical Chemistry, Ed. H. F. Schaefer, III, Plenum: New York, 1976, 1-28.
34.[] B. Krebs and K.-D. Hasse, Acta Cryst. B32, 1334 (1976).
35.[] J. L. Huston and H. H. Claassen, J. Chem. Phys. 52, 5646 (1970).
36.[] P. Carsky and E. Huback, Theor. Chim. Acta **80**, 407 (1991).

Article VI

"A Theoretical Evaluation of Steric and Electronic Effects on the Structure of [OsO4(NR3)] (NR3 = Bulky Chiral Alkaloid Derivate) complexes"

Gregori Ujaque, Feliu Maseras, Agustí Lledós

Theor. Chim. Acta, **94**, 67-73 (1996)

Theor Chim Acta (1996) 94: 67–73

Theoretica Chimica Acta

A theoretical evaluation of steric and electronic effects on the structure of $[OsO_4(NR_3)]$ (NR_3 = bulky chiral alkaloid derivative) complexes

Gregori Ujaque, Feliu Maseras, Agustí Lledós

Unitat de Química Física, Department de Química, Universitat Autònoma de Barcelona, E-08193 Bellaterra, Barcelona, Catalonia; Fax: 34-3-581-2920

Received February 26, 1996/Accepted March 1, 1996

Summary. The novel theoretical scheme IMOMM, integrating *ab initio* and molecular mechanics contributions in a single geometry optimization process, is applied to the structural determination of different $[OsO_4(NR_3)]$ (NR_3 = bulky chiral alkaloid derivative) species closely related to active catalysts for the asymmetric dihydroxylation of olefins. Computed values compare in a satisfactory way with available X-ray data, the relationship between the Os–N distance and the nature of the NR_3 ligand being properly reproduced. The computational scheme allows the separate quantification of electronic and steric effects, as well as the identification of the specific steric repulsions responsible for the difference.

Key words: IMOMM method – $[OsO_4(NR_3)]$ Complexes – Steric effects – Transition Metal chemistry

1. Introduction

The osmium-catalyzed asymmetric dihydroxylation of olefins is among the most efficient and better studied examples of the application of transition metal complexes to practical synthesis of biologically active compounds.[1] Although there has been recent mechanistic discussion in the chemical Literature,[2,3] there seems to exist a general agreement on the most efficient forms of the catalyst, that responds to the general formula $[OsO_4(NR_3)]$, with NR_3 being a bulky chiral alkaloid derivative. There are still however some open questions concerning the precise mechanism of the reaction, as well as on the exact origin of enantioselectivity.

Theoretical analysis seems appropriate for this kind of discussion, but its application has been so far hampered by the peculiarities of the problem. Full *ab initio* calculations cannot be carried out on the full experimental system because of its size, and have to be performed on the model system $[MO_4(NH_3)] + CH_2CH_2$ (M = Ru, Os),[4,5] where chirality effects are conspicously absent. Molecular mechanics calculations, that can indeed afford computing the full experimental system,[6,7] hit the problem of the scarceness of standard parameters for transition metal complexes, as well as problems in computation of transition states. The problem is therefore appropriate for a method able to combine *ab initio* and molecular mechanics contributions in a single calculation. Our laboratory has been

recently involved in the development of one of such algorithms,[8,9] which has been baptized as "integrated MO/MM" (IMOMM) scheme. This paper presents the results of its first application to complexes related to dihydroxylation of olefins, which in turn constitutes only its second application to transition and metal chemistry.[9]

In particular, the problem we address in this paper is the ability of this computational scheme to reproduce the X-ray geometry of two different $[OsO_4(NR_3)]$ complexes related to the osmium-catalyzed asymmetric dihydroxylation of olefins. These are $[OsO_4$(quinuclidine)] (**1**)[10] and $[OsO_4\{$(dimethylcarbamoyl)dihydroquinidine$\}]$ (2) [11]. The topic is especially appealing because, despite their similarity, the two compounds present quite different Os–N distances: 2.37 Å for **1**, 2.49 Å for **2**. That is, a difference of 0.12 Å, very likely due to steric effects.

2. Computational details

We performed calculations with a program built from modified versions [8] of the standard programs Gaussian 92/DFT [12] for the quantum mechanics part and mm3(92) [13] for the molecular mechanics part. *Ab initio* calculations were carried out on the $[OsO_4(NH_3)]$ fragment. We used two different basis sets I and II; and both the Hartree–Fock based (RHF, MP2 [14]) and density functional (BECKE3LYP [15]) formalisms were applied. Basis set I was the same used by Veldkamp and Frenking [5] in their thorough MO study of the reaction mechanism for the model system. It consists of a quasirelativistic effective core potential or the 60 innermost electrons of osmium with the associated basis set [16] in a (441/41/21) contraction, and a 3-21G basis set for all other atoms [17]. Basis set II uses the same effective core potential for osmium [16], with the basis set in the LANL2DZ standard contraction [12], the 6-31G* basis set for oxygen [18], and 6-31G for nitrogen and hydrogen [18a]. We shifted to this more complete basis set because we found different results from basis set I. The RHF optimized Os–N distance for the $[OsO_4(NH_3)]$ complex is 2.369 Å with basis set I and 2.613 Å with basis set II. We could also observe that the difference is mainly associated to the presence of the polarization d shell on the oxygen atom.

Molecular mechanics calculations used the force field contained in the mm3(92) program when possible [19]. All geometry optimizations were complete, except for the constraints required by the method [20].

3. Results of geometry optimization

The main geometrical features of the complexes were properly reproduced in the different geometry optimizations we carried out. Figures 1–4 show the results obtained with the BECKE3LYP formalism and the basis set II (IMOMM(BECKE3LYP/II:MM3) description). In both cases, the molecule adopts a trigonal bipyramidal structure around the metal center, with one oxygen and the NR_3 ligand in the axial positions. A staggered conformation around the Os–N bond, with O–Os–N–C dihedral angles near 60°, is found, in agreement with experiment [10, 11]. The bulky "antenna" of the (dimethylcarboamoyl)dihydroquinidine ligand of **2** presents also a disposition very similar to that of experiment [11].

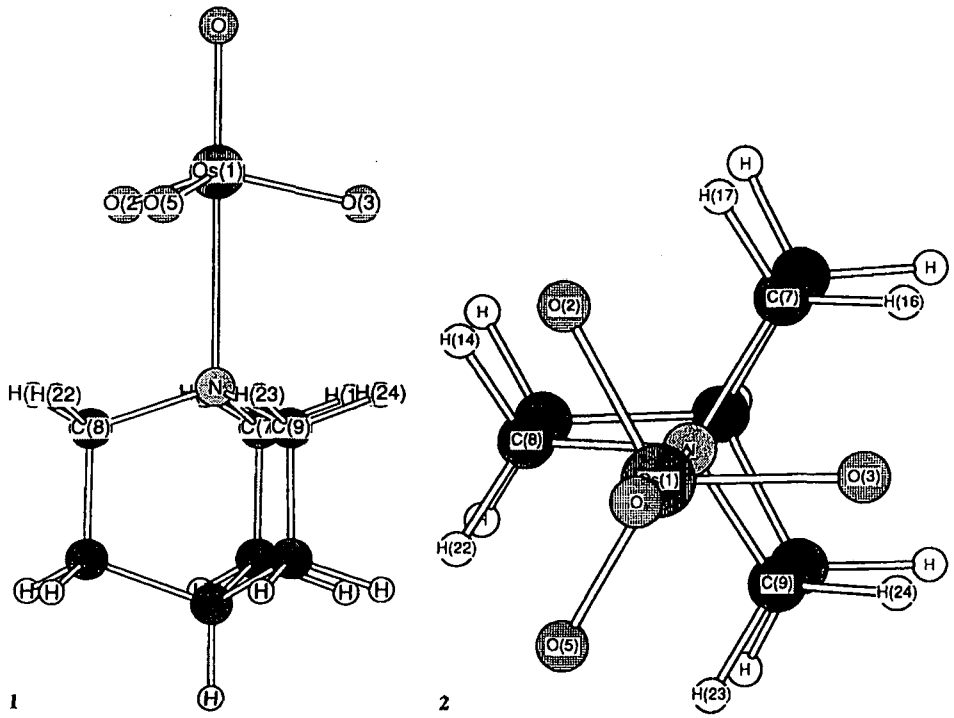

Fig. 1. IMOMM(BECKE3LYP/II:MM3) optimized geometry of complex **1** (side view)

Fig. 2. IMOMM(BECKE3LYP/II:MM3) optimized geometry of complex **1** (top view)

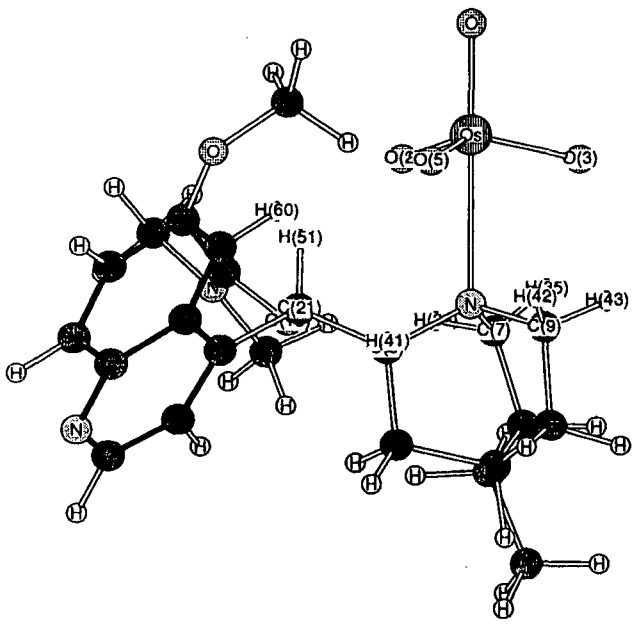

Fig. 3. IMOMM(BECKE3LYP/II:MM3) optimized geometry of complex **2** (side view)

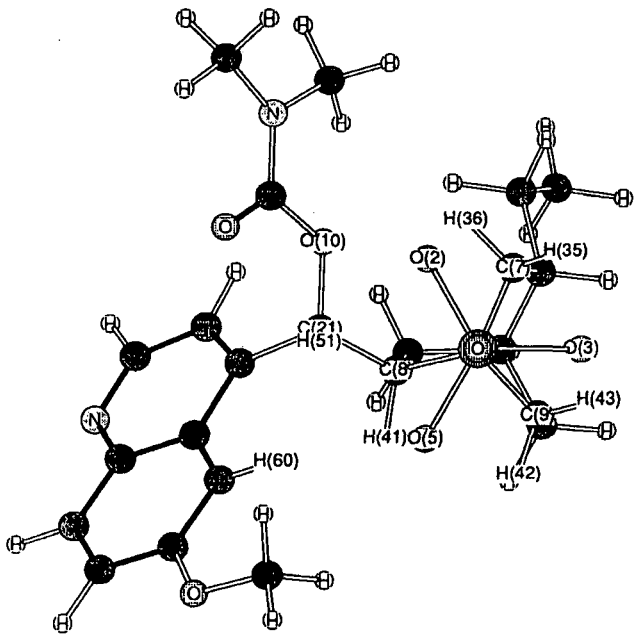

Fig. 4. IMOMM(BECKE3LYP/II:MM3) optimized geometry of complex **2** (top view)

Table 1. Optimized value for the Os–N distance (Å) in different $[OsO_4(NR_3)]$ complexes, as obtained with the IMOMM scheme. Results with different *ab initio* descriptions are presented

	RHF/I	MP2/II	BECKE3LYP/II
1	2.429	2.531	2.546
2	2.478	2.591	2.619
3	2.368	2.470	2.466
diff. **2** – **1**	0.049	0.060	0.073

The most significant result, from a quantitative point of view, of the geometry optimization is the Os–N distance. Values obtained for this parameter are collected in Table 1. Theoretical results for the hypothetical $[OsO_4(NH_3)]$ complex (**3**), that has not been synthesized, are also provided for comparison. The trend in the difference between complexes **1** and **2** is reproduced by our calculations. Complex **2** has always a longer distance than complex **1**, the precise computed value depending on the *ab initio* computational level. Although the computed differences (from 0.05 to 0.07 Å) fall short of the experimental value (0.12 Å), we consider this qualitative agreement itself a remarkable achievement of the integrated method. Some comment must also be made with respect to the absolute value of the Os–N distance. Besides the fact that agreement with experiment is rather poor (discrepancies up to 0.18 Å), the dispersion in computed values is also important (0.12 Å in **1**, 0.14 Å in **2**). Our interpretation is that the quantum mechanical descriptions that have been tested for the *ab initio* part are not accurate enough for the exact reproduction of this parameter. In other words, we would not blame the combination scheme for this problem, but rather the *ab initio* contribution.

4. Quantification of steric effects

Besides allowing the study of much larger systems, the IMOMM scheme provides additional tools to analyze the results. For instance, it is possible to quantify the relative weight of steric and electronic effects in the distortion of the system. In order to do this, we carried out some additional calculations. These were restricted geometry optimizations of **1** and **2** with the Os–N distance fixed to the optimized value for **3** at the corresponding computational level. From direct comparison of these restricted optimizations with the full optimizations discussed above, the energy gain associated to the elongation of the Os–N distance in presence of the bulky ligand can be measured. It comes out to be quite small. For complex **1**, it is 0.21, 0.15 and 0.24 kcal/mol at the RHF/I, MP2/II and BECKE3LYP/II *ab initio* descriptions, respectively. For complex **2**, the corresponding values are a little larger, 0.61, 0.68 and 0.69 kcal/mol. This total energy gain can be further decomposed in QM and MM contributions. For instance, in the IMOMM(BECKE3LYP/II:MM3) calculation for **1** it is found that the gain of 0.24 kcal/mol comes from a 0.46 kcal/mol gain at the MM level and a 0.22 kcal/mol loss at the QM level. Similarly, calculations for **2** at the same level yield an MM stabilization of 1.34 kcal/mol and a QM destabilization of 0.65 kcal/mol. These numbers, which are similar for other computational levels, bear an important consequence for the nature of bonding in these complexes. Certainly, they indicate that the Os–N bond is elongated essentially because of its intrinsic weakness (low force constant), and not because of the existence of strong steric repulsions, which are absent.

A last information to be extracted from the IMOMM results comes from a more detailed analysis of the MM part. The change in the MM energy associated to the lengthening of the Os–N distance is essentially associated to the relaxation of van der Waals (VDW) repulsions. In particular, for the IMOMM(BECKE3LYP/II:MM3) case, this term accounts for 0.44 of the total of 0.46 kcal/mol in complex **1**, and for 1.10 out of 1.34 kcal/mol in complex **2**. Moreover, these steric repulsions can even be tracked down to the particular pairs of atoms that are their responsible. We are going to carry now this type of analysis on the IMOMM(BECKE3LYP/II:MM3) results, in the understanding that they would be qualitatively reproduced in any of the two other computational levels. In complex **1** the change in van der Waals repulsions happens to be concentrated essentially in six particular pairs of atoms, which are (following the numbering scheme shown in Figs. 1 and 2) O(2)–H(14), O(2)–H(17), O(3)–H(16), O(3)–H(24), O(5)–H(22) and O(5)–H(23). The energy gain associated to the lengthening of the Os–N bond for each of this six VDW repulsions is of 0.08 kcal/mol. That is, if we were to consider only these six pairs of atoms, the VDW term would show a change of 0.48 kcal/mol, very close to the 0.44 kcal/mol associated to the real change in this term mentioned above. Let us now analyze what are these atoms pairs. Looking at Figs. 1 and 2, it can be seen that each pair if formed by one of the equatorial oxygen atoms bound to the metal and one of the γ hydrogen atoms of the quinuclidine ligand. This is actually what one would expect from this species, this is the place where steric repulsion is supposed to be located. The fact that the six repulsions are equivalent is consistent with the overall C_{3v} symmetry of the complex.

More interesting is the case of complex **2**, that has not such symmetry. In this case, analysis of the change in VDW energy associated to the lengthening of the Os–N bond can be concentrated in ten atom pairs, those indicated in Table 2. The energy gain associated to these ten atom pairs is 1.05 kcal/mol, which represents

Table 2. Decomposition in its most significant contributions (in kcal/mol) of the VDW energy gain associated to the lengthening of the Os–N distance in complex **2**. Results from IMOMM(BECKE3LYP/II:MM3) calculations. Numbering of atoms follows Figs. 3 and 4

Atom pair		Atom pair	
O(2)–O(10)	0.087	O(3)–H(43)	0.269
O(2)–C(21)	0.077	O(5)–H(41)	0.095
O(2)–H(36)	0.127	O(5)–H(42)	0.107
O(2)–H(51)	0.081	O(5)–H(51)	0.072
O(2)–H(35)	0.067	O(5)–H(60)	0.065

most of the 1.10 kcal/mol total VDW gain. By looking at Figs. 3 and 4, it is possible to see that the steric effect is still associated to repulsion between equatorial oxygen atoms bound to the metal center and the γ substituents of the NR_3 group, as happened in complex **1**. Here there is however the substantial difference that one of the γ substituents is not a hydrogen atom, but a much larger group (that starting at C(21)). Some interesting properties of complex **2** can be deduced from the data in Table 2. For instance, it is possible to group the ten contributions and see what corresponds to each γ substituent. By doing this, we find that the steric relaxation associated to the bulky C(21) group is 0.38 kcal/mol, which is a large part of the total, but not much larger than that corresponding to the value associated to the repulsion between O(3) and H(43) (0.27 kcal/mol). That is, the C(21) group is carefully arranged in such a way that it does not create a substantial steric repulsion. Another interesting application of Table 2 could be the prediction of which substituents would give a larger change upon substitution. For instance, it seems clear that any substitution of H(51), with sensible interactions to both O(2) and O(5) would bring a sharp increase in steric effects. Similarly, and somehow more unexpectedly, it is found that replacement of H(43) would be more critical than replacement of H(35).

5. Concluding remarks

We have shown the ability of the IMOMM scheme to reproduce the subtle differences in the Os–N bonding in complexes [OsO_4(quinuclidine)] and [OsO_4\{(dimethylcarbamoyl)dihydroquinidine\}]. This scheme has also allowed the separate quantification of electronic and steric effects, as well as the identification of the specific steric repulsions responsible for the difference. After this satisfactory test, the same computational scheme will be applied to topics directly related to the catalytic activity of this type of complexes, with the ultimate goal of reproducing computationally the whole reaction profile.

Acknowledgements. We thank Prof. Keiji Morokuma (Emory) for helpful discussions. Financial support is acknowledged from the Spanish "Dirección General de Investigación Cientifica y Técnica" (DGICYT) under projects No. PB92-0621 and PB95-0639.

References

1. Kolb HC, VanNieuwenhze MS, Sharpless KB (1994) Chem Rev 94:2483–2547, and references therein
2. Corey EJ, Noe MC (1993) J Am Chem Soc 115:2579–2580
3. Kolb HC, Andersson PF, Bennani YL, Crispino GA, Jeong K-S, Kwong HL, Sharpless KB (1993) J Am Chem Soc 115:12226–12227
4. Norrby P-O, Kolb HC, Sharpless KB (1994) Organometallics 13:344–347
5. Veldkamp A, Frenking G (1994) J Am Chem Soc 116:4937–4946
6. Norrby P-O, Kolb HC, Sharpless KB (1994) J Am Chem Soc 116:8470–8478
7. Wu Y-D, Wang Y, Houk KN (1992) J Org Chem 57:1362–1369
8. Maseras F, Morokuma K (1995) J Comp Chem 9:1170–1179
9. Matsubara T, Maseras F, Koga N, Morokuma K (1996) J Phys Chem 100:2573–2580
10. Griffith WP, Skapski AC, Woode KA, Wright MJ (1978) Inorg Chim Acta 31:L413–L414
11. Svendsen JS, Markó I, Jacobsen EN, Rao CP, Bott S, Sharpless KB (1989) J Org Chem 54:2264–2266
12. Frisch MJ, Trucks GW, Schlegel HB, Gill PMW, Johnson BG, Wong MW, Foresman JB, Robb MA, Head-Gordon M, Replogle ES, Gomperts R, Andres JL, Raghavachari K, Binkley JS, Gonzalez C, Martin RL, Fox DJ, Defrees DJ, Baker J, Stewart JJP, Pople JA (1993) Gaussian 92/DFT, Gaussian Inc, Pittsburgh PA
13. Allinger NL (1992) mm3(92), QCPE, Bloomington, IN
14. Møller C, Plesset MS (1934) Phys Rev 46:618
15. (a) Becke AD (1988) Phys Rev A 38:3098–3100 (b) Becke AD (1993) J Chem Phys 98:5648–5652 (c) Lee C, Yang W, Parr RG (1988) Phys Rev B 37:785–789
16. Hay PJ, Wadt WR (1985) J Chem Phys 82:299–310
17. Binkley JS, Pople JA, Hehre WJ (1980) J Am Chem Soc 102:939–947
18. (a) Hehre WJ, Ditchfield R, Pople JA (1972) J Chem Phys 56:2257–2261 (b) Hariharan PC, Pople JA (1973) Theor Chim Acta 28:213
19. Apart from the modifications required by the method [8], all torsional contributions associated to dihedral angles involving the metal atom were set to zero. Finally, the very few parameters of complex **2** that are not provided by the program were set to values corresponding to similar atoms
20. In the *ab initio* calculation, the N–H distances were frozen to 1.015 Å. In the molecular mechanics calculation, the corresponding N–C distances were frozen to their experimental value in the X-ray structure of **2**